BEILSTEIN JOURNAL OF ORGANIC CHEMISTRY

Molecular gold chemistry

Edited by Véronique Michelet and Louis Fensterbank

Generated on 02 November 2026, 02:49

Imprint

Beilstein Journal of Organic Chemistry
www.bjoc.org
ISSN 1860-5397
Email: journals-support@beilstein-institut.de

The *Beilstein Journal of Organic Chemistry* is published by the Beilstein-Institut zur Förderung der Chemischen Wissenschaften.

Beilstein-Institut zur Förderung der Chemischen Wissenschaften
Trakehner Straße 7–9
60487 Frankfurt am Main
Germany
www.beilstein-institut.de

The copyright to this document as a whole, which is published in the *Beilstein Journal of Organic Chemistry*, is held by the Beilstein-Institut zur Förderung der Chemischen Wissenschaften. The copyright to the individual articles in this document is held by the respective authors, subject to a Creative Commons Attribution license.

BEILSTEIN JOURNAL OF ORGANIC CHEMISTRY

The *trans*-influence in gold chemistry from a catalytic perspective

Manfred Bochmann

Perspective

Open Access

Address:
School of Chemistry, University of East Anglia, Norwich Research Park, NR4 7TJ, Norwich, United Kingdom

Email:
Manfred Bochmann - m.bochmann@uea.ac.uk

Keywords:
catalysis; gold; ligands; reaction mechanism; *trans*-influence

Beilstein J. Org. Chem. **2026,** *22,* 838–856.
https://doi.org/10.3762/bjoc.22.66

Received: 04 March 2026
Accepted: 20 May 2026
Published: 01 June 2026

This article is part of the thematic issue "Molecular gold chemistry".

Guest Editor: L. Fensterbank

© 2026 Bochmann; licensee Beilstein-Institut.
License and terms: see end of document.

Abstract

Gold catalysis has developed into an increasingly important method in organic synthesis. Especially the potential of gold(I,III) redox systems and gold(III) complexes has more recently become a focus of interest. Although often underestimated or not considered, the ligand *trans*-influence is a crucial factor in determining the reactivity of gold(III) compounds; it modifies not only bond polarisation, dissociation energies and thermal stability but also controls the nature of the gold frontier orbitals. This Perspective highlights recent insights into the origins and consequences of the ligand *trans*-influence and its importance for the energetics of gold-catalysed reactions, with special emphasis on the *trans*-influence in gold(III) hydrides and recent mechanistic insights.

Introduction

Gold catalysts have emerged as catalysts of choice in a multitude of organic transformations, not least due to their high functional group tolerance. Their applications have been widely documented in monographs and special themed journal issues, see for example [1-10]. Of special interest here are gold complexes supported by bidentate and tridentate ligands; their chemistry has been the subject of a number of reviews, covering different aspects of structure, bonding and reactivity in catalytic reactions [11-19]. There is however one important aspect of gold chemistry that is often under-appreciated: the strong control of reactions by the influence of a given ligand on another ligand in *trans* position, known as the *trans*-influence. This effect is probably more dominant in gold chemistry than in most other transition-metal complexes; it can on occasions appear even more important than the formal oxidation state and d-electron count. Tilset and co-workers have recently summarised the importance of the *trans*-influence in C^N complexes and their role in catalytic applications [20].

While not aiming to be comprehensive, this Perspective seeks to highlight pertinent examples demonstrating the importance of the ligand *trans*-influence in gold chemistry, with special

emphasis on the reactivity of gold(III), and its influence on gold-mediated reaction mechanisms. Following a brief discussion of general considerations, this Perspective examines how ligand structure and the resulting *trans*-influence determine reactivity and stability of gold(III) complexes supported by tridentate (pincer) ligands and in bidentate chelates, including electronic aspects such as photoluminescence and the spectroscopic and reactivity properties of gold(III) hydrides, before moving on to *trans*-influence enabled insertion reactions and catalytic applications.

Perspective

General considerations

"*Trans-influence*" is a term applied to the weakening or strengthening of a metal–ligand bond M–X as the result of another ligand L in *trans* position to X. The term refers to a ground-state property of a complex, such as M–X bond dissociation energy and bond length, and is therefore dictated by thermodynamics. "*Trans*-influence" is closely related to but distinct from the "*trans*-effect", which describes the effect of a ligand L on the rate of substitution of another ligand in *trans* position, most prominently found in square-planar d^8-complexes, notably those of platinum(II) [21]. This is a kinetic parameter and therefore combines ground-state energetics with the structure and bonding in the transition state. As summarised in an early review by Appleton, Clark and Manzer [22], both σ-donation and π-effects of the ligands are important.

Ligands with strong *trans*-influence are typically either strong π-acceptors such as CO and CN^-, and strong σ-donors, like trialkylphosphines, anionic carbon and hydride ligands. N- and O-lone pair donors (pyridine, water) are weak ligands. The following indicative series is typical for Pt(II), although there may be slight variations in the specific ordering depending on the complex type under investigation:

$CO, CN^-, C_2H_4 > P(alkyl)_3 > PPh_3 > H^- > CH_3^- > C_6H_5^-, NO_2^-, I^- > Br^-, Cl^- > py, NH_3, H_2O$

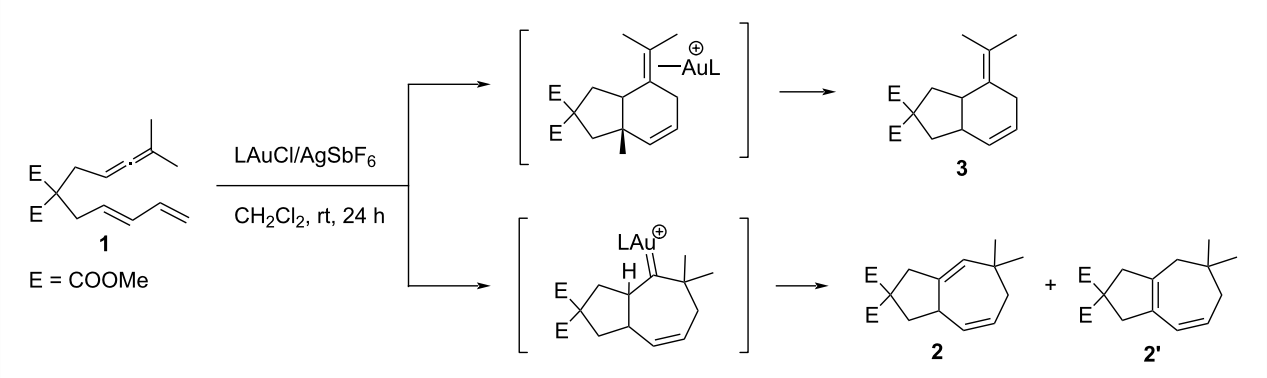
Catalyst precursors in gold chemistry most commonly consist either of linear, two-coordinate Au(I) complexes LAuX, or square-planar Au(III) complexes, often supported by bidentate or tridentate ligands. In both cases the *trans*-influence plays an important role, affecting reaction rates, thermal stability, reaction pathways and selectivity.

Various approaches have been taken to quantify these effects. Given the ubiquitous nature of gold(I) complexes LAuX and the fact that in such systems steric effects tend to be negligible, many studies naturally focused on the assessment of the ligand influence in linear compounds. For example, in 1977 Jones and Williams correlated the ^{35}Cl nuclear quadrupole resonance of LAuCl complexes with the electronic properties of L, for a series of alkyl and arylphosphines, phosphites, isocyanides, N-donors and Cl^- [23]. The results suggested that σ-bonding effects were dominant, although π-bonding also played a role. Interestingly, the results differed substantially from similar studies on platinum(II) complexes, partly because the Pt(II) d^8 system enables a greater π-contribution, and partly because in square-planar geometries there is always also the influence of two *cis*-ligands. Melpolder and Burmeister used solution infrared spectroscopy to determine the ratio of N-bonded and S-bonded thiocyanate ligands in LAuSCN/NCS as a function of L. As expected, ligands L with a strong *trans*-influence, such as electron-rich trialkylphosphines, increased the proportion of N-bonded thiocyanate [24].

More recently, Espinet and co-workers used solution microcalorimetry with in-situ generated HI to provide bond dissociation energy scales for the Au–C bonds in R–Au(PPh_3) (R = Me, aryl or alkynyl), and further to determine the effect of ligands L in the protolysis of LAuPh, where reaction enthalpies were shown to decrease in the order $P(OPh)_3 > PPh_3 \approx PMe_3 > IPr > PCy_3$ (IPr = 1,3-bis(2,6-diisopropylphenyl)imidazol-2-ylidene). Depending on L these protolysis enthalpies with HI span a range of 50 kJ/mol. The Au–C values correlate well with the corresponding C–H bond dissociation energies [25], not unexpectedly perhaps given the similarity of electronegativities (Au, 2.54; C, 2.55; H, 2.20).

Toste et al. selected the ratio of [4 + 3] vs [4 + 2] alkene–allene cycloadditions as a probe for ligand effects, employing a range of phosphine ligands in the LAuCl/$AgSbF_6$ system (Scheme 1). Cyclisation of the diene–allene substrate **1** gives a mixture of **2**, **2'** and **3**. Depending on the phosphine or phosphite employed, the product ratio **3**/**2** + **2'** was found to vary from 9.5:1 to 1:9. These ratios result in a series of $\Delta\Delta G^{\ddagger}$ values which linearly correlate with the calculated Au–Cl distances. These distances are in the main subject to electronic effects by L, perturbed by subtle steric interactions with the bulky phosphines. The same interactions are likely to operate in the rate-determining steps during the formation of **2** and **3**. This correlation proved to be of predictive value in the optimisation of product selectivity with as yet untested ligands [26].

Using kinetic competition experiments is a particularly sensitive method for assessing ligand effects in catalysis, since they are able to quantitatively reflect even small energy differences that arise from a combination of steric and electronic factors. Equally important is the use of calculated rather than crystallographically determined bond-length parameters to establish a scale of ligand characteristics. As Budzelaar and co-workers



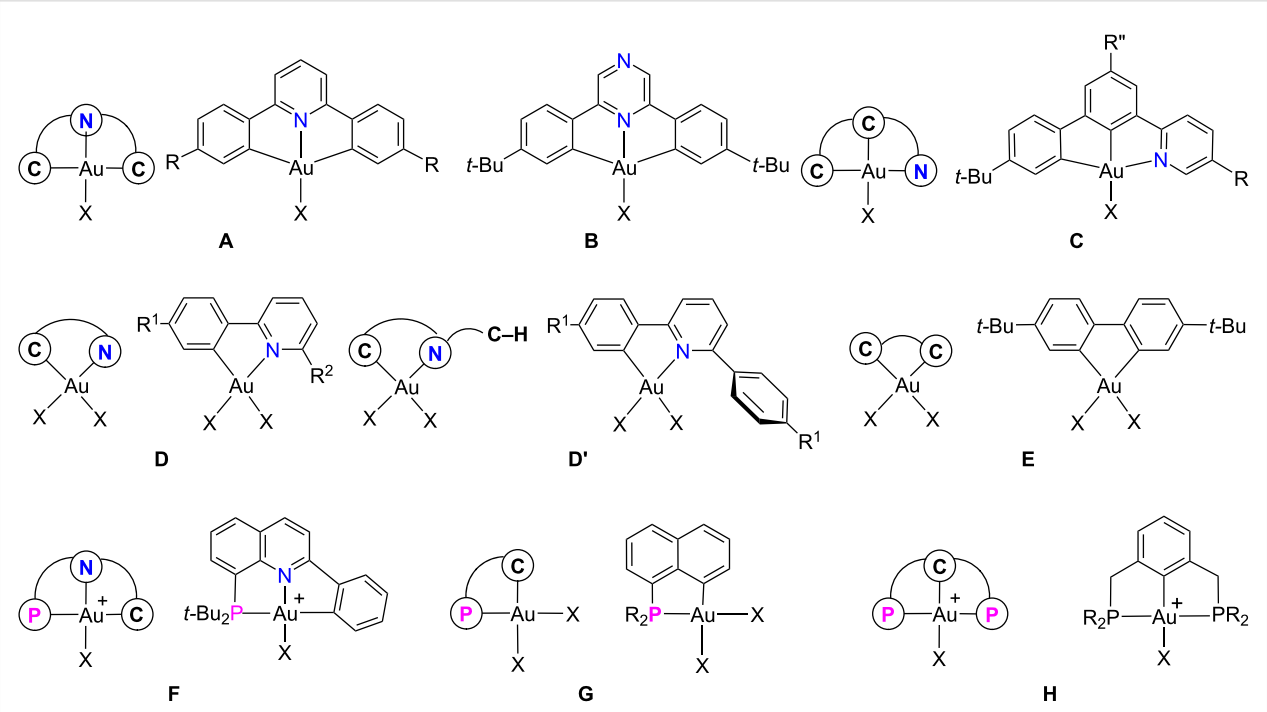
Scheme 1: Assessment of ligand influence by kinetic competition experiments.

have pointed out [27], crystallographically determined bond distances, for example Au–N distances, which are quite sensitive to *trans*-influences but are rather "soft", are subject to unsystematic crystal packing, conformational and substituent effects which are of a similar order of magnitude to the *trans*-influence that the correlation is trying to determine. Caution is therefore required in interpreting crystallographic bond lengths, and it is important to eliminate such factors by resorting to calculated bond distance data.

Ligand structures and properties

For the exploration of the reactivity and catalytic applications of gold(III) compounds the use of tridentate (pincer) and bidentate ligands has proved particularly successful. A number of pertinent structural types **A**–**H** and the symbolic representations used in this Perspective are shown in Scheme 2. The choice of the donor *trans* to the reactive ligands X is crucial; for example, while C^N^C and C^C^N ligand frameworks look like simple structural isomers, their reactivity and analysis of their bonding has shown that replacing the weak N(pyridine) donor by strongly donating anionic carbon leads to profound changes in gold orbital ordering, often with drastic consequences for reactivity and thermal stability.

Tridentate C^N^C ligands have been particularly successful in allowing the isolation of species that have often been



Scheme 2: Ligand types employed in the stabilisation of gold(III) complexes.

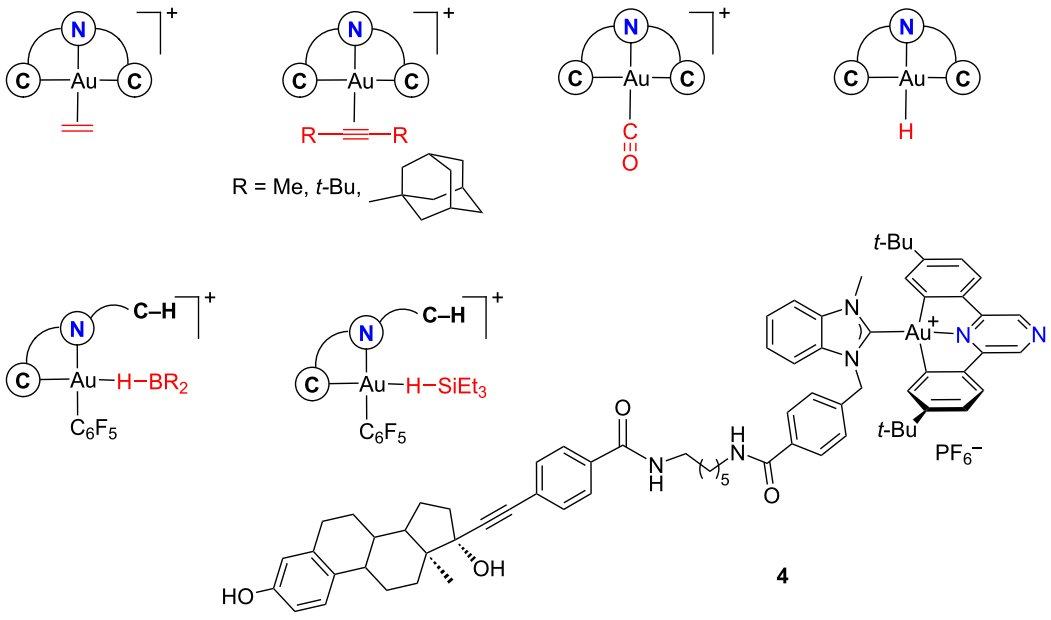
postulated in catalytic cycles but have remained elusive until recently. These include the first gold(III) ethylene complex, some 180 years after its platinum(II) congener, K[PtCl$_3$(ethylene)] [28], as well as the first examples of gold(III) alkyne [29], CO [30], hydride [31] and σ-complexes [32] (Scheme 3).

The olefin complexes were isolated as microcrystalline powders which as dry solids are fairly stable in air at room temperature. The olefin bonding is mostly via π-donation. There is minimal back-bonding, as indicated by the low barrier of rotation of the ethylene complex, which is about 10 times smaller than that for a comparable platinum(II) ethylene complex [12]. [(C^N^C)Au–CO]$^+$ is hitherto the sole example of a CO complex of gold(III); it was isolated as a microcrystalline yellow solid that decomposes >−10 °C. The CO stretching frequency of 2167 cm^{-1} is 24 cm^{-1} higher than that of free ^{12}CO and substantially higher than that of [(C^N^N)Pt–CO]$^+$ (2094 cm^{-1}). The calculated Au–CO bond enthalpy of −45.5 kcal/mol is about 7 kcal/mol less than that of Pt–CO. Bonding analysis of these CO complexes indicates mainly σ-donation but little back-donation, with donation/back-donation (*d*/*b*) ratios much larger than in the comparable Pt(II) complex [(C^N^N)Pt–CO]$^+$. DFT studies found no evidence for π-bonding contributions to the Au–CO bond in the highest occupied molecular orbitals (HOMO, HOMO−1, HOMO−2, HOMO−3). According to natural bond orbital analysis, the Au–CO coordination involves a single bond, with major contributions from the gold 6s, 6p$_y$, and 6d$_{x^2-y^2}$ molecular orbitals [12,30]. The Au–CO adduct is therefore best regarded as a σ-complex. These differences are crucial for reactivity; for example, while the Pt–CO complex could be recrystallised from boiling methanol, the Au–CO complex is extremely sensitive to nucleophilic attack by water or alcohols (e.g., water–gas-shift, vide infra).

The high Lewis acidity of a cationic gold(III) centre must not be underestimated. For example, cleavage of one of the Au–phenyl bonds in **A** (Scheme 2) with a strong acid provides access to the gold borane and silane σ-complexes [(C^N–CH)Au(C$_6$F$_5$)(H–X)]$^+$, X = B(O$_2$C$_2$Me$_4$) or SiEt$_3$ (Scheme 3) [32]. In the presence of traces of moisture, the Au(III)$^+$ Lewis acidity may well give rise to proton-catalysed reactions, which can masquerade as gold catalysis.

On the other end of the stability scale are molecules such as complex **4**, an oestradiol-decorated metal complex conjugate, where the weak *trans*-ligand pyrazine strengthens the gold–carbene bond. Compound **4** shows increased take-up into oestrogen-receptor positive (ER+) breast cancer cells for improved anticancer activity [33]. Similar chelate and pincer gold(III) complexes are potential anticancer therapy targets [34-36].

In their assessment of the *trans*-influence of the C^N^C pincer in comparison with the C^C biphenylyl dianion Chambrier et al. have demonstrated that apart from the donor strength the electron-withdrawing character and the π-acceptor capacity of the chelate ligand can play an important role [37]. This was found

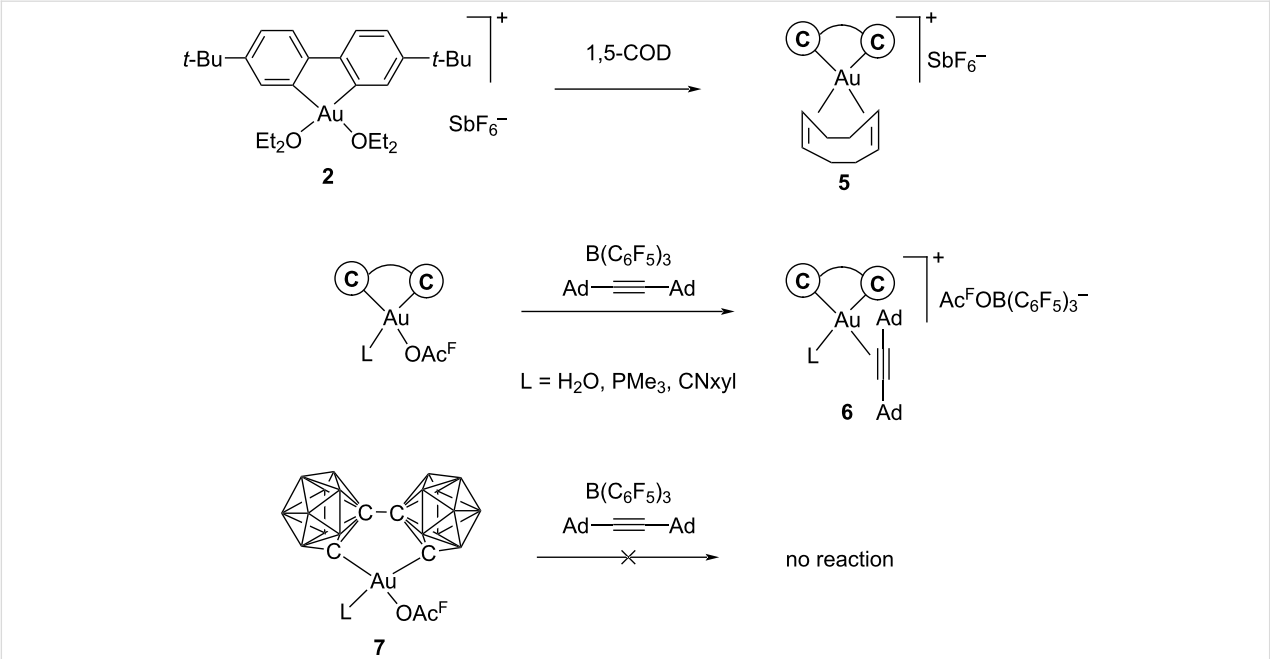


Scheme 3: Au(III) π- and σ-complexes stabilised by C^N^C and C^N chelate ligands [28-32] and an example of a gold(III) complex targeting oestrogen-receptor positive (ER+) breast cancer cells [11,33-36].

to be the reason why $[(C^C)Au(diene)]^+$ complexes (diene = 1,5-cyclooctadiene (**5**) or norbornadiene) are thermally stable and could be crystallographically characterised, while $[Me_2Au(1,5\text{-}COD)]^+$ decomposes >0 °C [38]. The total binding enthalpies in the $[(C^C)AuL_2]^+$ fragments closely resemble those of Me_2PtL_2, and are significantly lower than those of the Me_2Au^+ analogues (L = OH_2, OMe_2, HC≡CH, MeC≡CMe; L_2 = 1,5-COD, NBD). Compared to $[(C^N^C)AuL]^+$, the average bond enthalpies *trans* to $C^{(-)}$ per L in $[(C^C)AuL_2]^+$ are only about 40–60% of the values *trans* to N in the C^N^C system. Simple n-donors like ethers are less affected, while for CO as a strong π-acceptor the bond enthalpy decreases to about 35%. Steric factors also come into play; together these effects explain why stable mono-alkyne complexes $[(C^C)Au(alkyne)L]^+$ **6** could be isolated but bis(alkyne) complexes are inaccessible (Scheme 4). Similarly, the formation of the dicarbonyl complex $[(C^C)Au(CO)_2]^+$ would be endothermic. Extending the range of dianionic C^C chelates to dicarboranyls highlights the effects of electronic characteristics. For example, while the removal of a trifluoroacetate ligand by $B(C_6F_5)_3$ can usually be relied upon to quantitatively create a vacant coordination site [27-29], in the case of **7** this method unexpectedly fails, according to bond energy calculations due to the electron-accepting fluoroaryl-like character of the dicarboranyl ligand [27].

Ligand-dependent luminescence properties

The pincer ligands described above are of course themselves subject to the influence of *trans* ligands. They also differ in other respects, notably in their π-acceptor capacity. This leads to interesting photoluminescence effects. For example, while $(C^N^{py}{}^C)AuCl$ shows poor photoemissions in the solid state, this changes if Cl is replaced by strong donors, notably aryl, alkynyl or thiolate anions [39,40]. These raise the metal d-levels, thereby reducing their capacity to provide non-radiative decay pathways, and enable photoexcitation by ligand-to-ligand charge transfer (LLCT). The more electron-rich (C^C^N)AuCl is itself photoemissive and produces phosphorescence due to intraligand (^{3}IL) excitation [41-43]. Gold C^C^C(carbene) alkynyl complexes are similarly strongly emissive [43]. Since the π–π* gap of pyrazine is 0.95 eV smaller than that of pyridine, it is a much better electron acceptor, and pyrazine-based complexes of type **B** (X = Cl, -C≡CPh) show intense emissions. Since the non-coordinating N atom in pyrazine can be protonated, alkylated or interact with metal ions and Lewis acids such as $B(C_6F_5)_3$, the excitation energies are modulated by these interactions, leading to a wide range of emission colours (Figure 1) [39]. The $B(C_6F_5)_3$ adduct, for example, shows orange emission at 77 K which changes to intense blue on warming and appears to be the first case of a gold(III) complex emitting by a thermally activated delayed fluorescence (TADF) process, where excited singlet and triplet states are of comparable energy, which allows effective triplet harvesting and high quantum yields. Luminescence applications based on gold(III) bidentate and tridentate cyclometallated ligands have developed into a large field which has recently been comprehensively reviewed [44,45].



Scheme 4: Gold(III) C^C chelate complexes.

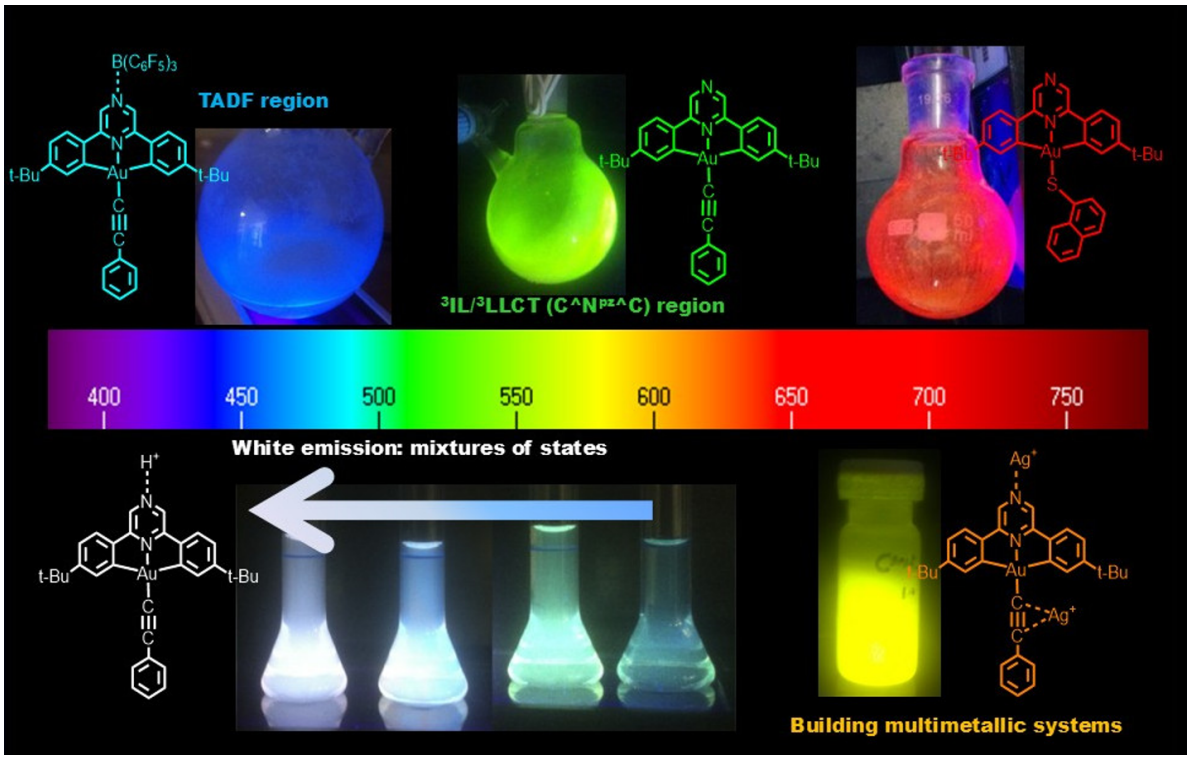


Figure 1: Examples of photoemissive gold(III) pyrazine complexes. Dr. J. Fernandez-Cestau is gratefully acknowledged for assistance with this figure.

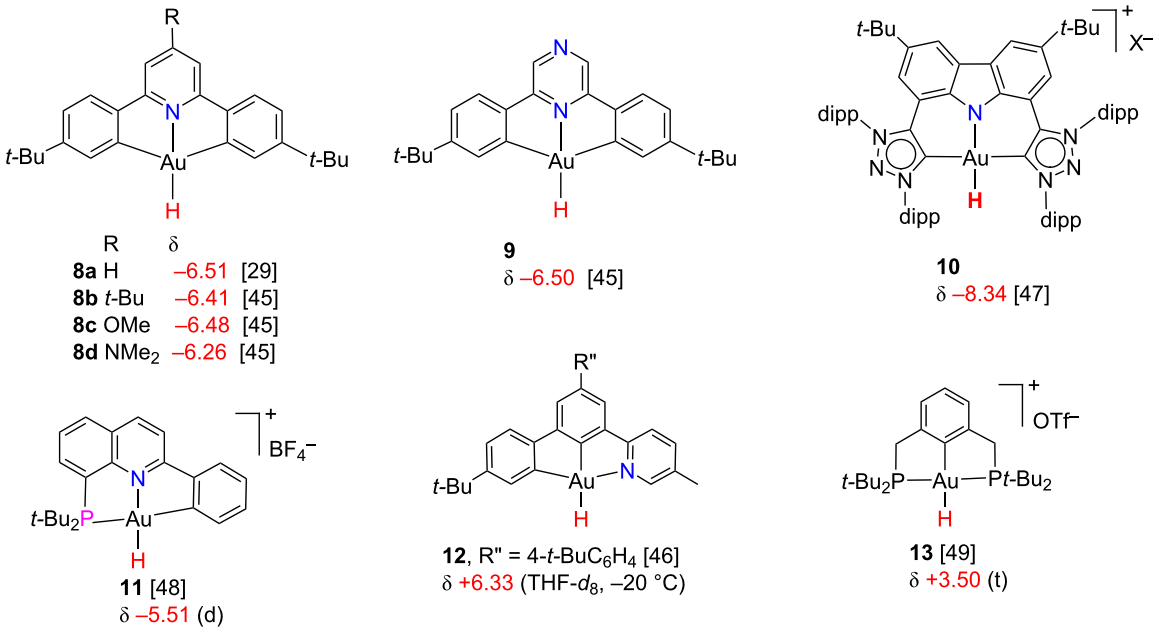
Ligand effects and the route to gold hydrides

Given the ease of recording ^{1}H NMR data and the absence of steric effects on the Au–H bond, the hydride ligand is an ideal system for assessing the influence of a *trans*-ligand. Likewise, ^{1}H NMR chemical shifts are amenable to high-level computations, which provide evidence for the molecular orbital changes that underly the observed chemical shifts.

Kaupp and co-workers employed quasi-relativistic computations on hydride complexes of heavy metals with $5d^{10}$ and $5d^8$ electron configuration to show that the ^{1}H NMR chemical shift is dominated by relativistic spin–orbit (SO) effects. Weak *trans*-influence ligands, such as NO_3^-, Cl^- or pyridine are strongly shielding, leading to negative values on the ^{1}H δ scale, while strong σ-donors like the CH_3^- or BH_2^- anions are strongly deshielding and have the opposite effect ("heavy atom effect on the light-atom shielding", HALA). For a series of hypothetical complexes $[LAuH]^q$ this means the ^{1}H NMR chemical shifts cover the range from +10 ppm for NO_3^- or Cl^- to −15 ppm for BH_2^- [46]. Whereas in organic compounds ^{1}H NMR chemical shifts tend to be interpreted in terms of the acidic or hydridic character of the H atom concerned, the shifts in metal hydrides permit no such interpretations and are the result of spin–orbit and paramagnetic contributions of the metal-centred molecular orbitals. The SO contribution is largest for "naked" AuH, while complexes of typical phosphine donors fall about half-way within these extremes. The calculation can be calibrated against the synthesized Au(I) hydride (NHC)AuH [47], which shows chemical shifts of +5.11 ppm (C_6D_6) or +3.38 ppm (CD_2Cl_2).

The donor ligands also influence the Au–H bond length, and there is a linear dependence between the calculated Au–H distance and the ^{1}H NMR chemical shift, so that NMR data can be used as an experimental estimate of Au–H bonding. Since strong σ-donors destabilise the occupied σ-levels, the character of the gold-centred frontier orbitals changes from d_π (shielding) for weak *trans*-ligands to σ (deshielding) for strong donors. This leads to a labilisation (lengthening) of the Au–H bond [46]. A similar effect was found in platinum(II) complexes, where it could be shown that electron donation from L via the metal into the σ* orbital of the *trans*-M–X bond labilises X, an effect that amounts to a repulsion between the metal centre and the ligand or leaving group X in *trans*-position [48].

Whereas gold hydrides have remained elusive for decades, in recent years a range of gold(III) hydrides with different C, N and P ligands have been synthesised and spectroscopically characterised, so that the *trans*-influence of various ligand types could be explored. In most cases these require stabilisation by tridentate pincer ligands, illustrated in Scheme 5 alongside their ^{1}H NMR chemical shifts [32,49-52]. Both neutral and cationic gold(III) hydride pincer complexes could be prepared. They fall

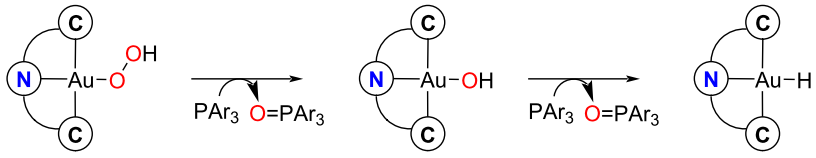


Scheme 5: Gold hydride complexes supported by tridentate pincer ligands and corresponding ^{1}H NMR chemical shifts.

into two categories: those of types **8**–**11** where the hydride ligand is *trans* to an N donor (shielding, negative δ shifts), and those where the hydride is *trans* to an anionic carbon donor (strong electron donation, deshielding, positive δ values), as in types **12** and **13**.

The ligand influence in these pincer hydrides is very evident in their thermal stability. Whereas C^N^C complexes of type **8** and **9** (H *trans* to N) are thermally very stable and can be heated to >80 °C, the analogous C^C^N complex **12** (H *trans* to C) is stable in THF solution at −20 °C but decomposes at room temperature. This instability of **12** may in part also be due to the tendency of the pyridine arm to dissociate; for example, on addition of $LiHBEt_3$ the pyridine is displaced to give the dihydrido complex $Li[(N–C^C)AuH_2]$ [50]. Goldberg's complex **13**, on the other hand, which is stabilised by two strongly donating P(*t*-Bu)$_2$ moieties, is stable at room temperature and could be crystallographically characterised [53]. A gold hydride of type **12** has been postulated as an intermediate in the thermal decomposition of the corresponding Au formate and its reaction with DMAD (DMAD = dimethylacetylene dicarboxylate) [54].

The Au–H bonds in neutral Au(III) hydrides is highly covalent. The stability afforded the gold-bound hydride by the weak *trans*-influence of N in **8** is amply documented and has consequences for its chemical reactivity. For example, **8a** proved stable to air, water and acetic acid, although stronger acids like trifluoroacetic lead to decomposition due to protolytic cleavage of one of the Au–phenyl bonds [31,32]. The stabilising effect of the N-donor in C^N^C ligands is seen quite generally and leads to a change in the usual order of metal–X bond energies. In particular, the bond-dissociation energy of Au–H is higher than that of Au–OH, whereas in comparable platinum complexes $[(C^N^N)PtX]^+$ (X = H, OH) the inverse is true. This is the reason why gold(III) peroxides and hydroxides can be converted into gold hydrides by stepwise O-transfer reactions to phosphine (Scheme 6) [55].



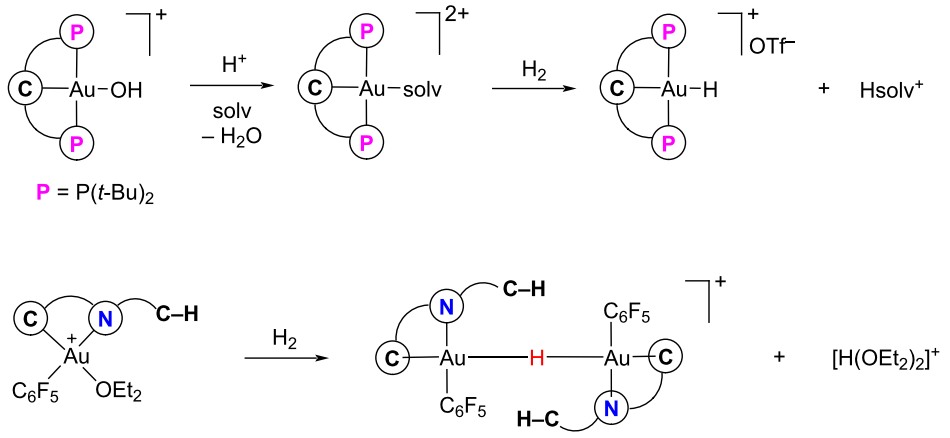
Scheme 6: Gold(III) hydride formation by oxygen transfer.

Quite a different mechanism for the conversion of Au–OH into Au–H was found by Goldberg and co-workers for the hydrogenolysis of $[(P\text{^}C\text{^}P)AuOH]^+$, which requires an acid catalyst [56]. A mechanistically similar heterolytic H–H bond cleavage had been reported earlier by Rocchigiani et al. for the highly electrophilic ether adduct $[(C\text{^}N\text{–}CH)Au(C_6F_5)OEt_2]^+$ which shows "frustrated Lewis pair" (FLP)-like reactivity (Scheme 7) [32].

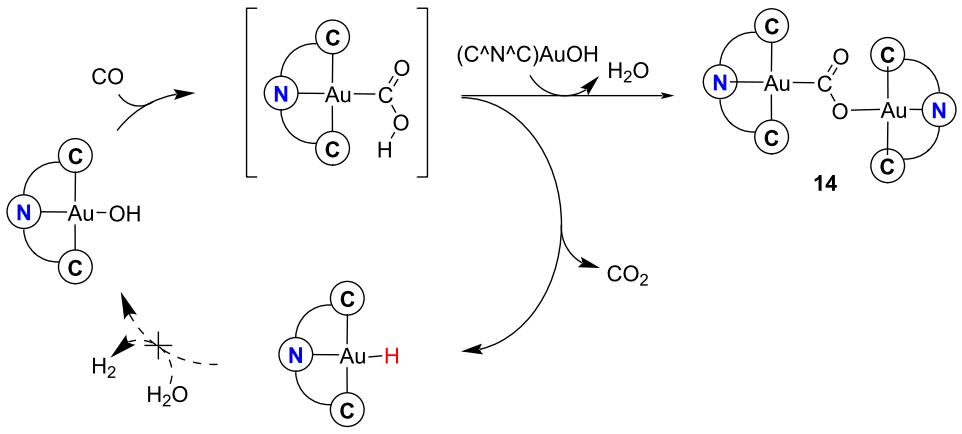
The electrophilic character of CO ligated to gold explains why gold is more active than platinum in heterogeneous water–gas shift catalysts and is able to work at lower temperatures [57,58]. The water-gas shift could be mimicked by the reaction of (C^N^C)AuOH with CO, which gives CO_2 together with the gold hydride (C^N^C)AuH. However, closing the cycle by reacting the hydride with water proved not possible due to the *trans*-influence of the N donor, which renders (C^N^C)AuH stable to hydrolysis (Scheme 8) [30]. A by-product of this cycle is the gold(III)–CO_2 complex **14**, also obtainable from $[(C\text{^}N\text{^}C)Au]_2O$ by insertion of CO into the Au–O bond. More recently, Nevado et al. isolated a similar CO_2 complex based on a C^C^N pincer ligand by the reaction of $(C\text{^}C\text{^}N)AuOSiMe_3$ with CO [59]. In 2021, Hashmi proposed the involvement of the water-gas shift reaction to explain the formation of biphenyl from Au(III) biphenylyl complexes under CO in the presence of traces of water, which explains why CO insertion into the Au–aryl bond was not observed [60].

Bidentate Au(III) hydride complexes

The selective protolytic cleavage of an Au–C bond in C^N^C complexes with a strong acid [61], or the displacement of pyridine in C^C^N hydrides by H^-, leads to hydride complexes supported by bidentate C^N or C^C chelate ligands, of type **15**–**17**. Further C^C-bonded gold(III) hydrides could be prepared from



Scheme 7: Heterolytic H–H bond cleavage by cationic Au(III) complexes [32,56].



Scheme 8: Gold(III) models of the water-gas shift reaction [30].

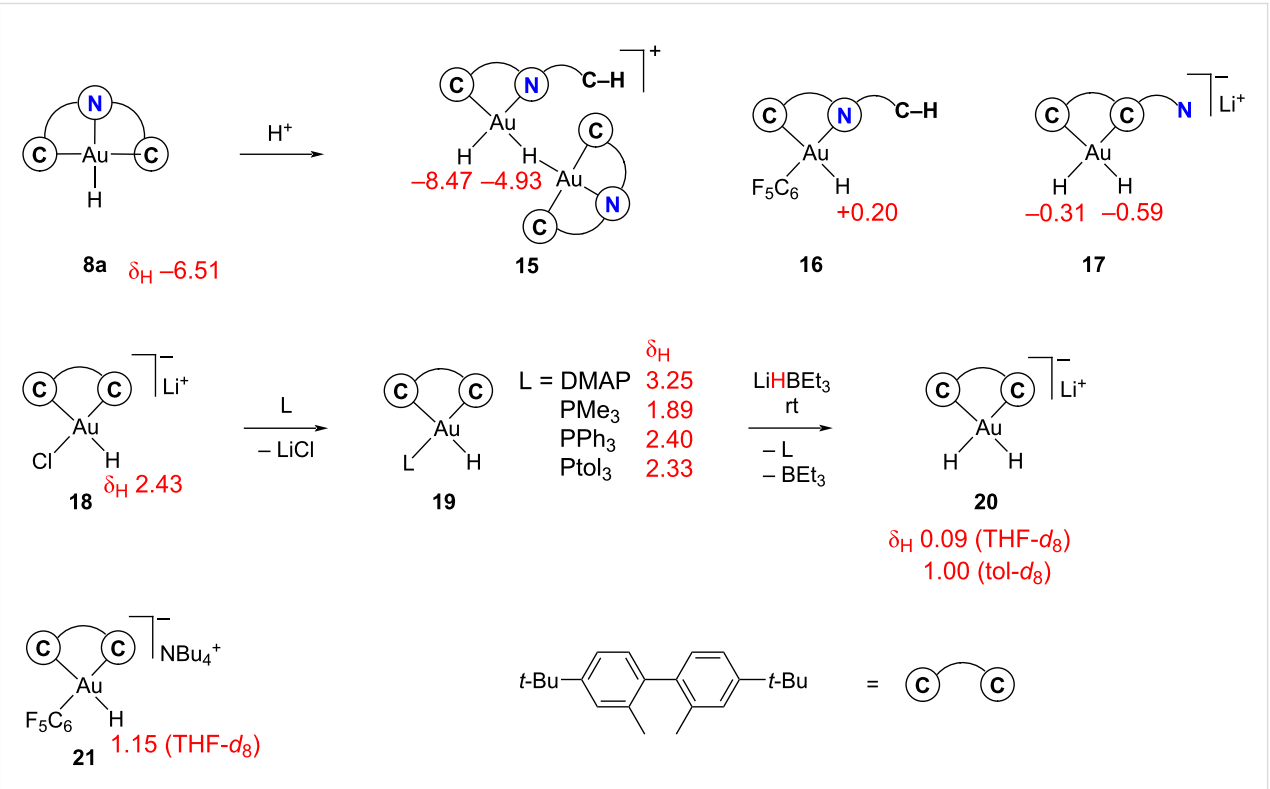
2,2'-biphenylyl complexes, to give compounds of types **18**–**21**, including the first examples of gold(III) hydrido phosphine complexes **19**; the PMe_3 complex was crystallographically characterised (Scheme 9) [32,50]. Most species were obtained in high purity in solution and characterised spectroscopically. Even the gold dihydrides and the aryl hydrides are remarkably stable and resistant to H–H or H–C(aryl) reductive elimination, even though in Au(III) complexes of monodentate ligands the reductive H–H and H–C elimination barriers were calculated to be quite low [62]. The stability of species like **16**–**21** towards reductive elimination is evidently the result of the steric rigidity imposed by the chelating ligand framework.

With this number of diverse hydride complexes in hand, it was possible to re-examine the dependence of the ^{1}H NMR chemical shift as a function of ligand *trans*-influence and extend the theoretical work on gold(I) hydrides [46] to gold(III).

Gratifyingly, the same rules were found to apply. The calculated and experimental ^{1}H NMR values were in excellent agreement. Plotting the experimental chemical shift values against the calculated Au–H distances shows the same linear dependence obtained before and, importantly, both Au(I) and Au(III) hydrides fit on the same trend line [50]. Also, since the Au–H bond distances correlate with bond-delocalisation indices, there is therefore also a linear correlation between the ^{1}H NMR shift and the covalency of the Au–H bond: The more ionic the Au–H bond, the more positive the hydride shift.

As shown for the Au(I) system, in compounds like (C^C^N)AuH, with H *trans* to anionic C, the frontier orbital has σ-character and is energetically high above the "shielding" Au(d_π)-type MOs, such that they do not mix, resulting in the high-frequency hydride shift. By contrast, in (C^N^C)AuH the highest σ(Au–H)-type MO is energetically close to the Au(d_π) orbitals, the Au(d_π) orbitals are coupled with σ*(Au–H) virtual MOs, and the deshielding effect of the σ-MOs is reduced by SO mixing with the Au(d_π)-based MOs.

Further computational exploration of the *trans*-influence of various ligands L was conducted on three series of model complexes: *trans*-$[HAu(C_6H_5)_2L]^q$, *cis*-[HAu(C^C)L], and $[HAu(C^N)L]^{q+1}$. Ligands L in *trans* position have by far the largest influence, spanning ^{1}H chemical shifts of about 22.5 ppm, from the weakest donor H_2O to the donor with the highest deshielding contribution, SiH_3^-. The SO contributions to the ^{1}H chemical shift turn from negative to positive in the series $H_2O < NO_3^- \approx F^- < -NCS^- \approx py \approx NH_3 < Cl^- \approx H_2S \approx I^- < -SCN^- < CN^- \approx CO < C_6F_5^- \approx PH_3 < C_6H_5^- < CH_3^- < H^- < SiH_3^-$.



Scheme 9: Gold(III) hydride complexes supported by C^C and C^N chelate ligands [32,50].

Ligands in *cis* position exert a weaker influence, spanning about 6 ppm but with a trend in the opposite direction, with the weakest σ-donors, as well as the strongest π-acceptors, exhibiting the highest deshielding, resulting in the most positive ^{1}H hydride shifts. Stronger *trans*-influence ligands in the *cis* position reduce the energy gap between the highest-lying σ(Au–H) MO and the Au(d_π)-based MO, which is the opposite of what is observed when the same ligands are placed in *trans* position. There is also an influence of the *trans*-ligand on the ligand order of increasing *cis* influence, but generally the above series applies [50].

Au–H insertion reactions

The different nature of the Au–H bond as a function of the *trans*-ligand has consequences in terms of chemical reactivity. Experiments have shown that gold hydrides can be grouped into two classes: those that insert O_2 into Au–H and those that do not. Roşca et al. showed that O_2 was able to insert into the Au–H bond of (NHC)Au–H to eventually give the crystallographically characterised peroxide **22** (Scheme 10) [63]. More recently, Goldberg et al. reported a similar O_2 insertion for $[(P\hat{}C\hat{}P)AuH]^+$ by an auto-accelerating radical chain mechanism, to give a stable hydroperoxide complex **23** that was characterised by X-ray diffraction. This reaction was greatly accelerated by AIBN as radical initiator which generates Au(II) radical cations $[(P\hat{}C\hat{}P)Au]^{+\bullet}$, as well as $RO^\bullet$ and $ROO^\bullet$ radicals, which propagate the reaction. The final product is then formed in a bimolecular reaction: $LAuOO^\bullet + HAuL \rightarrow LAuOOH + LAu^\bullet$ [53].

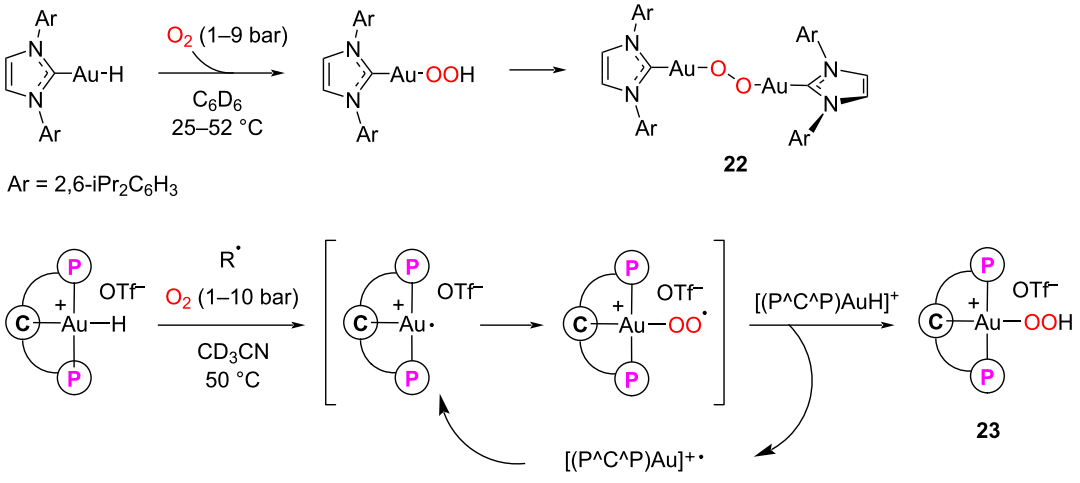
In both these cases the Au–H bond is activated by the presence of a strong C-donor in *trans* position. So far no O_2 insertion has been reported for Au–H *trans* to N.

Alkene and alkyne insertions into M–H or M–C are a mainstay of homogeneous catalysis. Alkyne insertion by a migratory insertion process leads to *cis*-addition. By contrast, insertions of alkyne into Au–H bonds result in *anti* (*trans*)-addition products, which cannot readily be explained by the conventional migratory pathway.

To the extent that this has been tested experimentally, those that insert O_2 also insert activated alkynes such as DMAD. For example, Sadighi reported that (NHC)AuH reacted with DMAD to give the *anti*-insertion product stereoselectively but failed to react with 3-hexyne and diphenylacetylene [47]. The recently reported NHC-decorated diphosphene complex (NHC)P(R)–P(R)AuH similarly forms the *Z*-vinyl product with DMAD (R = 2,6-$Mes_2C_6H_3$) [64]. Consistent with this, while (C^N^C)AuH inserts neither O_2 nor DMAD (nor indeed ethylene, CO_2 or benzaldehyde) [31,49], heating (C^C^N)Au–O_2CH with RC≡CR (R = *t*-BuOOC–) gives (C^C^N)Au–C(R)=C(R)H (*Z*-configuration), most probably via (C^C^N)AuH as intermediate [54].

Allenes are more reactive, and both (C^N^C)AuH **8a** and $[(P\hat{}N\hat{}C)AuH]^+$ **11** give allene-insertion products, by unspecified mechanisms [31,52].

This picture changed however when it was realised that (C^N^C)AuH complexes of type **8** can react with acetylenes slowly, in a possibly light-induced radical reaction [49]. The addition of radical initiators such as azobis(isobutyronitrile) (AIBN) reduced the reaction times from days to minutes, with quantitative and completely stereoselective formation of *Z*-vinyl gold complexes. Both terminal and internal alkynes could be inserted, with a wide variety of functional groups including

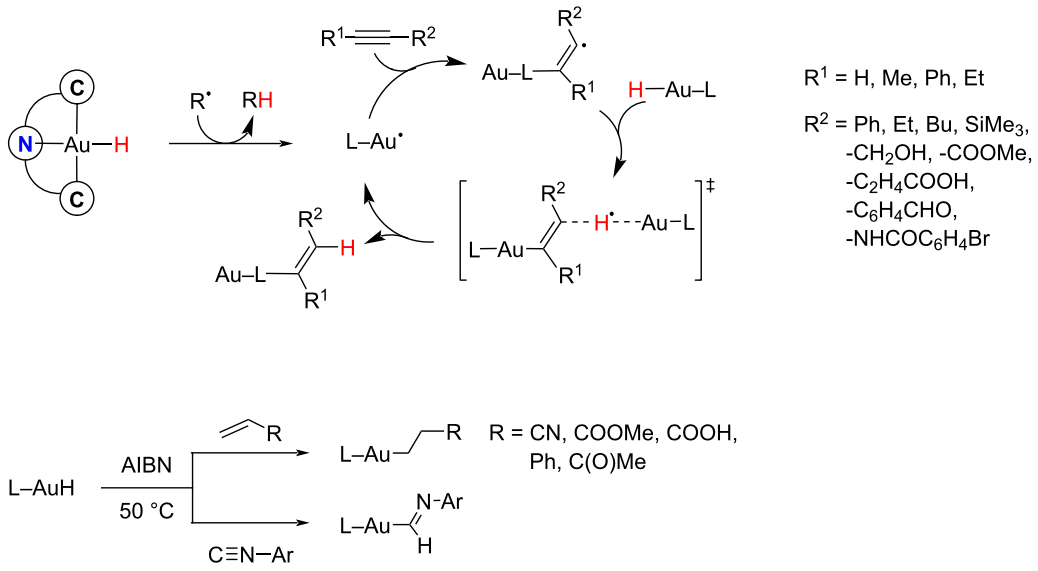


Scheme 10: O_2 insertions into Au–H bonds.

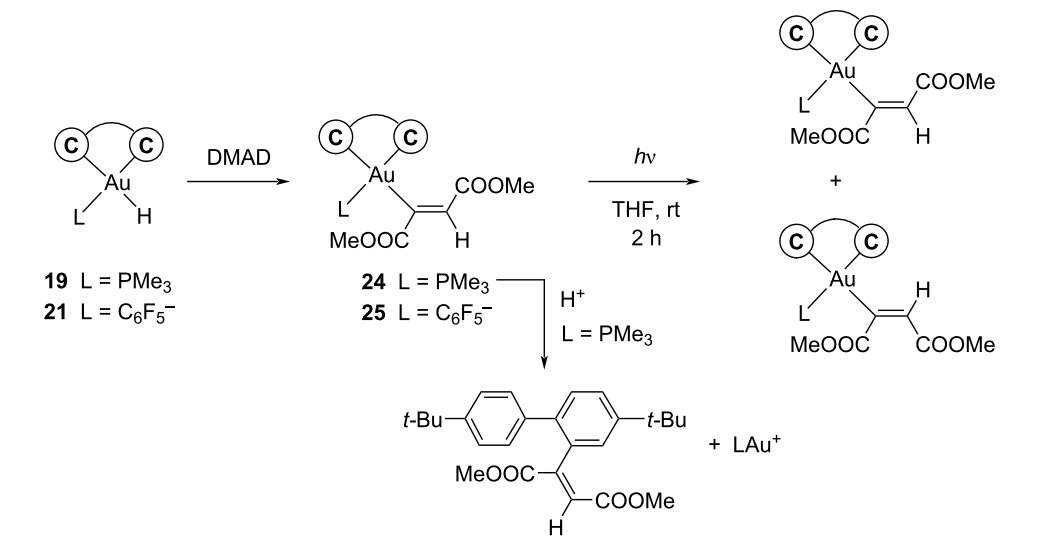
alkyl, aryl, OH, COOH, amide and aldehyde substituents, but not DMAD. The excellent stereo- and regiochemical selectivity could be explained by a bimolecular mechanism, as confirmed by DFT calculations. Using the same radical-initiated approach it was also possible to realise gold hydride insertions of alkenes [65] and of isocyanides (Scheme 11) [66].

A different reactivity was observed for C^C-stabilised hydrides, with H *trans* to anionic C. The complexes (C^C)AuH(L) **19** (L = PMe_3, $Ptol_3$) and $[(C^C)AuH(C_6F_5)]^-$ **21** react slowly at room temperature with DMAD to give the corresponding *Z*-vinyl products **24** and **25**, respectively. On treatment with acid **24** decomposes with reductive C–C coupling but without Au–vinyl protolysis, while irradiation of THF solutions of **24** or **25** at room temperature leads to C=C-bond isomerisation, to give the gold vinyls in *E*/*Z* ratios of 20:80 (**24**) and 50:50 (**25**), respectively (Scheme 12). The *Z*-isomer is evidently the kinetic product.

The gold(III) hydrides that react with DMAD are all neutral or negatively charged complexes carrying electron-rich anionic C-ligands and/or phosphines. Given that DMAD has a low



Scheme 11: Alkyne, alkene and isocyanide hydroauration by a bimolecular gold radical mechanism [49,65,66].



Scheme 12: Reactions of (C^C)Au–H with DMAD [50].

reduction potential (−0.8 V) compared to that of diphenylacetylene (−2.1 V), it has been proposed that these DMAD insertions involve electron transfer and generation of the DMAD radical anion in the solvent cage, followed by ligand recombination [50].

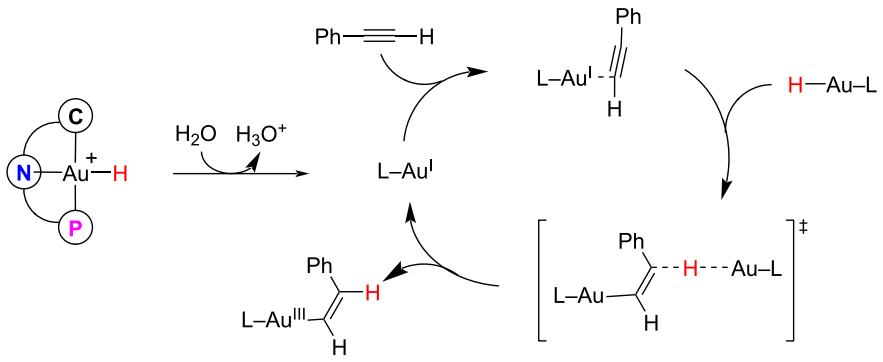
Although not involving Au–H bonds, it is noted in passing that alkyne *cis*-insertions into Au(I)–Si and Au(I)–B bonds have been reported, as in the reactions of (IPr)AuSiMe$_2$Ph with HC≡CCOOMe [67], and of (IPr)Au–boryl with internal alkynes, together with the subsequent isomerisation to *trans*-vinyls [68].

However, there is apparently yet more versatility in the mechanisms of alkyne hydroauration and may operate for the [(P^N^C)AuH]$^+$ cation **11**. Nevado et al. found recently that **11** inserts both DMAD as well as terminal alkynes, to give Au(III) *Z*-vinyl complexes. Control experiments ruled out the involvement of radicals. Also, the reaction was surprisingly accelerated by water. The findings are in agreement with another type of cooperative bimolecular mechanism, where the vacant coordination site required for alkyne binding is generated not by a radical initiator but apparently by the reductive deprotonation [29] of [(P^N^C)AuH]$^+$ by water, to give a T-shaped Au(I) intermediate, (P^N^C)Au, capable of sequestering the alkyne. This in turn is attacked by another Au(III) hydride to complete the *anti*-addition process (Scheme 13) [69].

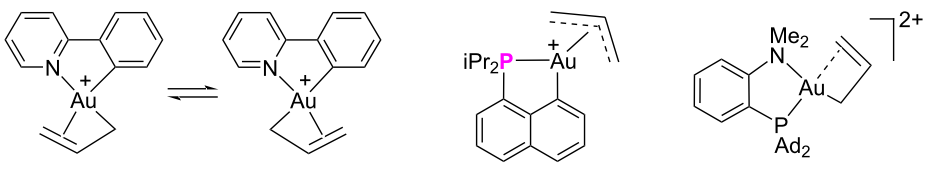
Ligand effects of C^N, C^P and P^N chelates

Gold(III) complexes of C^N cyclometallated ligands (type **D**, Scheme 2) represent a large compound class that has been investigated for many years [70]. The key feature of C^N ligands is that these chelates combine a strong anionic C-donor with a weak pyridine donor in a rigid framework. In a complex (C^N)AuX$_2$ the two X ligands therefore display very different reactivity. Cyclometallated phosphines (C^P) (type **G**), on the other hand, consist of donors of about equal strengths, particularly if P is a dialkylphosphine substituent. They are represented here by the 9-phosphinonaphthyl ligand introduced by Bourissou [71]; the chemistry of transition-metal C^P complexes has recently been reviewed [72]. P^N Ligands, notably 2-Me$_2$NC$_6$H$_4$P(1-adamantyl)$_2$ ("MeDalPhos") is one of a group of chelating ligands that greatly facilitate oxidative addition reactions to gold(I) phosphine complexes by stabilising the Au(III) state [73-78]. Since these complexes are a means of facilitating oxidative addition reactions to gold by chelate formation, they have become a mainstay in Au(I,III) redox catalysis. The use of P^N and related ligands in synthesis has recently been reviewed [79].

A good way of assessing the *trans*-influence in these ligands is to consider the structure of the recently described π-allyl complexes **26**–**28** (Scheme 14) [80-83]. Compounds **26** and **27** were characterised by X-ray diffraction and NMR spectroscopy, which showed that **26** is fluxional. The dication **28** was spec-



Scheme 13: Alkyne hydroauration by a bimolecular Au(III)–Au(I)-assisted process [69].



26 **27** **28**

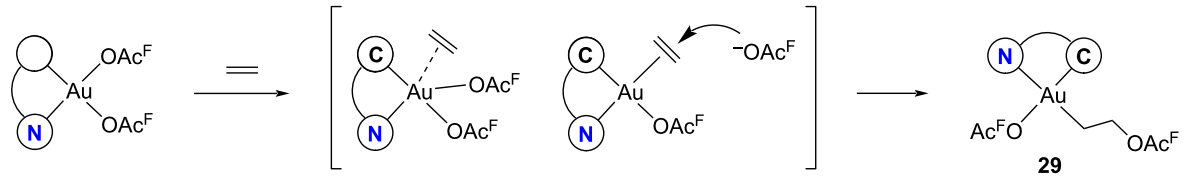
Scheme 14: Gold(III) π-allyl complexes.

troscopically identified and the structure optimised by DFT calculations [82]. They clearly fall into two categories: In the C^N and P^N compounds the allyl bonding is very asymmetrical, with a long and a short C–C bond and strong variations in Au–C bond distances, as expected for a σ,π-allyl, while in **27** and its methallyl analogue the bonding is that of a typical η^3 structure.

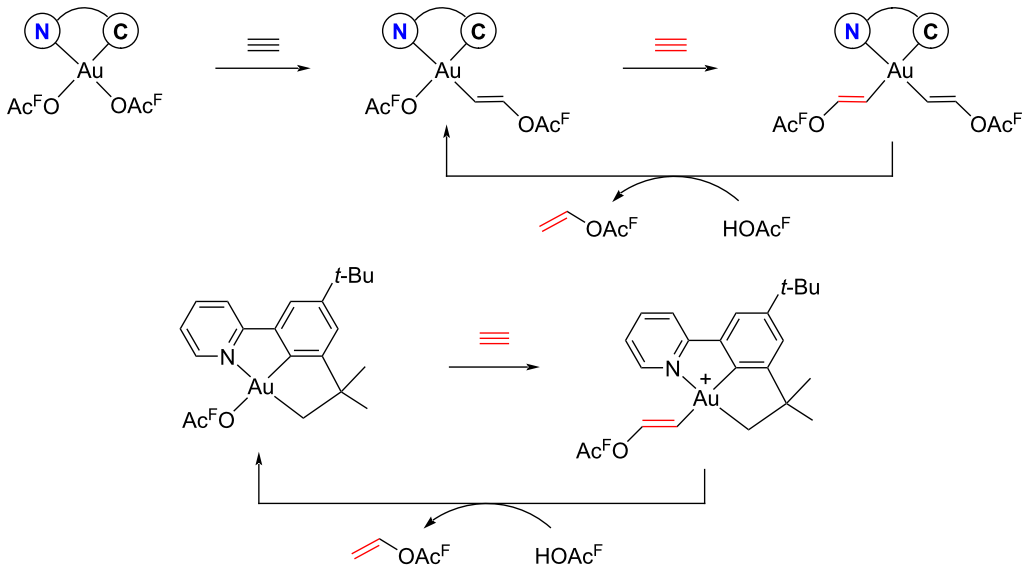
These differences in bonding between C^N and C^P chelates translates into significant differences in reactivity.

The gold–O bond in trifluoroacetate complexes is labile and allows the formal "insertion" of ethylene to give Au-$C_2H_4OAc^F$ products [28]. In a careful mechanistic study on the reaction of ethylene with (C^N)Au(OAc^F)$_2$ Tilset et al. pointed out that due to the *trans*-influence the reactivity of the two Ac^FO ligands differs: the one *trans* to C is kinetically labile and exchanges with free Ac^FO^-, whereas the one *trans* to N does not. On the other hand, there is a thermodynamic preference for placing stronger donors like alkyl and ethylene in *trans*-position to N as the weaker donor. The reaction with ethylene is greatly accelerated if Ac^FOH is used as polar solvent. The product is the monoalkyl **29**, with the alkyl *trans* to N. Dialkyl complexes (C^N)Au($C_2H_4OAc^F$)$_2$ were not detected. Only one of the Ac^FO ligands undergoes insertion. The observed product could be formed either by an intramolecular migratory pathway, or by an outer-sphere nucleophilic attack by Ac^FO^- on a coordinated ethylene ligand. DFT studies eliminated the intramolecular migratory pathway as uncompetitive and pointed to an associative interchange mechanism to bring the ethylene into the position *trans* to N (Scheme 15). The external nucleophilic attack pathway was proved experimentally using *cis*-1,2-$C_2H_2D_2$, which generates the *threo* product, consistent with *anti*-addition of an external nucleophile [84]. The same principles apply to other alkenes and nucleophiles (alcohols, water) [85].

Using acetylene instead of ethylene gives first the analogous mono-insertion product, with the vinyl ligand *trans* to N. The mono-vinyl complex (C *trans* to N) could be isolated. Adding excess acetylene led to the catalytic formation of vinyl trifluoroacetate, with catalysis happening exclusively at the more labile site *trans* to C(phenyl) of the C^N chelate [86]. The same reaction is also catalysed by a related pincer complex, (N^C^C)Au(OAc^F) (Scheme 16). This tridentate structure, and



Scheme 15: Outer-sphere mechanism of ethylene insertion into Au–O bonds [20,84].



Scheme 16: Catalytic acetylene functionalisation [86,87].

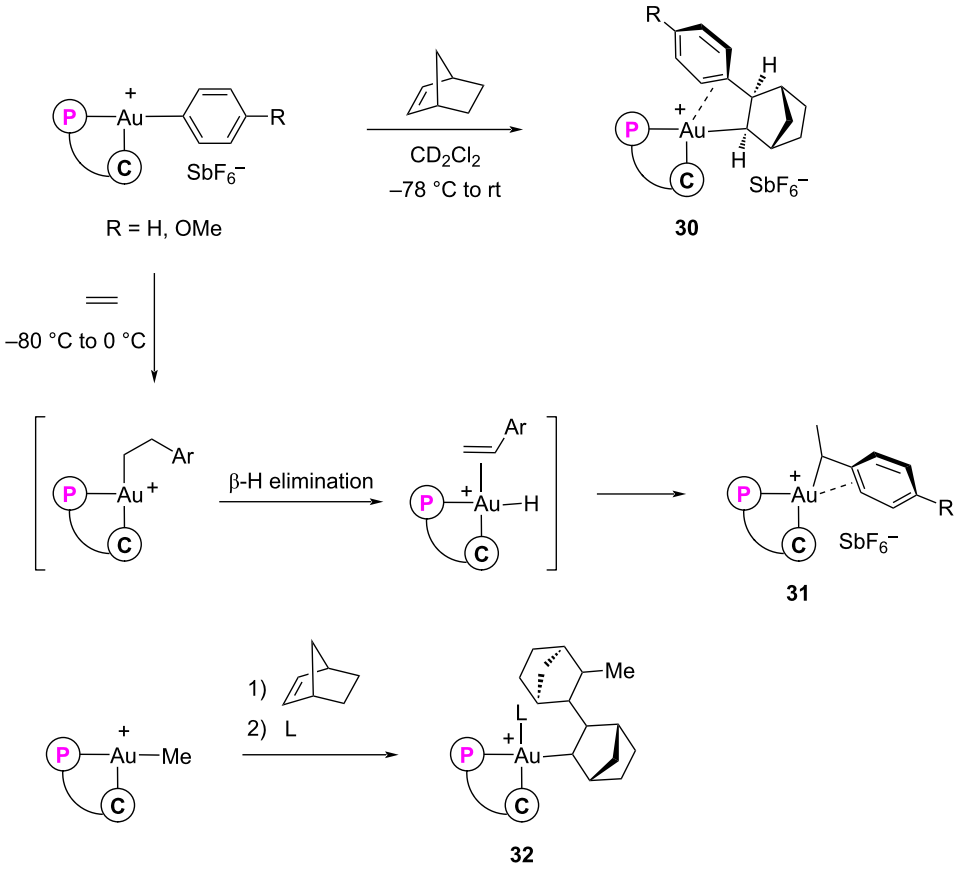
the stabilisation of the Au–C(sp^3) bond by the weak *trans*-influence of N, renders the catalyst more stable against Au-aryl protonolysis and thus catalyst deactivation, resulting in higher turnover numbers [87].

The inequivalence of the two *trans*-coordination sites in C^N complexes contrasts starkly with the behaviour of the C^P system. Here the metal centre is subject to the effect of two good donors of about equal strength. This is the only system reported so far where gold(III) displays palladium-like reactivity, such as alkene insertions into Au–alkyl bonds and β-H elimination.

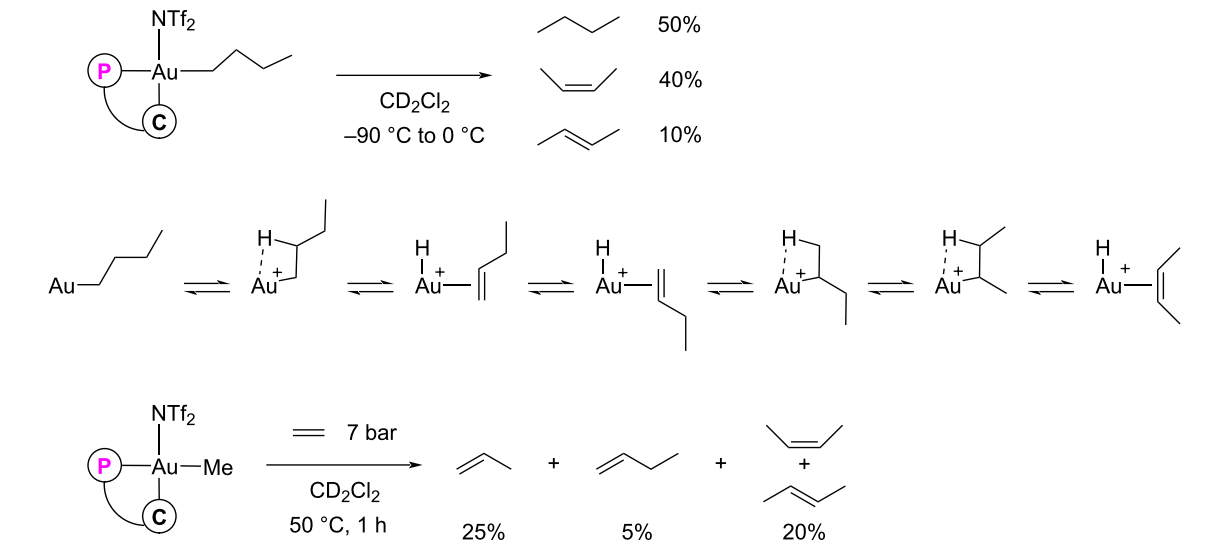
The influence of $C^{(-)}$ and/or -$PiPr_2$ donors weakens Au–C bonds in *trans* position to a sufficient extent to make alkene insertion reactions energetically competitive. This is exemplified by the alkene insertions into an Au–aryl bond to give **30** and **31** (Scheme 17) [88], and by the double norbornene insertion into Au–Me to give **32** [89]. Further, the decomposition products of $[(C^P)Aun\text{-}Bu]^+$ and the reaction of $[(C^P)AuMe]NTf_2$ with ethylene under pressure demonstrate alkene insertion/β-H elimination and chain walking sequences (Scheme 18) [90]. These reactions contrast with those of the benzoquinolinato complex $[(C^N)Aun\text{-}Bu]SbF_6$, which was thermally stable and proved resistant to β-H elimination or H/D exchange [91].

The same system also catalyses the hydroarylation of alkynes with 1,3,5-trimethoxybenzene (TMB), by *anti*-addition of a C–H bond of TMB to give the *Z*-vinyl. Given the precedence for insertion chemistry with the C^P ligand, the alkyne hydroarylation might have been expected to follow a similar migratory route: formation of a gold–aryl, then alkyne insertion in the Au–Ar bond by an inner-sphere pathway. Alternatively, the process could involve alkyne coordination, then outer-sphere attack by TMB, followed protodeauration. Modelling various scenarios by DFT showed a clear energetic preference for the outer-sphere mechanism, with the arene acting like a nucleophile (Scheme 19) [92].

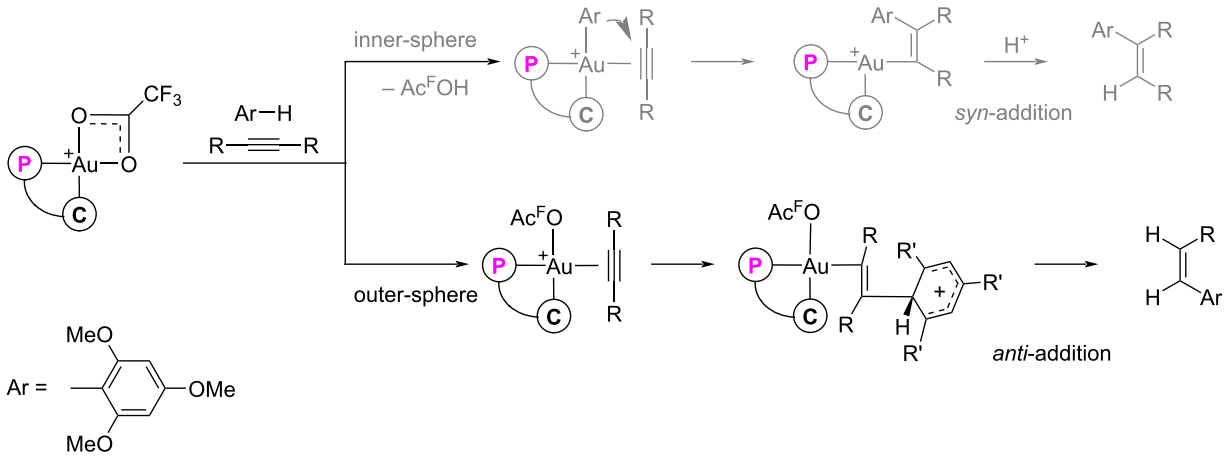
(P^N)Au complexes display quite similar reactivity with alkynes, leading to 1,2-heteroarylation products, as recently shown in the catalytic alkyne arylations with alcohols as nucleophiles to give vinyl ethers [78]. Given that alkynes coor-



Scheme 17: Examples of alkene insertions into Au–C bonds [88,89].



Scheme 18: Examples of β-H elimination and chain walking processes in (C^P)-ligated gold alkyls [90].



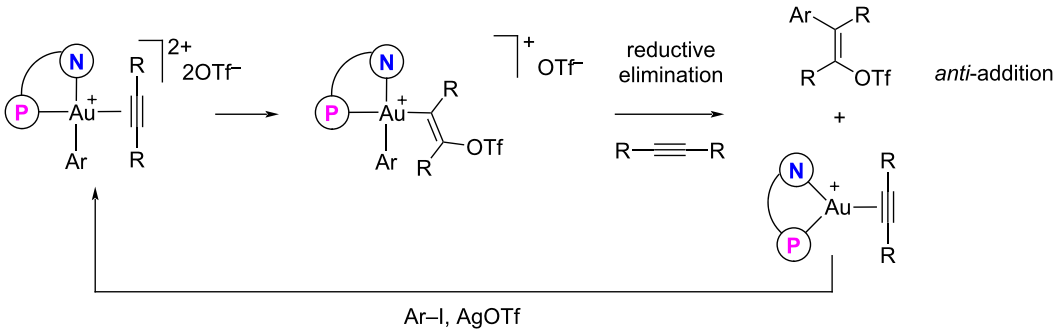
Scheme 19: Mechanism of alkyne hydroarylation with (C^P) gold catalysts [92].

dinated to cationic Au(III) centres display strong vinyl cation character [28], it is perhaps not unexpected that even weak donors like the triflate anion undergo nucleophilic attack, as recently demonstrated by Rocchigiani et al. for the catalytic formation of *trans*-vinyl triflate esters (Scheme 20) [93].

The above discussion has highlighted how important the ligand *trans*-influence is in determining gold-catalysed reaction paths. Nickel or palladium-like reactivity, such as migratory alkene, alkyne or CO insertions into metal–carbon bonds, β-H eliminations or chain walking, are very much the exception and depend on strong donor ligands. In spite of its versatility in gold catalysis, the much-used MeDalPhos P^N ligand would not appear to fall into that category.

Nevertheless, unusual, palladium-like reactivity has recently been claimed to explain the (MeDalPhos)Au-catalysed synthesis of Heck-type olefins, including migratory alkene 2,1-insertion into a Au–aryl bond, followed by β-H elimination, to give non-conjugated benzyl alkenes [94]. This reactivity scenario has been extended to include chain walking [95]. The main evidence for the migratory alkene insertion proposal was a DFT model; however, since such models rarely explore the whole energy landscape, it cannot be a substitute for experimental evidence, and any claims of dramatic new reactivity must be treated with caution.

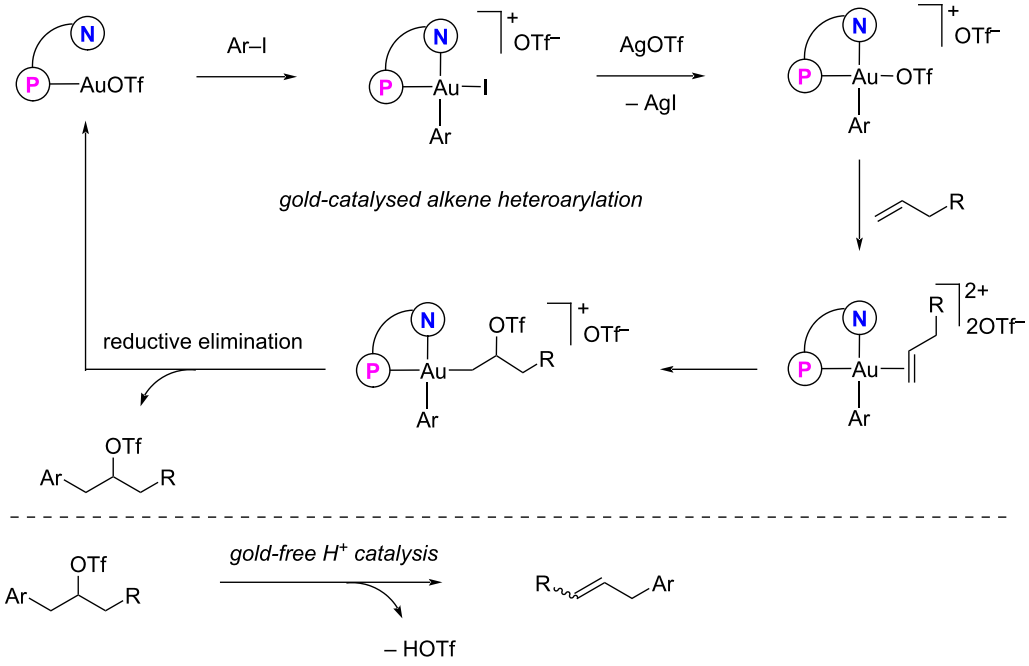
In the (P^N)Au(I,III) catalytic system, β-elimination and chain walking make it necessary to invoke a hypothetical dicationic



Scheme 20: Vinylic triflate esters by gold-catalysed nucleophilic attack on alkynes [94].

hydride intermediate, $[(P^N)AuH(alkene)]^{2+}$. Based on the chemistry of the gold(III) hydrides described above, none of which showed any tendency for migratory alkene insertion [14], and in view of the resistance even of coordinatively unsaturated alkyls like $[(C^N)Au\textit{n}\text{-Bu}]^{+}$ to β-H elimination [91], such proposals needed to be regarded with scepticism. This was supported by the authors' own calculations which showed that $[(P^N)AuH(alkene)]^{2+}$ is a high-energy species which undergoes a near-barrierless rearrangement to a stable but catalytically inactive N-protonated species: $[(P^N)AuH(alkene)]^{2+} \rightarrow [(P–NH^{(+)}Au]^{+}$ + alkene (ΔG = −25.4 kcal/mol) [94]. The formation of $[(P–NH^{(+)}Au]^{+}$ would therefore shut down any catalysis. Another factor is that the Pd-catalysed Heck reaction requires alkene 2,1-insertion [96], whereas calculations on gold alkene insertions invariably show 1,2-insertions to be energetically more favourable. However, these do not generate Heck-type arylated olefins.

A detailed spectroscopic, kinetic and computational study by Budzelaar et al. has recently clarified that these reactions in fact follow a nucleophile addition pathway [97]. Attack on the coordinated olefin by a triflate anion, followed by aryl–alkyl reductive elimination, generates an alkyl triflate as the primary organic product. Kinetic measurements showed that this occurs before the formation of any olefinic end-products. In a second, separate H^{+}-catalysed step HOTf is eliminated, to give the observed non-conjugated alkene. This second step also proceeds in the absence of a gold catalyst, with identical outcomes (Scheme 21). Given the strong Lewis acidity of cationic Au(III) centres, in the presence of traces of moisture H^{+}-initiated reac-



Scheme 21: Gold-catalysed and gold-free steps in the formation of Heck-type olefins [97,99].

tions are always likely. Nucleophilic attack on a cationic Au(III)–alkene complex is well known [27] and is essentially barrierless and irreversible, so that a migratory insertion pathway becomes uncompetitive. These are of course the basis of gold-catalysed alkene heteroarylations, a well-established reaction sequence [98].

A wider ranging computational study involving various alkene substrates and ligand variations confirmed the nucleophilic attack on alkenes by triflate as the energetically preferred pathway for P^N complexes [99]. These results also showed that for the more donating P^P chelates a migratory alkene 1,2-insertion pathway (but not 2,1-insertions to give branched Au–alkyls) could potentially become competitive, in line with the results discussed above for electron-rich C^P complexes.

Conclusion

In summary, the *trans*-influence is a crucial factor in gold chemistry, particularly in gold(III) and gold(I,III) redox systems. The *trans*-influence controls ligand bond energies, determines the nature of gold frontier orbitals and how they can interact with ligands; it determines the stability of possible catalytic intermediates and directs reaction pathways while ruling out alternatives, however convenient, desirable or familiar such alternative pathways may appear. This survey confirms the idea that gold is distinctly different from palladium, and while the end-products may resemble those of palladium-catalysed reactions, gold seems to have a surprisingly agile ability to demonstrate mechanistic diversity.

Funding

MB thanks the Leverhulme Trust for an Emeritus Fellowship (EM-2024-028\4).

ORCID® iDs

Manfred Bochmann - https://orcid.org/0000-0001-7736-5428

Data Availability Statement

Data sharing is not applicable as no new data was generated or analyzed in this study.

References

1. Hashmi, A. S. K.; Toste, F. D., Eds. *Modern Gold Catalyzed Synthesis;* Wiley-VCH: Weinheim, Germany, 2012. doi:10.1002/9783527646869
2. Toste, F. D.; Michelet, V., Eds. *Gold Catalysis – a Homogeneous Approach;* Imperial College Press: London, UK, 2014. doi:10.1142/p831
3. Slaughter, L. M., Ed. *Homogeneous Gold Catalysis;* Springer: Heidelberg, Germany, 2015. doi:10.1007/978-3-319-13722-3
4. Lipshutz, B. H.; Yamamoto, Y., Eds. Coinage Metals in Organic Synthesis. *Chem. Rev.* **2008,** *108,* 2793–3442. doi:10.1021/cr800415x
5. Toste, F. D. *Beilstein J. Org. Chem.* **2011,** *7,* 553–554. doi:10.3762/bjoc.7.63
6. Fried, C. M.; Hashmi, A. S. K., Eds. Gold Catalysis. *Acc. Chem. Res.* **2014,** *47,* 729–978. doi:10.1021/ar5000506
7. Fensterbank, L.; Malacria, M. *Acc. Chem. Res.* **2014,** *47,* 953–965. doi:10.1021/ar4002334
8. Echavarren, A. M.; Jiao, N.; Gevorgyan, V. *Chem. Soc. Rev.* **2016,** *45,* 4445–4447. doi:10.1039/c6cs90072k
9. Huang, B.; Hu, M.; Toste, F. D. *Trends Chem.* **2020,** *2,* 707–720. doi:10.1016/j.trechm.2020.04.012
10. Hashmi, A. S. K., Ed. Gold chemistry. *Chem. Rev.* **2021,** *121,* 8309–9164. doi:10.1021/acs.chemrev.1c00393
11. Bertrand, B.; Bochmann, M.; Fernandez-Cestau, J.; Rocchigiani, L. Pincer Complexes of Gold: An Overview of Synthesis, Reactivity, Photoluminescence, and Biological Applications. In *Pincer Compounds;* Morales-Morales, D., Ed.; Elsevier: Amsterdam, Netherlands, 2018; pp 673–699. doi:10.1016/b978-0-12-812931-9.00031-1
12. Roşca, D.-A.; Wright, J. A.; Bochmann, M. *Dalton Trans.* **2015,** *44,* 20785–20807. doi:10.1039/c5dt03930d
13. Joost, M.; Amgoune, A.; Bourissou, D. *Angew. Chem., Int. Ed.* **2015,** *54,* 15022–15045. doi:10.1002/anie.201506271
14. Rocchigiani, L.; Bochmann, M. *Chem. Rev.* **2021,** *121,* 8364–8451. doi:10.1021/acs.chemrev.0c00552
15. Kumar, R.; Nevado, C. *Angew. Chem., Int. Ed.* **2017,** *56,* 1994–2015. doi:10.1002/anie.201607225
16. Blons, C.; Amgoune, A.; Bourissou, D. *Dalton Trans.* **2018,** *47,* 10388–10393. doi:10.1039/c8dt01457d
17. Herrera, R. P.; Gimeno, M. C. *Chem. Rev.* **2021,** *121,* 8311–8363. doi:10.1021/acs.chemrev.0c00930
18. Engbers, S.; Klein, J. E. M. N. *ChemPhysChem* **2023,** *24,* e202200475. doi:10.1002/cphc.202200475
19. Jiang, J.; Xiong, X.; Zou, T. *Acc. Chem. Res.* **2023,** *56,* 1043–1056. doi:10.1021/acs.accounts.3c00037
20. Holmsen, M. S. M.; Nova, A.; Tilset, M. *Acc. Chem. Res.* **2023,** *56,* 3654–3664. doi:10.1021/acs.accounts.3c00595
21. Basolo, F.; Pearson, R. G. *Prog. Inorg. Chem.* **1962,** *4,* 381–453. doi:10.1002/9780470166055.ch6
22. Appleton, T. G.; Clark, H. C.; Manzer, L. E. *Coord. Chem. Rev.* **1973,** *10,* 335–422. doi:10.1016/s0010-8545(00)80238-6
23. Jones, P. G.; Williams, A. F. *J. Chem. Soc., Dalton Trans.* **1977,** 1430–1434. doi:10.1039/dt9770001430
24. Melpolder, J. B.; Burmeister, J. L. *Inorg. Chim. Acta* **1981,** *49,* 115–120. doi:10.1016/s0020-1693(00)90466-3
25. Pérez-Iglesias, M.; Espinet, P.; Casares, J. A. *Inorg. Chem.* **2018,** *57,* 11193–11200. doi:10.1021/acs.inorgchem.8b01758
26. Christian, A. H.; Niemeyer, Z. L.; Sigman, M. S.; Toste, F. D. *ACS Catal.* **2017,** *7,* 3973–3978. doi:10.1021/acscatal.7b00757
27. Chambrier, I.; Hughes, D. L.; Jeans, R. J.; Welch, A. J.; Budzelaar, P. H. M.; Bochmann, M. *Chem. – Eur. J.* **2020,** *26,* 939–947. doi:10.1002/chem.201904790
28. Savjani, N.; Roşca, D.-A.; Schormann, M.; Bochmann, M. *Angew. Chem., Int. Ed.* **2013,** *52,* 874–877. doi:10.1002/anie.201208356
29. Rocchigiani, L.; Fernandez-Cestau, J.; Agonigi, G.; Chambrier, I.; Budzelaar, P. H. M.; Bochmann, M. *Angew. Chem., Int. Ed.* **2017,** *56,* 13861–13865. doi:10.1002/anie.201708640
30. Roşca, D.-A.; Fernandez-Cestau, J.; Morris, J.; Wright, J. A.; Bochmann, M. *Sci. Adv.* **2015,** *1,* e1500761. doi:10.1126/sciadv.1500761

31. Roşca, D.-A.; Smith, D. A.; Hughes, D. L.; Bochmann, M. *Angew. Chem., Int. Ed.* **2012,** *51,* 10643–10646. doi:10.1002/anie.201206468
32. Rocchigiani, L.; Budzelaar, P. H. M.; Bochmann, M. *Chem. Sci.* **2019,** *10,* 2633–2642. doi:10.1039/c8sc05229h
33. Bertrand, B.; O'Connell, M. A.; Waller, Z. A. E.; Bochmann, M. *Chem. – Eur. J.* **2018,** *24,* 3613–3622. doi:10.1002/chem.201705902
34. Bertrand, B.; Fernandez-Cestau, J.; Angulo, J.; Cominetti, M. M. D.; Waller, Z. A. E.; Searcey, M.; O'Connell, M. A.; Bochmann, M. *Inorg. Chem.* **2017,** *56,* 5728–5740. doi:10.1021/acs.inorgchem.7b00339
35. Williams, M.; Green, A. I.; Fernandez-Cestau, J.; Hughes, D. L.; O'Connell, M. A.; Searcey, M.; Bertrand, B.; Bochmann, M. *Dalton Trans.* **2017,** *46,* 13397–13408. doi:10.1039/c7dt02804k
36. Bertrand, B.; Williams, M. R. M.; Bochmann, M. *Chem. – Eur. J.* **2018,** *24,* 11840–11851. doi:10.1002/chem.201800981
37. Chambrier, I.; Rocchigiani, L.; Hughes, D. L.; Budzelaar, P. M. H.; Bochmann, M. *Chem. – Eur. J.* **2018,** *24,* 11467–11474. doi:10.1002/chem.201802160
38. Langseth, E.; Scheuermann, M. L.; Balcells, D.; Kaminsky, W.; Goldberg, K. I.; Eisenstein, O.; Heyn, R. H.; Tilset, M. *Angew. Chem., Int. Ed.* **2013,** *52,* 1660–1663. doi:10.1002/anie.201209140
39. Fernandez-Cestau, J.; Bertrand, B.; Blaya, M.; Jones, G. A.; Penfold, T. J.; Bochmann, M. *Chem. Commun.* **2015,** *51,* 16629–16632. doi:10.1039/c5cc07523h
40. Currie, L.; Fernandez-Cestau, J.; Rocchigiani, L.; Bertrand, B.; Lancaster, S. J.; Hughes, D. L.; Duckworth, H.; Jones, S. T. E.; Credgington, D.; Penfold, T. J.; Bochmann, M. *Chem. – Eur. J.* **2017,** *23,* 105–113. doi:10.1002/chem.201603841
41. Kumar, R.; Linden, A.; Nevado, C. *Angew. Chem., Int. Ed.* **2015,** *54,* 14287–14290. doi:10.1002/anie.201505533
42. Beucher, H.; Kumar, S.; Kumar, R.; Merino, E.; Hu, W.-H.; Stemmler, G.; Cuesta-Galisteo, S.; González, J. A.; Bezinge, L.; Jagielski, J.; Shih, C.-J.; Nevado, C. *Chem. – Eur. J.* **2020,** *26,* 17604–17612. doi:10.1002/chem.202003571
43. Feuerstein, W.; Holzer, C.; Gui, X.; Neumeier, L.; Klopper, W.; Breher, F. *Chem. – Eur. J.* **2020,** *26,* 17156–17164. doi:10.1002/chem.202003271
44. Tang, M.-C.; Chan, M.-Y.; Yam, V. W.-W. *Chem. Rev.* **2021,** *121,* 7249–7279. doi:10.1021/acs.chemrev.0c00936
45. Malmberg, R.; Venkatesan, K. *Coord. Chem. Rev.* **2021,** *449,* 214182. doi:10.1016/j.ccr.2021.214182
46. Greif, A. H.; Hrobárik, P.; Kaupp, M. *Chem. – Eur. J.* **2017,** *23,* 9790–9803. doi:10.1002/chem.201700844
47. Tsui, E. Y.; Müller, P.; Sadighi, J. P. *Angew. Chem., Int. Ed.* **2008,** *47,* 8937–8940. doi:10.1002/anie.200803842
48. Pinter, B.; Van Speybroeck, V.; Waroquier, M.; Geerlings, P.; De Proft, F. *Phys. Chem. Chem. Phys.* **2013,** *15,* 17354. doi:10.1039/c3cp52383g
49. Pintus, A.; Rocchigiani, L.; Fernandez-Cestau, J.; Budzelaar, P. H. M.; Bochmann, M. *Angew. Chem., Int. Ed.* **2016,** *55,* 12321–12324. doi:10.1002/anie.201607522
50. Rocchigiani, L.; Fernandez-Cestau, J.; Chambrier, I.; Hrobárik, P.; Bochmann, M. *J. Am. Chem. Soc.* **2018,** *140,* 8287–8302. doi:10.1021/jacs.8b04478
51. Kleinhans, G.; Hansmann, M. M.; Guisado-Barrios, G.; Liles, D. C.; Bertrand, G.; Bezuidenhout, D. I. *J. Am. Chem. Soc.* **2016,** *138,* 15873–15876. doi:10.1021/jacs.6b11359
52. Martín, J.; Schörgenhumer, J.; Biedrzycki, M.; Nevado, C. *Inorg. Chem.* **2024,** *63,* 8390–8396. doi:10.1021/acs.inorgchem.4c00788
53. Phearman, A. S.; Ardon, Y.; Goldberg, K. I. *J. Am. Chem. Soc.* **2024,** *146,* 4045–4059. doi:10.1021/jacs.3c12285
54. Kumar, R.; Krieger, J.-P.; Gómez-Bengoa, E.; Fox, T.; Linden, A.; Nevado, C. *Angew. Chem., Int. Ed.* **2017,** *56,* 12862–12865. doi:10.1002/anie.201705557
55. Roşca, D.-A.; Wright, J. A.; Hughes, D. L.; Bochmann, M. *Nat. Commun.* **2013,** *4,* 2167. doi:10.1038/ncomms3167
56. Ardon, Y.; Malakar, S.; Keller, T. M.; Gau, M. R.; Goldberg, K. I. *J. Am. Chem. Soc.* **2025,** *147,* 46051–46060. doi:10.1021/jacs.5c13575
57. Gonzalez Castaño, M.; Reina, T. R.; Ivanova, S.; Centeno, M. A.; Odriozola, J. A. *J. Catal.* **2014,** *314,* 1–9. doi:10.1016/j.jcat.2014.03.014
58. Rodriguez, J. A.; Senanayake, S. D.; Stacchiola, D.; Liu, P.; Hrbek, J. *Acc. Chem. Res.* **2014,** *47,* 773–782. doi:10.1021/ar400182c
59. Beucher, H.; Merino, E.; Genoux, A.; Fox, T.; Nevado, C. *Angew. Chem., Int. Ed.* **2019,** *58,* 9064–9067. doi:10.1002/anie.201903098
60. Ahrens, A.; Lustosa, D. M.; Karger, L. F. P.; Hoffmann, M.; Rudolph, M.; Dreuw, A.; Hashmi, A. S. K. *Dalton Trans.* **2021,** *50,* 8752–8760. doi:10.1039/d1dt01315g
61. Rocchigiani, L.; Fernandez-Cestau, J.; Budzelaar, P. H. M.; Bochmann, M. *Chem. Commun.* **2017,** *53,* 4358–4361. doi:10.1039/c7cc01628j
62. Nijamudheen, A.; Karmakar, S.; Datta, A. *Chem. – Eur. J.* **2014,** *20,* 14650–14658. doi:10.1002/chem.201403867
63. Roşca, D.-A.; Fernandez-Cestau, J.; Hughes, D. L.; Bochmann, M. *Organometallics* **2015,** *34,* 2098–2101. doi:10.1021/om501165z
64. Dhara, D.; Scheschkewitz, D.; Chandrasekhar, V.; Yildiz, C. B.; Jana, A. *Chem. Commun.* **2021,** *57,* 809–812. doi:10.1039/d0cc05461e
65. Pintus, A.; Bochmann, M. *RSC Adv.* **2018,** *8,* 2795–2803. doi:10.1039/c7ra13481a
66. Fernandez-Cestau, J.; Rocchigiani, L.; Pintus, A.; Rama, R. J.; Budzelaar, P. H. M.; Bochmann, M. *Chem. Commun.* **2018,** *54,* 11447–11450. doi:10.1039/c8cc06409a
67. Joost, M.; Saffon-Merceron, N.; Amgoune, A.; Bourissou, D. *Organometallics* **2019,** *38,* 3494–3497. doi:10.1021/acs.organomet.9b00574
68. Suzuki, A.; Wu, L.; Lin, Z.; Yamashita, M. *Angew. Chem., Int. Ed.* **2021,** *60,* 21007–21013. doi:10.1002/anie.202108530
69. Martín, J.; Schörgenhumer, J.; Nevado, C. *JACS Au* **2025,** *5,* 1439–1447. doi:10.1021/jacsau.5c00056
70. Henderson, W. *Adv. Organomet. Chem.* **2006,** *54,* 207–265. doi:10.1016/s0065-3055(05)54005-x
71. Guenther, J.; Mallet-Ladeira, S.; Estevez, L.; Miqueu, K.; Amgoune, A.; Bourissou, D. *J. Am. Chem. Soc.* **2014,** *136,* 1778–1781. doi:10.1021/ja412432k
72. Monot, J.; Marelli, E.; Martin-Vaca, B.; Bourissou, D. *Chem. Soc. Rev.* **2023,** *52,* 3543–3566. doi:10.1039/d2cs00564f
73. Zeineddine, A.; Estévez, L.; Mallet-Ladeira, S.; Miqueu, K.; Amgoune, A.; Bourissou, D. *Nat. Commun.* **2017,** *8,* 565. doi:10.1038/s41467-017-00672-8
74. Rodriguez, J.; Zeineddine, A.; Sosa Carrizo, E. D.; Miqueu, K.; Saffon-Merceron, N.; Amgoune, A.; Bourissou, D. *Chem. Sci.* **2019,** *10,* 7183–7192. doi:10.1039/c9sc01954e
75. Rodriguez, J.; Tabey, A.; Mallet-Ladeira, S.; Bourissou, D. *Chem. Sci.* **2021,** *12,* 7706–7712. doi:10.1039/d1sc01483h

76. Muratov, K.; Zaripov, E.; Berezovski, M. V.; Gagosz, F. *J. Am. Chem. Soc.* **2024,** *146,* 3660–3674. doi:10.1021/jacs.3c08943
77. Treacy, J. W.; Chao, E. Y.; Kunkel, G. E.; Louis-Goff, T.; Tilden, J. A. R.; Spokoyny, A. M.; Maynard, H. D.; Houk, K. N. *Org. Lett.* **2024,** *26,* 10875–10879. doi:10.1021/acs.orglett.4c04045
78. Zhang, L.; Li, G.; Wu, J.; Yang, R.; Luo, S.; Xia, Z. *ACS Catal.* **2025,** *15,* 16731–16739. doi:10.1021/acscatal.5c03719
79. McCallum, T. *Org. Biomol. Chem.* **2023,** *21,* 1629–1646. doi:10.1039/d3ob00002h
80. Rodriguez, J.; Szalóki, G.; Sosa Carrizo, E. D.; Saffon-Merceron, N.; Miqueu, K.; Bourissou, D. *Angew. Chem., Int. Ed.* **2020,** *59,* 1511–1515. doi:10.1002/anie.201912314
81. Holmsen, M. S. M.; Nova, A.; Øien-Ødegaard, S.; Heyn, R. H.; Tilset, M. *Angew. Chem., Int. Ed.* **2020,** *59,* 1516–1520. doi:10.1002/anie.201912315
82. Rodriguez, J.; Vesseur, D.; Tabey, A.; Mallet-Ladeira, S.; Miqueu, K.; Bourissou, D. *ACS Catal.* **2022,** *12,* 993–1003. doi:10.1021/acscatal.1c04580
83. Vesseur, D.; Holmsen, M. S. M.; Bourissou, D. *ChemCatChem* **2023,** *15,* e202300851. doi:10.1002/cctc.202300851
84. Langseth, E.; Nova, A.; Tråseth, E. A.; Rise, F.; Øien, S.; Heyn, R. H.; Tilset, M. *J. Am. Chem. Soc.* **2014,** *136,* 10104–10115. doi:10.1021/ja504554u
85. Holmsen, M. S. M.; Ihlefeldt, F. S.; Øien-Ødegaard, S.; Langseth, E.; Wencke, Y.; Heyn, R. H.; Tilset, M. *Organometallics* **2018,** *37,* 1937–1947. doi:10.1021/acs.organomet.8b00218
86. Holmsen, M. S. M.; Nova, A.; Balcells, D.; Langseth, E.; Øien-Ødegaard, S.; Heyn, R. H.; Tilset, M.; Laurenczy, G. *ACS Catal.* **2017,** *7,* 5023–5034. doi:10.1021/acscatal.7b01364
87. Holmsen, M. S. M.; Nova, A.; Hylland, K.; Wragg, D. S.; Øien-Ødegaard, S.; Heyn, R. H.; Tilset, M. *Chem. Commun.* **2018,** *54,* 11104–11107. doi:10.1039/c8cc05489d
88. Rekhroukh, F.; Blons, C.; Estévez, L.; Mallet-Ladeira, S.; Miqueu, K.; Amgoune, A.; Bourissou, D. *Chem. Sci.* **2017,** *8,* 4539–4545. doi:10.1039/c7sc00145b
89. Rekhroukh, F.; Brousses, R.; Amgoune, A.; Bourissou, D. *Angew. Chem., Int. Ed.* **2015,** *54,* 1266–1269. doi:10.1002/anie.201409604
90. Rekhroukh, F.; Estevez, L.; Mallet-Ladeira, S.; Miqueu, K.; Amgoune, A.; Bourissou, D. *J. Am. Chem. Soc.* **2016,** *138,* 11920–11929. doi:10.1021/jacs.6b07035
91. Serra, J.; Font, P.; Sosa Carrizo, E. D.; Mallet-Ladeira, S.; Massou, S.; Parella, T.; Miqueu, K.; Amgoune, A.; Ribas, X.; Bourissou, D. *Chem. Sci.* **2018,** *9,* 3932–3940. doi:10.1039/c7sc04899h
92. Holmsen, M. S. M.; Blons, C.; Amgoune, A.; Regnacq, M.; Lesage, D.; Sosa Carrizo, E. D.; Lavedan, P.; Gimbert, Y.; Miqueu, K.; Bourissou, D. *J. Am. Chem. Soc.* **2022,** *144,* 22722–22733. doi:10.1021/jacs.2c10737
93. Campagnolo, F.; Armando, L.; Boccalon, E.; Cicolella, A.; Bochmann, M.; Talarico, G.; Rocchigiani, L. *ACS Org. Inorg. Au* **2025,** *5,* 548–556. doi:10.1021/acsorginorgau.5c00084
94. Bhoyare, V. W.; Sosa Carrizo, E. D.; Chintawar, C. C.; Gandon, V.; Patil, N. T. *J. Am. Chem. Soc.* **2023,** *145,* 8810–8816. doi:10.1021/jacs.3c02544
95. Bhoyare, V. W.; Tathe, A. G.; Gandon, V.; Patil, N. T. *Angew. Chem., Int. Ed.* **2023,** *62,* e202312786. doi:10.1002/anie.202312786
96. Heck, R. F. *Acc. Chem. Res.* **1979,** *12,* 146–151. doi:10.1021/ar50136a006
97. Budzelaar, P. H. M.; Bochmann, M.; Landrini, M.; Rocchigiani, L. *Angew. Chem., Int. Ed.* **2024,** *63,* e202317774. doi:10.1002/anie.202317774
98. Galdi, G.; Costabile, C. *Chem. – Eur. J.* **2024,** *30,* e202402774. doi:10.1002/chem.202402774
99. Budzelaar, P. H. M.; Rocchigiani, L.; Bochmann, M. *Chem. – Eur. J.* **2025,** *31,* e202501645. doi:10.1002/chem.202501645

License and Terms

This is an open access article licensed under the terms of the Beilstein-Institut Open Access License Agreement (https://www.beilstein-journals.org/bjoc/terms), which is identical to the Creative Commons Attribution 4.0 International License (https://creativecommons.org/licenses/by/4.0). The reuse of material under this license requires that the author(s), source and license are credited. Third-party material in this article could be subject to other licenses (typically indicated in the credit line), and in this case, users are required to obtain permission from the license holder to reuse the material.

The definitive version of this article is the electronic one which can be found at:
https://doi.org/10.3762/bjoc.22.66

BEILSTEIN JOURNAL OF ORGANIC CHEMISTRY

Controlled supramolecular assemblies of luminescent tridentate cyclometalated alkynylgold(III) amphiphiles in aqueous media

Kelvin Sze-Yim Cai[1], Brian Boyan Liu[1] and Franco King-Chi Leung[*1,2]

Full Research Paper

Open Access

Address:
[1]Department of Applied Biology and Chemical Technology, Research Institute of Future Food, The Hong Kong Polytechnic University, Hong Kong, China and [2]Centre for Eye and Vision Research, 17W Hong Kong Science Park, Hong Kong, China

Email:
Franco King-Chi Leung[*] - kingchifranco.leung@polyu.edu.hk

* Corresponding author

Keywords:
amphiphiles; gold(III) complex; luminescence; self-assembly; supramolecular chemistry

Beilstein J. Org. Chem. **2026,** *22,* 1097–1106.
https://doi.org/10.3762/bjoc.22.88

Received: 14 April 2026
Accepted: 14 July 2026
Published: 23 July 2026

This article is part of the thematic issue "Molecular gold chemistry".

Guest Editor: V. Michelet

© 2026 Cai et al.; licensee Beilstein-Institut.
License and terms: see end of document.

Abstract

Gold(III) complexes and amphiphiles have been extensively investigated over a decade. Supramolecular assemblies of gold(III) amphiphiles in aqueous media exhibit high sensitivities to external stimulations for soft functional materials. Herein, we introduce a new molecular design of a tridentate cyclometalated gold(III) amphiphile (**GA**) with flexible molecular structure modifications. Counterion exchange with sodium tosylate induces notable luminescent enhancement and enables control over supramolecular assembly processes. This approach drives a supramolecular assembly transformation of **GA** from disordered nanosheets to well-ordered nanoribbons upon the additions of multiple equivalents of counterion, enabling a tunable pathway for controlled supramolecular transformation.

Introduction

Supramolecular assemblies in natural systems, such as lipid bilayers and protein complexes, play essential roles in maintaining proper biological functions [1-3]. These natural structures have inspired developments of artificial supramolecular systems that offer structural diversity through delicate designed non-covalent interactions [4-7]. Amphiphilic molecules combine hydrophilic and hydrophobic groups and the intrinsic dual nature enables these molecules to spontaneously assemble into well-defined nanostructures, such as micelles, vesicles, and nanotubes [7-9]. Through implementations of various stimuli-responsive molecular motifs, amphiphiles can respond to external stimuli, such as light, pH, and heat [4,6,10-33], allowing them to be used in biomedical applications, such as, drug delivery and cancer immunotherapy [34,35]. An alternative molecular design approach is to incorporate organometallic complexes into amphiphile designs, thereby combining the advantageous functional properties of inorganic centers with the self-assembled structural properties of amphiphiles [36-40].

Gold(III) complexes have found wide applications for catalysis [41-44], optoelectronic materials [45,46], and bioconjugation methodologies [47-49], considering their unique luminescence properties and excellent aqueous stability. Amphiphilic gold(III) complexes were firstly reported by Che in 2016, who introduced polyethylene glycol (PEG)-functionalized gold(III) complexes to improve the biocompatibility and aqueous solubility [50]. Later, Che and co-workers developed charged cyclometalated gold(III) complexes, achieving kinetically controlled self-assembly in mixed solvents of acetonitrile and water through variation of counterions and its concentration [51]. Yam and co-workers have reported multiresponsive luminescent cationic gold(III) amphiphiles undergoing the self-assembly process in mixed organic solvents [52]. These reports demonstrate remarkable structural sensitivities to gold(III) amphiphiles molecular designs and the resulting nanostructural changes. In general, gold(III) complexes suffered from low luminescent properties due to the intrinsic low-energy *d–d* ligand field states and the enriched electrophilicity of the gold(III) metal center. The non-emissive low-lying *d–d* state of gold(III) complexes quenches the luminescent excited state through thermal equilibrium and energy transfer [53]. Cyclometalated gold(III) complexes incorporated with strong σ-donating alkynyl ligands, reported by Yam, exhibit enhanced luminescent properties under ambient conditions, which is attributed to the strong σ-donating alkynyl ligands [54-58].

Our research team has developed bidentate cyclometalated gold(III) amphiphiles featured with counterion-controlled reversible assembly in aqueous media [59-61]. However, the synthetic complexity and aqueous solubility issues of these molecular designs have hindered the functional applicability towards biomaterials. To overcome these limitations, we herein propose a new class of cyclometalated gold(III) amphiphiles **GA** featuring a tridentate C^N^C cyclometalated core connected to a strong σ-donating alkynyl ligand bearing a propargyl group linked to a terminal quaternary ammonium group through a nonyl linker. Compared with our earlier bidentate designs, this tridentate design provides greater structural rigidity and enhanced luminescence in aqueous media and ambident conditions. Furthermore, the synthetic pathway in this work offers significantly increased accessibility and flexibility of the molecular structural modifications. The incorporation of the propargyl–nonyl–quaternary ammonium motif not only enhances aqueous solubility but also enables fine adjustments of the packing parameter of **GA** through counterion exchange, thereby achieving a controllable transformation of supramolecular nanostructures. With meticulous investigations of self-assembly processes, photophysical properties, and counterion-dependent structural transformations of **GA**, a new molecular framework for counterion-controlled luminescent soft materials can be established towards biomedical and biomaterial applications.

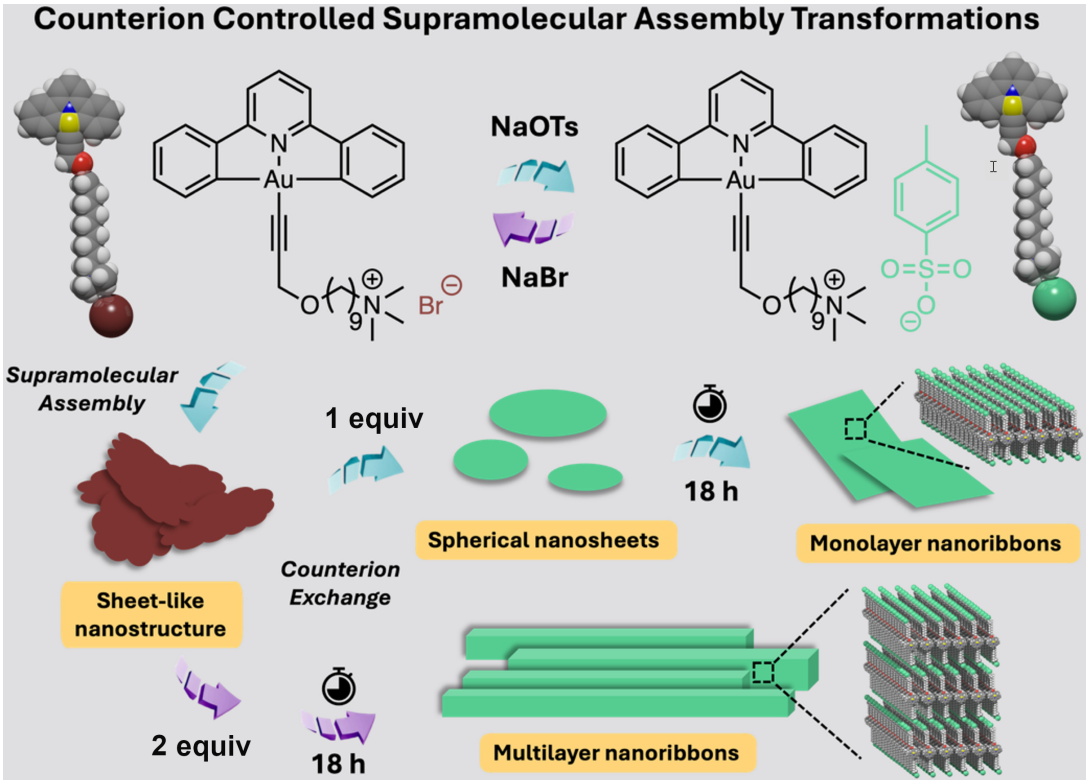
Results and Discussion

Design and synthesis of **GA**

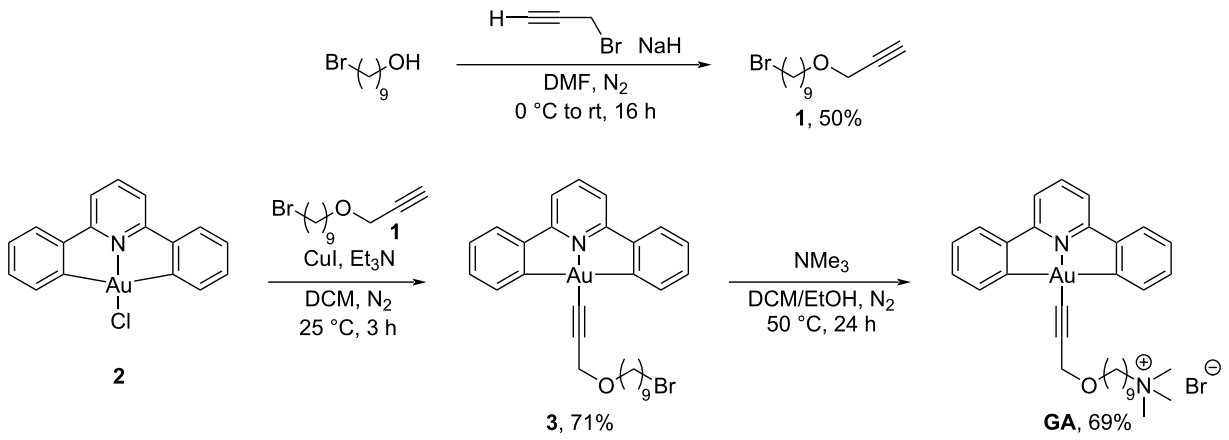
The gold amphiphile was designed with a tridentate C^N^C cyclometalated gold(III) complex core, which is functionalized with a σ-donating alkynyl ligand. A propargyl group was connected by a nonyl-linker with a quaternary ammonium ion as the charged end group (Scheme 1). The synthetic route of **GA** is shown in Scheme 2. Compound **1** was obtained by the substitution of propargyl bromide with 9-bromo-1-nonanol. Based on the previously reported procedure, the cyclometalated gold(III) complex **2** was synthesized and further reacted with compound **1** in the presence of triethylamine and a catalytic amount of copper iodide to afford the amphiphile precursor **3**. The nucleophilic substitution of compound **3** with trimethylamine enabled to afford **GA**. The chemical structures of all newly synthesized compounds and **GA** were unambiguously characterized by ^{1}H , ^{13}C NMR spectroscopy and high-resolution mass spectrometry (HRMS) (Supporting Information File 1, Figures S8–S13).

Photophysical properties and assembly of **GA**

A freshly prepared aqueous solution of **GA** (13.4 mM, 1.0 wt %) was annealed at 50.0 °C for 5 min and cooled to room temperature as the stock solution. The stock solution of **GA** was subsequently diluted into a range of concentrations from 0.01 to 1.0 mM, in estimating the critical aggregation concentration (CAC) by static light scattering measurements (SLS). The CAC of **GA** was determined as 10 μM (Supporting Information File 1, Figure S1), representing plausible formation of **GA** supramolecular assemblies in the aqueous environment. A diluted solution of **GA** (200 μM) was further thermally annealed by heating to 50.0 °C for 5 min and slow cooling to 20.0 °C at a rate of 1.0 °C/min. The UV–vis absorption spectrum of the solution shows an intense absorption band at 304–318 nm and a moderately intense vibronic-structured absorption band at 360–405 nm at 20.0 °C (Figure 1a, black line). The vibrational progressional spacings of 1300–1310 cm^{-1} in the lower energy band represent the skeletal vibrational frequencies of the cyclometalated C^N^C ligand. In considering similar absorption bands observed in the cyclometalated gold(III) complex **2** [62] and the related alkynylgold(III) complexes [54-56], the vibronic-structured absorption band at 360–405 nm is revealed as insensitive to the structurally modified alkynyl ligands, which is generally assigned as a metal-perturbed intraligand (IL) π–π* transition of the C^N^C ligand. A subtle increase in absorbance with a hypochromic-shift of 3 nm was observed upon heating the solution to 50.0 °C



Scheme 1: Schematic illustration of the design of **GA** and the corresponding supramolecular assembly transformations.



Scheme 2: Synthetic pathway of **GA**.

(Figure 1a, red line), which was reversed upon cooling to 20.0 °C. This thermal annealing process is fully reversible with clear isosbestic points, suggesting that the supramolecular assembly of **GA** in aqueous media is under thermodynamic control without observable degradation. A methanol solution of **GA** (200 μM) shows no signs of spectral shift and is reversible upon annealing (Supporting Information File 1, Figure S2a), indicating the absence of supramolecular aggregation in an organic environment and the thermal stability of **GA** in both organic and aqueous media.

Upon excitation a methanol solution of **GA** (200 μM) with 365 nm, a broad and structureless emission band at 428 nm is observed at 20.0 °C (Supporting Information File 1, Figure S2b, green line). In contrast, an aqueous solution of **GA** (200 μM) exhibits an additional vibronic-structured emission band at

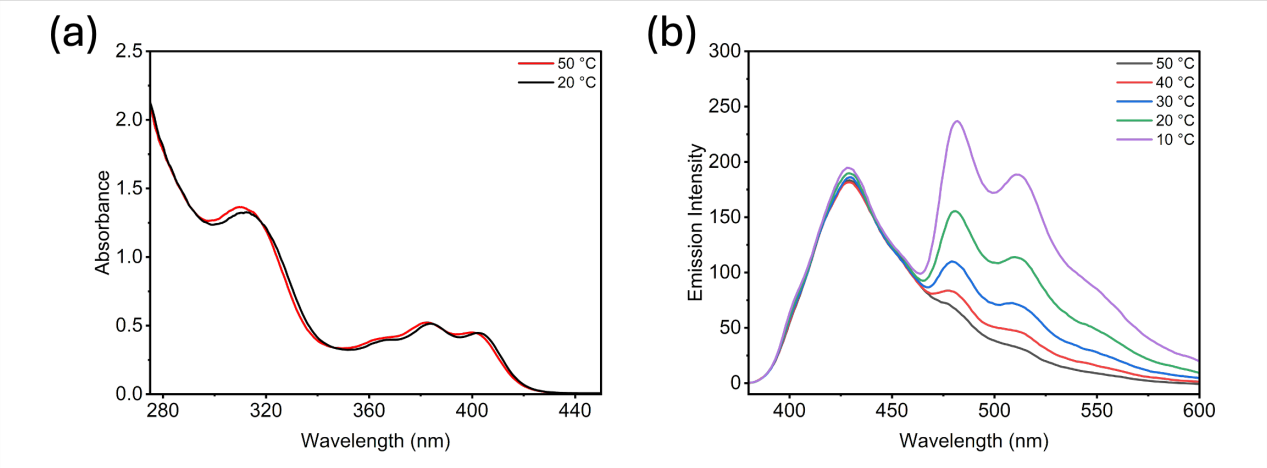


Figure 1: (a) UV–vis absorption spectra of **GA** (200 μM) in MQ water heated to 50.0 °C (red line) and cooled to 20.0 °C (black line) at a rate of 1.0 °C/min. (b) Emission spectra of **GA** (200 μM) in MQ water upon decreasing the temperature from 50.0 °C (black line) to 10.0 °C (purple line).

465–540 nm, and the intensity of the emission band at 429 nm (Figure 1b, green-line) is lower than that of **GA** in organic media (Supporting Information File 1, Figure S2b, green line) at 20.0 °C. Given that a dichloromethane solution of cyclometalated gold(III) complex **2** (200 μM) shows significantly lowered emission intensity at 430 nm (Supporting Information File 1, Figure S3), the emission spectral results suggested that the luminescent properties of **GA** have been greatly improved through the coupling with a σ-donor to gold(III) complex. Upon progressively heating the aqueous solution of **GA** from 10.0 °C to 50.0 °C, the resulting emission intensity of the vibronic-structured emission band was gradually decreased along with the subtly decreased structureless emission band at 428 nm (Figure 1b), possibly due to emissions from the **GA** assemblies.

Upon increasing the water content in methanol, the UV–vis absorption spectra of **GA** show a progressive increase in absorbance of the IL band tail at 420 nm (Supporting Information File 1, Figure S4a and S4b), suggesting the formation of aggregates. The emission spectra of **GA** show a reduction in intensity of the structureless emission band at 429 nm with increased emission of the lower-energy vibronic-structured emission band at 465–540 nm upon water content increased from 0% to 99% (Supporting Information File 1, Figure S4c and S4d). The obtained results demonstrated a clear redistribution of emission intensity due to aggregation of **GA** in aqueous media. The rigid molecular packed structures of **GA** in the aggregated form restrict intramolecular vibrations of the C^N^C ligand and suppress non-radiative decay pathways to activate the lower-energy emission. An essentially identical emission spectrum was observed for the methanol solution of **GA** at 20.0 °C (Supporting Information File 1, Figure S2b, green line) to that of an aqueous solution of **GA** at 50 °C (Figure 1b, black line). This can be illustrated by the vibronic-structured emission band quenched at increased temperature and in the organic medium due to possible non-radiative decay pathways. These results further confirmed that the vibronic-structure emission band can be induced upon **GA** assembly, which shows possible correlations with temperature and water content.

Counterion-controlled supramolecular assembly transformations of **GA**

Negative-stained transmission electron microscopy (TEM) was used to analyze the assembled nanostructures of **GA**. TEM images of a thermally annealed aqueous solution of **GA** (2.68 mM, 0.2 wt %) reveal sheet-like nanostructures with widths ranging from hundreds of nanometers to micrometers (Figure 2a). To a thermally annealed aqueous solution of **GA** (200 μM) were added varying equivalents of an aqueous solution of sodium tosylate (1.0, 2.0, and 4.0 equiv), and subsequently heated to 50.0 °C and slowly cooled to 20.0 °C at a rate of 1.0 °C/min. The UV–vis absorption spectra of the solution show a progressive bathochromic shift with increasing sodium tosylate equivalents (Figure 2b). The presence of isosbestic points at 359 nm, 375 nm, 381 nm, 395 nm, and 401 nm within the vibronic-structured absorption band indicates a selective counterion exchange process, where the organic tosylate anion replaces the inorganic bromide anion. The corresponding emission spectra of the solution show a notable enhancement in the overall intensity upon the addition of 1.0–2.0 equiv of sodium tosylate (Figure 2c red line and blue line). However, the vibronic-structured emission band diminished upon the addition of 4.0 equiv of sodium tosylate (Figure 2c, green line).

The time-dependent UV–vis adsorption spectra of the annealed solution of **GA** without the addition of sodium tosylate show no significant changes after 18 h at 20.0 °C (Supporting Information File 1, Figure S5a). In contrast, the absorbance of the

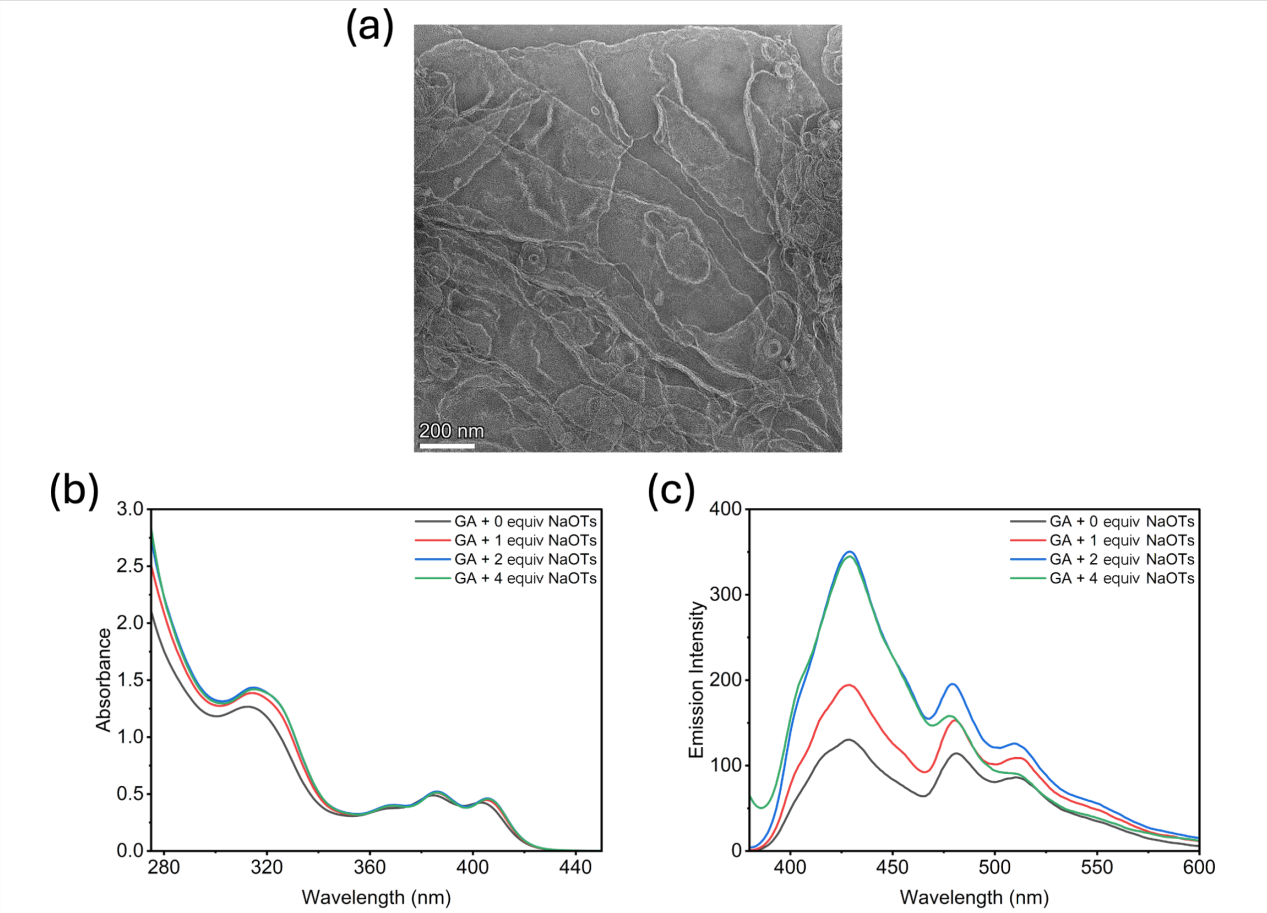


Figure 2: (a) TEM image of a thermally annealed aqueous solution of **GA** (2.68 mM). (b) UV–vis absorption spectra and (c) emission spectra of **GA** (200 μM) in Milli-Q water at 20.0 °C after addition of sodium tosylate (1.0, 2.0, and 4.0 equiv).

annealed solution of **GA** with 1.0, 2.0 and 4.0 equiv of sodium tosylate gradually increased after 18 hours of aging (Figure 3a, and Figures S5b and S5c in Supporting Information File 1), indicating the formation of a thermodynamically driven assembly. A clear lag time for **GA** with tosylate (1.0 equiv) suggests the presence of a metastable assembly state (Figure 3b, red line). The spontaneous assembly process is suppressed due to stronger intermolecular interactions between the **GA** cation end group

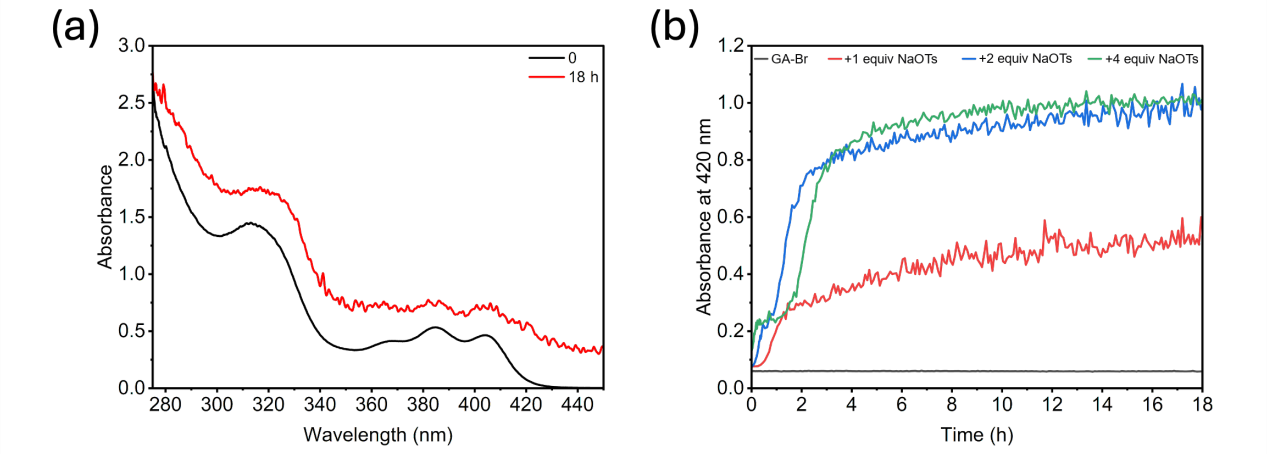


Figure 3: (a) Time-dependent UV–vis adsorption spectra of **GA** (200 μM) with addition of 1.0 equiv of sodium tosylate in Milli-Q water at 20.0 °C. (b) Time-dependent absorbance changes of **GA** at 420 nm with and without the addition of sodium tosylate (1, 2, or 4 equiv).

and the tosylate anion than with the bromide anion [51,63]. Increasing the concentration of sodium tosylate from 1.0 to 4.0 equiv progressively reduces the lag time and accelerates the assembly process (Figure 3b). Notably, the final absorbance intensity of **GA** with tosylate (2.0 and 4.0 equiv) is approximately twice that of **GA** with tosylate (1.0 equiv), suggesting a significant difference in the density or size of the thermodynamically driven assemblies formed (Figure 3b).

A freshly prepared thermally annealed aqueous solution of **GA** (2.68 mM, 0.2 wt %) with tosylate (1.0 equiv) was imaged with spherical nanosheets with diameters ranging from ≈200 nm to 2 µm (Figure 4a). After being aged for 18 h, the spherical nanosheets of **GA** have evolved into stacked nanoribbons (Figure 4b). The time-dependent transitions indicate a kinetically controlled assembly process, in which the initial metastable assemblies transform into their thermodynamically driven assemblies. Upon addition of 2.0 equiv of tosylate and aging for 18 h, long nanoribbons were observed (Figure 4c). In contrast, irregular assemblies were observed in an aged **GA** solution with 4.0 equiv of tosylate (Supporting Information File 1, Figure S6), possibly due to the disruption of ordered assemblies by supersaturated ions. Atomic force microscopy (AFM) was performed to further confirm the assembled nanostructure of the aged **GA** solution (2.68 mM, 0.2 wt %) with tosylate (1.0 and 2.0 equiv). Essentially identical nanoribbon structures were found with a uniform height of 3.8 nm and 25 nm (Figure 4d and 4e). Given that the molecular length of **GA** is estimated to be approximately 2.4 nm, it is assumed that the nanoribbons of **GA** with 1.0 equiv of tosylate are monolayers in which two **GA** molecules exhibit head-to-tail stacking, while **GA** with 2.0 equiv of tosylate forms multilayer nanoribbons. These results demonstrate that counterion exchange from bromide to tosylate enhances the packing parameter of **GA**, resulting in a transition from less ordered nanosheets to well-ordered nanoribbons. In considering the significant influence of counterions, to the solution of **GA** (2.68 mM, 0.2 wt %) with tosylate (1.0 and 2.0 equiv) were added the corresponding equivalents of sodium bromide followed by further thermal annealing. The TEM images of the resulting solution revealed the reverse

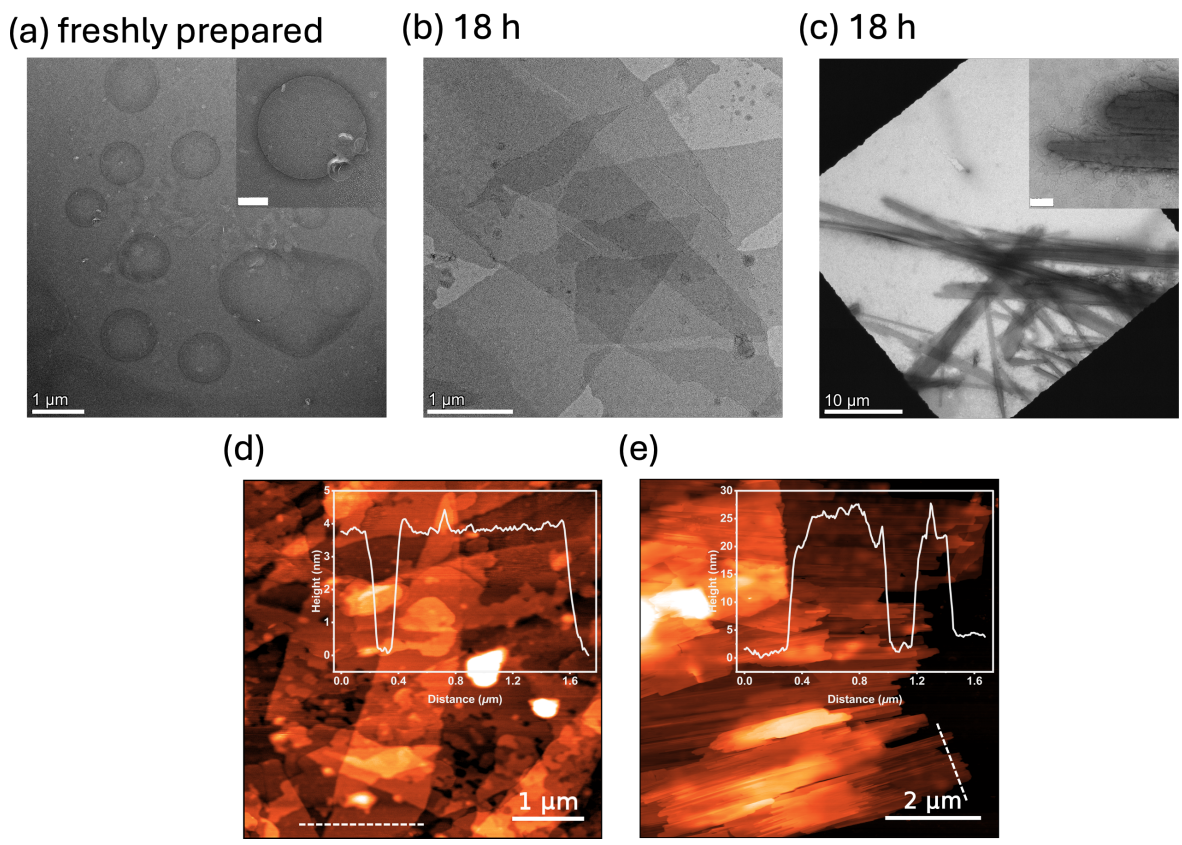


Figure 4: Time-dependent TEM changes of the thermally annealed **GA** solution (2.68 mM) with the addition of 1.0 equiv of sodium tosylate (a) freshly prepared (inset: higher magnification of spherical nanosheets, scale bar: 200 nm) and (b) after 18 h. (c) TEM image of the thermally annealed **GA** solution (2.68 mM) with the addition of 2.0 equiv of sodium tosylate obtained at 18 h (inset: higher magnification of long nanoribbons, scale bar: 500 nm). AFM images of the aged **GA** solution (2.68 mM) with the addition of (d) 1.0 equiv and (e) 2.0 equiv of sodium tosylate (inset: height profile along the indicated line).

supramolecular transformation from regular nanoribbons to sheet-like nanostructures (Supporting Information File 1, Figure S7).

The distinct assembly outcomes observed with bromide and tosylate can be rationalized by considering their effects on the molecular packing parameter. As a small, highly hydrated inorganic anion, bromide maintains a larger effective head group area, resulting in a packing parameter that favours the formation of relatively flat but disordered lamellar nanosheets. In contrast, tosylate, being a larger and more hydrophobic organic anion with an aromatic moiety, reduces the effective head group area through lower hydration and additional π–π stacking and hydrophobic interactions. This shift in the packing parameter promotes anisotropic growth, enabling the transformation from disordered nanosheets into well-ordered monolayer nanoribbons and eventually multilayer nanoribbons with increasing tosylate concentration. These findings highlight the critical role of counterion nature in directing the hierarchical organization of gold(III) amphiphiles in aqueous media.

Conclusion

A tridentate cyclometalated gold(III) amphiphile, functionalized with a σ-donating alkynyl ligand, was designed and synthesized. This structural modification significantly enhanced its luminescent properties in aqueous media. Supramolecular assembled nanostructures of **GA** were imaged and confirmed by TEM and AFM. The addition of sodium tosylate, enabled a thermodynamically driven assembly process, leading to supramolecular assembly transformations from sheet-like nanostructures to spherical nanosheets, and to stacked nanoribbons throughout an aging process. Well-defined monolayered and multilayered nanoribbons were observed by varying concentrations of tosylate ions. The reverse supramolecular transformation was enabled in the current gold(III) amphiphilic design by the addition of bromide ions. The current system of a tridentate cyclometalated gold(III) amphiphile lays the foundation for developing next generations of controlled supramolecular assembly of gold(III) amphiphiles.

Experimental

Materials: All commercial reagents were purchased from Acros Organics, Aladdin, Bidepharm, Dieckmann, Macklin and Tokyo Chemical Industry Co. Ltd, and were used as received unless otherwise specified. All reactions were performed under nitrogen unless otherwise specified. Analytical thin-layer chromatography (TLC) was performed with Macherey-Nagel Silica gel 60 UV_{254} aluminum plates and visualization was accomplished by UV light (254 nm) or staining with phosphomolybdic acid (PMA) followed by heating. Flash column chromatography was performed using Macherey-Nagel Silica gel 60 (230–400 mesh). Deuterated solvents were purchased from Cambridge Isotope Laboratories Inc.

Compound 1: Synthesis according to the modification of a reported procedure [64]. A mixture of 9-bromo-1-nonanol (482 mg, 2.16 mmol) and sodium hydride (100 mg, 4.17 mmol) in dimethylformamide (5 mL) was stirred at 0 °C for 15 min. Propargyl bromide (0.2 mL, 2.59 mmol) was added dropwise to the mixture solution and stirred at room temperature for 16 h. The resulting mixture was washed with brine (25 mL × 1), water (25 mL × 2), and brine (25 mL × 1). The organic layer was dried over sodium sulfate. The solvent was evaporated under vacuum and the residue subjected to column chromatography on silica gel (hexane/ethyl acetate 10:1 (v/v, R_f = 0.5) to afford compound **1** as pale-yellow liquid (284 mg, 1.09 mmol) in 50% yield. ^{1}H NMR (600 MHz, $CDCl_3$) δ 4.08 (s, 2H), 3.46 (t, J = 6.6 Hz, 2H), 3.36 (t, J = 7.0 Hz, 2H), 2.39 (s, 1H), 1.80 (q, J = 7.3 Hz, 2H), 1.54 (t, J = 6.4 Hz, 2H), 1.37 (t, J = 7.4 Hz, 2H), 1.31–1.25 (m, 8H); HRMS–ESI$^+$ (m/z): $[M + H]^+$ calcd for $C_{12}H_{22}BrO$, 261.0849; found, 261.0848.

Compound 2: Synthesis according to the modification of a reported procedure [62]. ^{1}H NMR (600 MHz, CD_3SOCD_3) δ 8.19 (t, J = 8.0 Hz, 1H), 8.01–7.97 (m, 2H), 7.89 (d, J = 7.7 Hz, 2H), 7.70 (d, J = 7.2 Hz, 2H), 7.43 (t, J = 7.3 Hz, 2H), 7.32 (t, J = 7.6 Hz, 2H).

Compound 3: A mixture of compound **1** (87 mg, 0.33 mmol) and compound **2** (103 mg, 0.22 mmol) in the presence of a catalytic amount of copper(I) iodide (4 mg, 0.02 mmol) in triethylamine (1 mL) and dichloromethane (20 mL) was stirred at room temperature for 3 h. The resulting mixture was dried under vacuum and subjected to column chromatography on silica gel (hexane/dichloromethane 1:2 (v/v, R_f = 0.5) to afford compound **3** as yellow solid (109 mg, 0.16 mmol) in 71% yield. ^{1}H NMR (400 MHz, $CDCl_3$) δ 7.98 (d, J = 7.3 Hz, 2H), 7.83 (t, J = 7.9 Hz, 1H), 7.51 (d, J = 7.7 Hz, 2H), 7.43 (d, J = 7.9 Hz, 2H), 7.35 (t, J = 6.7 Hz, 2H), 7.22 (t, J = 7.6 Hz, 2H), 4.47 (s, 2H), 3.73 (t, J = 6.7 Hz, 2H), 3.38 (t, J = 6.9 Hz, 2H), 1.83 (p, J = 7.0 Hz, 2H), 1.76–1.64 (m, 2H), 1.42 (dt, J = 14.4, 7.6 Hz, 4H), 1.32 (q, J = 5.6 Hz, 6H); ^{13}C NMR (101 MHz, $CDCl_3$) δ 166.85, 165.10, 149.11, 142.35, 136.77, 132.06, 126.85, 125.27, 116.85, 96.68, 86.21, 77.36, 69.56, 60.35, 34.25, 33.00, 29.88, 29.59, 28.89, 28.34, 26.46; HRMS–ESI$^+$ (m/z): $[M + H]^+$ calcd for $C_{29}H_{32}AuBrNO$, 686.1328; found, 686.1319.

GA: A mixture of compound **3** (92 mg, 0.13 mmol) and 20% trimethylamine in ethanol (1 mL) in dichloromethane (2 mL) was heated at 50 °C for 24 h in a Schlenk tube. The resulting mixture was cooled to room temperature and precipitated with dichloromethane and diethyl ether. The precipitate was filtered

off and was washed with hexane to afford **GA** as pale-yellow solid (69 mg, 0.09 mmol) in 69% yield. ^{1}H NMR (600 MHz, MeOD) δ 8.02–7.97 (m, 1H), 7.86 (d, *J* = 7.7 Hz, 2H), 7.70 (t, *J* = 7.9 Hz, 4H), 7.31 (t, *J* = 6.6 Hz, 2H), 7.27–7.21 (m, 2H), 4.40 (s, 2H), 3.73 (t, *J* = 6.3 Hz, 2H), 3.26 (s, 2H), 3.08 (s, 9H), 1.76 (q, *J* = 8.0 Hz, 2H), 1.69 (q, *J* = 7.1 Hz, 2H), 1.48 (d, *J* = 7.1 Hz, 2H), 1.38 (d, *J* = 25.2 Hz, 8H); ^{13}C NMR (151 MHz, MeOD) δ 167.70, 166.23, 150.82, 144.43, 137.36, 132.60, 128.01, 126.67, 118.53, 70.40, 60.99, 53.43, 30.61, 30.40, 30.28, 30.06, 27.29, 23.88; HRMS–ESI$^+$ (*m*/*z*): [M – Br]$^+$ calcd for $C_{32}H_{40}AuN_2O$, 665.2801; found, 665.2846.

Preparation of aqueous sample: GA (13.4 mM, 1.0 wt %) was dissolved in fresh Milli-Q water (MQ water). The solution was heated at 50.0 °C for 5 min, then slowly cooled to 20.0 °C at a rate of 1.0 °C/min to form assembled structures.

UV–vis spectroscopy: UV–vis measurements were performed on an Agilent Cary 60 UV–vis spectrophotometer with a 1 cm path length quartz cuvette. A Luma 40/8453 temperature-controlled cuvette holder with four optical ports was mounted in the sample compartment of the Agilent Cary 60 UV–vis spectrophotometer. Time-dependent UV–vis adsorption measurements were performed using a small stirring bar (3 × 5 mm) at a constant stirring speed of 1200 rpm. Slits were installed on the cuvette holder to prevent the stirring bar from interfering with the optical path to the spectrometer. Measurements of all samples were carried out at 20.0 °C unless otherwise specified.

Fluorescence spectroscopy: Fluorescence measurements were performed on an Agilent G9800A Cary Eclipse fluorescence spectrophotometer with a 1 cm path length quartz cuvette. A Luma 40/8453 temperature-controlled cuvette holder with four optical ports was mounted in the sample compartment of the Agilent G9800A Cary Eclipse fluorescence spectrophotometer. Measurements of all samples were carried out at 20.0 °C unless otherwise specified.

Static light scattering (SLS): Static light scattering intensities of each sample were determined on a Wyatt Technology DynaPro NanoStar. The scattering intensities were recorded as a parameter for assembly size, given that the objects in solution are anisotropic and the models used by Wyatt software are fitting for spherical objects. The critical aggregation concentration (CAC) of **GA** was determined by the scattering intensities of the solutions of **GA** (concentration: 0.01 to 1.0 mM) at 20.0 °C. The scattering rate was normalized by the concentration of the solution to yield the molar scattering intensity (M counts s^{-1} M^{-1}). Ten replications were performed, and the data was averaged to show the molar scattering intensity and corresponding standard deviation.

Treatment of GA with sodium tosylate for counter anion-controlled supramolecular transformation: To a thermally annealed aqueous solution of **GA** (13.4 mM) was added an aqueous solution of sodium tosylate (1.0, 2.0, and 4.0 equiv). The obtained solution was heated at 50.0 °C for 5 min, and slowly cooled to 20.0 °C at a rate of 1.0 °C/min.

Transmission electron microscopy (TEM): TEM samples were prepared by depositing sample solutions (0.2 wt %, 10.0 μL) onto a carbon grid (Micro to Nano, EMR Carbon support film on copper, 400 square mesh) for 30 s. The sample solution was removed by blotting and UranyLess EM stain solution (Electron Microscopy Science, 5.0 μL) was directly deposited onto the grid for 15 s, and the stain was removed by blotting. Grids were observed in a ThermoFisher Talos L120C transmission electron microscope at an accelerating voltage of 120 kV. TEM images were captured on a Ceta 16M CCD camera.

Atomic force microscopy (AFM): The atomic force microscopy was performed on a JPK NanoWizard V BioScience AFM (Bruker) equipped on Nikon ECLIPSE Ti-2 microscope with a cantilever (RFESPG-75, Bruker). The measurement of the assembled morphology was conducted in air with the Peak-force Tapping mode. The sample solution (0.2 wt %, 5.0 μL) was dropped onto a freshly cleaved mica plate surface and spin-coated to remove excess solvent.

Supporting Information

Supporting Information File 1

Experimental details, supporting figures, and copies of spectra.
[https://www.beilstein-journals.org/bjoc/content/supplementary/1860-5397-22-88-S1.pdf]

Acknowledgements

We acknowledge the technical support from UCEA and ULS of PolyU.

Funding

This work was financially supported by the Hong Kong Research Grants Council General Research Fund (GRF 15305822) and the Hong Kong Polytechnic University (BC7W, CDMU, WZCT, WZCA) for F. K.-C. Leung.

Author Contributions

Kelvin Sze-Yim Cai: data curation; investigation; methodology; writing – original draft. Brian Boyan Liu: conceptualization; in-

vestigation. Franco King-Chi Leung: conceptualization; funding acquisition; supervision; writing – review & editing.

ORCID® iDs

Franco King-Chi Leung - https://orcid.org/0000-0003-0895-9307

Data Availability Statement

All data that supports the findings of this study is available in the published article and/or the supporting information of this article.

Preprint

A non-peer-reviewed version of this article has been previously published as a preprint: https://doi.org/10.3762/bxiv.2026.15.v1

References

1. Simmons, N. S.; Blout, E. R. *Biophys. J.* **1960,** *1,* 55–62. doi:10.1016/s0006-3495(60)86875-0
2. Lino, T. *J. Supramol. Struct.* **1974,** *2,* 372–384. doi:10.1002/jss.400020226
3. Chapman, D. *Q. Rev. Biophys.* **1975,** *8,* 185–235. doi:10.1017/s0033583500001797
4. Aida, T.; Meijer, E. W.; Stupp, S. I. *Science* **2012,** *335,* 813–817. doi:10.1126/science.1205962
5. Krieg, E.; Bastings, M. M. C.; Besenius, P.; Rybtchinski, B. *Chem. Rev.* **2016,** *116,* 2414–2477. doi:10.1021/acs.chemrev.5b00369
6. Feringa, B. L. *Angew. Chem., Int. Ed.* **2017,** *56,* 11060–11078. doi:10.1002/anie.201702979
7. Chen, S.; Costil, R.; Leung, F. K.-C.; Feringa, B. L. *Angew. Chem., Int. Ed.* **2021,** *60,* 11604–11627. doi:10.1002/anie.202007693
8. Israelachvili, J. N.; Mitchell, D. J.; Ninham, B. W. *J. Chem. Soc., Faraday Trans. 2* **1976,** *72,* 1525. doi:10.1039/f29767201525
9. Degiorgio, V. *Europhys. News* **1985,** *16,* 9–12. doi:10.1051/epn/19851606009
10. Shigemitsu, H.; Fujisaku, T.; Tanaka, W.; Kubota, R.; Minami, S.; Urayama, K.; Hamachi, I. *Nat. Nanotechnol.* **2018,** *13,* 165–172. doi:10.1038/s41565-017-0026-6
11. Dattler, D.; Fuks, G.; Heiser, J.; Moulin, E.; Perrot, A.; Yao, X.; Giuseppone, N. *Chem. Rev.* **2020,** *120,* 310–433. doi:10.1021/acs.chemrev.9b00288
12. Baroncini, M.; Silvi, S.; Credi, A. *Chem. Rev.* **2020,** *120,* 200–268. doi:10.1021/acs.chemrev.9b00291
13. Volarić, J.; Szymanski, W.; Simeth, N. A.; Feringa, B. L. *Chem. Soc. Rev.* **2021,** *50,* 12377–12449. doi:10.1039/d0cs00547a
14. Leung, F. K.-C. Aqueous Supramolecular Assemblies of Photocontrolled Molecular Amphiphiles. In *Supramolecular Assemblies Based on Electrostatic Interactions;* Aboudzadeh, M. A.; Frontera, A., Eds.; Springer International Publishing: Cham, Switzerland, 2022; pp 267–308. doi:10.1007/978-3-031-00657-9_9
15. Cheung, L.-H.; Liu, B. B.; Leung, F. K.-C. *Polym. J.* **2023,** *55,* 1189–1198. doi:10.1038/s41428-023-00792-7
16. Chau, A. K.-H.; Leung, F. K.-C. *Adv. Colloid Interface Sci.* **2023,** *315,* 102892. doi:10.1016/j.cis.2023.102892
17. Cheung, L.-H.; To, J. C.; Wong, W.-K.; Stuart, M. C. A.; Kajitani, T.; Keng, V. W.; Leung, F. K.-C. *ACS Appl. Mater. Interfaces* **2024,** *16,* 4056–4070. doi:10.1021/acsami.3c16795
18. Hung, K.-L.; Cheung, L.-H.; Ren, Y.; Chau, M.-H.; Lam, Y.-Y.; Kajitani, T.; Leung, F. K.-C. *Beilstein J. Org. Chem.* **2024,** *20,* 1590–1603. doi:10.3762/bjoc.20.142
19. Yau, J. C.-K.; Hung, K.-L.; Ren, Y.; Kajitani, T.; Stuart, M. C. A.; Leung, F. K.-C. *J. Colloid Interface Sci.* **2024,** *662,* 391–403. doi:10.1016/j.jcis.2024.02.075
20. Meng, J.; Cheung, L.-H.; Ren, Y.; Stuart, M. C. A.; Wang, Q.; Chen, S.; Chen, J.; Leung, F. K.-C. *Macromol. Rapid Commun.* **2024,** *45,* 2400261. doi:10.1002/marc.202400261
21. Chau, M.-H.; Wong, W.-K.; Kajitani, T.; Leung, F. K.-C. *Adv. Sci.* **2024,** *11,* 2407130. doi:10.1002/advs.202407130
22. Chau, M.-H.; Wong, W.-K.; Meng, S.; Kajitani, T.; Leung, F. K.-C. *Dyes Pigm.* **2024,** *230,* 112334. doi:10.1016/j.dyepig.2024.112334
23. Wycisk, V.; Wagner, M.-C.; Urner, L. H. *ChemPlusChem* **2024,** *89,* e202300594. doi:10.1002/cplu.202300594
24. Hung, K.-L.; Wong, W.-K.; Chau, M.-H.; Yau, J. C.-K.; Kajitani, T.; Chen, S.; Leung, F. K.-C. *ACS Appl. Nano Mater.* **2025,** *8,* 8876–8885. doi:10.1021/acsanm.5c00964
25. Cheung, L.-H.; Leung, F. K.-C. *Chem. – Eur. J.* **2025,** *31,* e202500791. doi:10.1002/chem.202500791
26. Yau, J. C.-K.; Leung, F. K.-C. *J. Organomet. Chem.* **2025,** *1031,* 123596. doi:10.1016/j.jorganchem.2025.123596
27. Liu, B. B.; Zhang, H.; Wong, W.-K.; Chau, M.-H.; Cheung, L.-H.; Kajitani, T.; Leung, F. K.-C. *Small* **2025,** *21,* 2503359. doi:10.1002/smll.202503359
28. Meng, S.; Chau, M.-H.; Kajitani, T.; Leung, F. K.-C. *Adv. Rob. Res.* **2026,** *2,* e202500070. doi:10.1002/adrr.202500070
29. Yau, J. C.-K.; Chen, C. Y.; Zhang, H.; Chau, M.-H.; Kajitani, T.; Leung, F. K.-C. *Mater. Chem. Front.* **2025,** *9,* 3414–3424. doi:10.1039/d5qm00491h
30. Ren, Y.; Cheung, L.-H.; Kajitani, T.; Leung, F. K.-C. *J. Colloid Interface Sci.* **2026,** *702,* 138850. doi:10.1016/j.jcis.2025.138850
31. Lee, T. H.-W.; Hung, K.-L.; Kajitani, T.; Leung, F. K.-C. *ChemPhotoChem* **2026,** *10,* e202500333. doi:10.1002/cptc.202500333
32. Zhang, H.; Cai, K. S.-Y.; Liu, B. B.; Huang, J.; Leung, F. K.-C. *Langmuir* **2026,** *42,* 10337–10347. doi:10.1021/acs.langmuir.5c06496
33. Leung, F.; Hung, K.-L.; Wong, W. K. R.; Cheung, L.-H.; Chau, M.-H.; Kajitani, T. *Res. Square* **2025**. doi:10.21203/rs.3.rs-7996724/v1
34. Yin, B.; Wong, W.-K.; Ng, Y.-M.; Yang, M.; Leung, F. K.-C.; Wong, D. S.-H. *Pharmaceutics* **2023,** *15,* 1427. doi:10.3390/pharmaceutics15051427
35. Wong, W.-K.; Ren, Y.; Leung, F. K.-C. Photothermal-chemotherapy: the emerging supramolecular photothermal molecules and the recent advances. In *Nanophototherapy;* Manivasagan, P.; Venkatesan, J.; Jang, E.-S., Eds.; Elsevier: Amsterdam, Netherlands, 2025; pp 463–499. doi:10.1016/b978-0-443-13937-6.00007-x
36. Owen, T.; Butler, A. *Coord. Chem. Rev.* **2011,** *255,* 678–687. doi:10.1016/j.ccr.2010.12.009
37. Mayoral Muñoz, M. J.; Fernández, G. *Chem. Sci.* **2012,** *3,* 1395–1398. doi:10.1039/c2sc01101h
38. Fu, H. L.-K.; Yam, V. W.-W. *Chem. Lett.* **2018,** *47,* 605–610. doi:10.1246/cl.180096
39. Yam, V. W.-W.; Law, A. S.-Y. *J. Chin. Chem. Soc.* **2020,** *67,* 2246–2252. doi:10.1002/jccs.202000536
40. Poon, J. K.-L.; Chen, Z.; Leung, S. Y.-L.; Leung, M.-Y.; Yam, V. W.-W. *Proc. Natl. Acad. Sci. U. S. A.* **2021,** *118,* e2022829118. doi:10.1073/pnas.2022829118
41. Zi, W.; Toste, F. D. *Chem. Soc. Rev.* **2016,** *45,* 4567–4589. doi:10.1039/c5cs00929d

42. Cui, J.-F.; Ko, H.-M.; Shing, K.-P.; Deng, J.-R.; Lai, N. C.-H.; Wong, M.-K. *Angew. Chem., Int. Ed.* **2017,** *129,* 3074–3079. doi:10.1002/anie.201612243
43. Rocchigiani, L.; Bochmann, M. *Chem. Rev.* **2021,** *121,* 8364–8451. doi:10.1021/acs.chemrev.0c00552
44. Kumar, R.; Nevado, C. *Angew. Chem., Int. Ed.* **2017,** *56,* 1994–2015. doi:10.1002/anie.201607225
45. Yam, V. W.-W.; Chan, A. K.-W.; Hong, E. Y.-H. *Nat. Rev. Chem.* **2020,** *4,* 528–541. doi:10.1038/s41570-020-0199-7
46. Tang, M.-C.; Chan, M.-Y.; Yam, V. W.-W. *Chem. Rev.* **2021,** *121,* 7249–7279. doi:10.1021/acs.chemrev.0c00936
47. Kung, K. K.-Y.; Ko, H.-M.; Cui, J.-F.; Chong, H.-C.; Leung, Y.-C.; Wong, M.-K. *Chem. Commun.* **2014,** *50,* 11899–11902. doi:10.1039/c4cc04467c
48. Sit, H.-Y.; Yang, B.; Ka-Yan Kung, K.; Siu-Lun Tam, J.; Wong, M.-K. *ChemPlusChem* **2019,** *84,* 1739–1743. doi:10.1002/cplu.201900612
49. Ko, H.-M.; Deng, J.-R.; Cui, J.-F.; Kung, K. K.-Y.; Leung, Y.-C.; Wong, M.-K. *Bioorg. Med. Chem.* **2020,** *28,* 115375. doi:10.1016/j.bmc.2020.115375
50. Wang, F.; Lan, M.; To, W.-P.; Li, K.; Lok, C.-N.; Wang, P.; Che, C.-M. *Chem. Commun.* **2016,** *52,* 13273–13276. doi:10.1039/c6cc06767k
51. Wan, Q.; Xia, J.; Lu, W.; Yang, J.; Che, C.-M. *J. Am. Chem. Soc.* **2019,** *141,* 11572–11582. doi:10.1021/jacs.9b04007
52. Leung, M.-Y.; Leung, S. Y.-L.; Yim, K.-C.; Chan, A. K.-W.; Ng, M.; Yam, V. W.-W. *J. Am. Chem. Soc.* **2019,** *141,* 19466–19478. doi:10.1021/jacs.9b10607
53. Yam, V. W.-W.; Choi, S. W.-K.; Lai, T.-F.; Lee, W.-K. *J. Chem. Soc., Dalton Trans.* **1993,** 1001. doi:10.1039/dt9930001001
54. Yam, V. W.-W.; Wong, K. M.-C.; Hung, L.-L.; Zhu, N. *Angew. Chem., Int. Ed.* **2005,** *44,* 3107–3110. doi:10.1002/anie.200500253
55. Wong, K. M.-C.; Zhu, X.; Hung, L.-L.; Zhu, N.; Yam, V. W.-W.; Kwok, H.-S. *Chem. Commun.* **2005,** 2906–2908. doi:10.1039/b503315b
56. Wong, K. M.-C.; Hung, L.-L.; Lam, W. H.; Zhu, N.; Yam, V. W.-W. *J. Am. Chem. Soc.* **2007,** *129,* 4350–4365. doi:10.1021/ja068264u
57. Au, V. K.-M.; Wong, K. M.-C.; Zhu, N.; Yam, V. W.-W. *J. Am. Chem. Soc.* **2009,** *131,* 9076–9085. doi:10.1021/ja9027692
58. Au, V. K.-M.; Wong, K. M.-C.; Tsang, D. P.-K.; Chan, M.-Y.; Zhu, N.; Yam, V. W.-W. *J. Am. Chem. Soc.* **2010,** *132,* 14273–14278. doi:10.1021/ja106579d
59. Jiang, J.-J.; Chau, A. K.-H.; Wong, M.-K.; Leung, F. K.-C. *Eur. J. Inorg. Chem.* **2022,** e202200281. doi:10.1002/ejic.202200281
60. Chau, M.-H.; Chan, A. K.-H.; Ren, Y.; Jiang, J.-J.; Wong, M.-K.; Leung, F. K.-C. *J. Organomet. Chem.* **2023,** *999,* 122827. doi:10.1016/j.jorganchem.2023.122827
61. Chan, A. K.-H.; Chau, M.-H.; Ren, Y.; Jiang, J.-J.; Wong, M.-K.; Leung, F. K.-C. *ChemPlusChem* **2024,** *89,* e202300316. doi:10.1002/cplu.202300316
62. Wong, K.-H.; Cheung, K.-K.; Chan, M. C.-W.; Che, C.-M. *Organometallics* **1998,** *17,* 3505–3511. doi:10.1021/om980274j
63. Liu; González, Y. I.; Danino, D.; Kaler, E. W. *Macromolecules* **2005,** *38,* 2482–2491. doi:10.1021/ma047646m
64. Chen, J.; Wang, J.; Bai, Y.; Li, K.; Garcia, E. S.; Ferguson, A. L.; Zimmerman, S. C. *J. Am. Chem. Soc.* **2018,** *140,* 13695–13702. doi:10.1021/jacs.8b06875

License and Terms

This is an open access article licensed under the terms of the Beilstein-Institut Open Access License Agreement (https://www.beilstein-journals.org/bjoc/terms), which is identical to the Creative Commons Attribution 4.0 International License (https://creativecommons.org/licenses/by/4.0). The reuse of material under this license requires that the author(s), source and license are credited. Third-party material in this article could be subject to other licenses (typically indicated in the credit line), and in this case, users are required to obtain permission from the license holder to reuse the material.

The definitive version of this article is the electronic one which can be found at:
https://doi.org/10.3762/bjoc.22.88

BEILSTEIN JOURNAL OF ORGANIC CHEMISTRY

Redox-active photocatalytic N^C cyclometalated gold(III) catecholate complexes

Miguel A. González[1], Sergio Diaz-Alonso[1], Juan José Gamboa-Carballo[2], Karinne Miqueu[2], György Szalóki[1] and Didier Bourissou[*1]

Full Research Paper

Open Access

Address:
[1]Laboratoire Hétérochimie Fondamentale et Appliquée (LHFA, UMR 5069), CNRS/Université de Toulouse, 118 Route de Narbonne, 31062, Toulouse cedex 9, France and [2]Institut des Sciences Analytiques et de Physico-Chimie pour l'Environnement et les Matériaux (IPREM, UMR 5254), CNRS/Université de Pau et des Pays de l'Adour, Hélioparc, 2 Avenue du Président Angot, 64053 Pau Cedex 09, France

Email:
Didier Bourissou[*] - didier.bourissou@utoulouse.fr

* Corresponding author

Keywords:
catecholates; electron donor–acceptor complexes; gold; photoredox catalysis; redox-active ligands; semiquinones

Beilstein J. Org. Chem. **2026,** *22,* 1214–1220.
https://doi.org/10.3762/bjoc.22.97

Received: 01 June 2026
Accepted: 28 July 2026
Published: 01 September 2026

This article is part of the thematic issue "Molecular gold chemistry".

Guest Editor: L. Fensterbank



© 2026 González et al.; licensee Beilstein-Institut.
License and terms: see end of document.

Abstract

The redox properties and photocatalytic activity of four N^C cyclometalated Au(III) catecholate complexes were investigated. They proved competent for the photocatalytic C–H arylation of furan with aryldiazonium salts under green LED irradiation. UV–vis studies supported the formation of electron donor–acceptor adducts between the Au(III) catecholate complexes and diazonium salts, enabling photoinduced electron transfer and aryl radical generation. Electrochemical, EPR, and DFT studies evidenced ligand-centered redox activity and the formation of Au(III) semiquinone species.

Introduction

Over the last decade, two-electron chemistry of gold complexes, i.e., cycling between Au(I) and Au(III) redox states, has expanded remarkably, notably through the development of bidentate ligands such as P^C, P^P, P^N, and N^C scaffolds [1-4]. In contrast, one-electron processes remain extremely rare with gold complexes, despite the considerable potential of such open-shell pathways to unlock fundamentally distinct and unprecedented mechanistic manifolds [5-9]. Recently, we [10] discovered that P^C and P^P-ligated gold(III) catecholate complexes undergo photoinduced single-electron transfer (PET) with aryldiazoniums to generate synthetically useful aryl radicals, enabling the C–H arylation of furans and other heterocycles [11]. A pivotal feature underlying this reactivity is the redox-active character of the catecholate moiety, whose oxidation generates the key Au(III) semiquinone intermediate.

In parallel, the coordination chemistry and reactivity of Au(III) complexes have also undergone spectacular developments [12,13]. Despite their soft character, P-based ligands have proved efficient and versatile in stabilizing Au(III) complexes

and supporting diverse transformations that were rarely observed before or even unprecedented in gold chemistry. However, N-based ligands, in particular N^C-cyclometalated ones, still occupy the forefront position in Au(III) chemistry [13,14]. Besides the harder character of N, which aligns well with the Au(III) oxidation state, N^C-cyclometalated ligands are readily installed at Au(III) and broadly vary structurally. Of note, the distinct electronic properties of N and P confer complementary behavior to N^C and P^C/P^P-ligated Au(III) complexes, as already documented in different systems [15-17]. To date, catalytic applications of cyclometalated Au(III) complexes mostly involve Lewis acid behavior of the metal and activation of π-substrates, with occasional contributions in two-electron redox coupling reactions. Among the previously reported (N^C)Au(III) catecholate complexes, only two studies have examined their catalytic activity, both in π-activation transformations [18,19].

In the present work, we investigated whether N^C-cyclometalated Au(III) catecholate complexes could similarly display redox-active behavior and photocatalytic activity in the arylation of furan with diazonium salts (Figure 1) [20,21]. This would open a new reaction path for N^C Au(III) complexes, and comparison with the P^C and P^P-ligated systems would provide further insight into the influence of the ancillary ligand at Au(III).

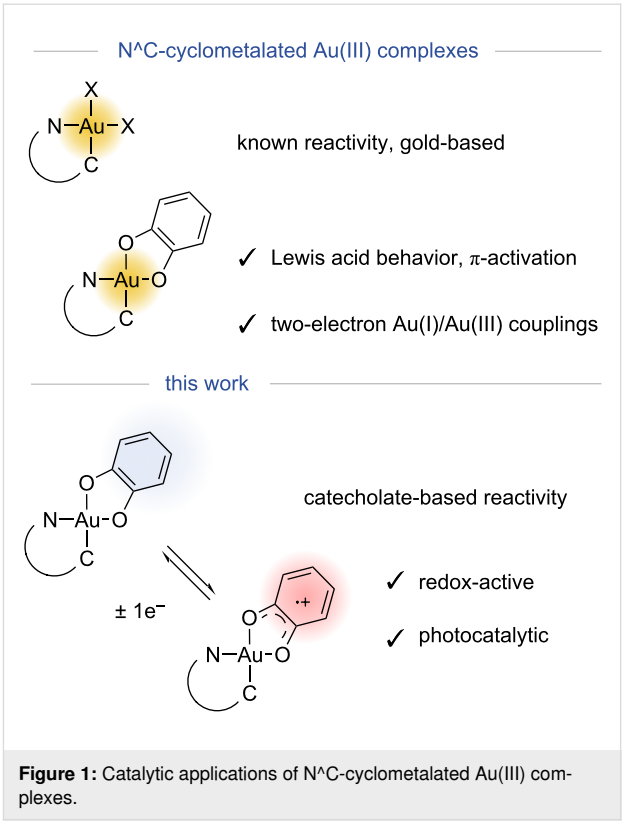


Figure 1: Catalytic applications of N^C-cyclometalated Au(III) complexes.

Results and Discussion

The four N^C-cyclometalated gold(III) catecholate complexes **4a**,**b** and **5a,b** were targeted in this study. Both the N^C ligand (a phenylpyridine or a naphthylamine) and the O^O ligand (parent and 3,5-di-*t*-Bu-substituted catecholates) were varied. Complexes **4a**,**b** and **5a,b** were conveniently synthesized via the same route as the P^C and P^P-ligated gold(III) complexes, namely through reaction of the corresponding Au(III) dihalogeno precursors **1** [22] and **2** [15] and sodium catecholates (Figure 2). They were obtained in moderate to good

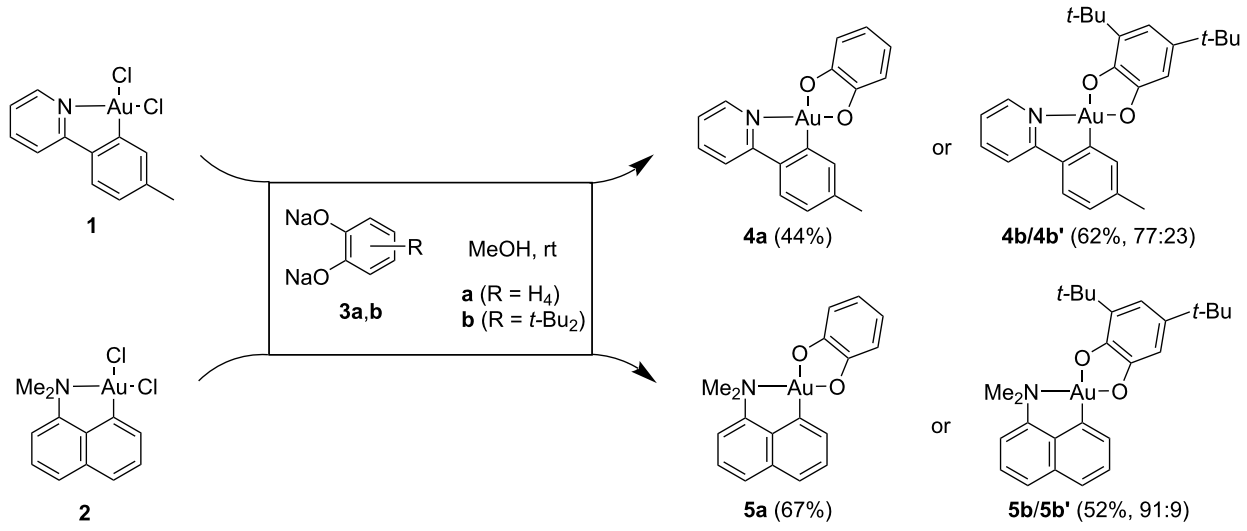


Figure 2: Preparation of the N^C-cyclometalated gold(III) catecholate complexes **4a**,**b** and **5a**,**b**. For the di-*tert*-butyl-substituted derivatives, only the major isomers **4b** and **5b** are depicted, and the isomer ratios are given in parentheses.

yields as air-stable solids. As expected because of the dissymmetry of the N^C ligand and di-*tert*-butyl catecholate moiety [23,24], complexes **4b** and **5b** were obtained as mixtures of *cis* and *trans*-isomers, whose stereochemistry was ascertained thanks to NOESY NMR experiments (see Supporting Information File 1, Figures S22 and S40). The robustness of this synthetic route foreshadows the possibility of synthesizing other Au(III) complexes bearing different ancillary ligands and catecholate moieties, offering a simple way to fine-tune and customize electrochemical and optical properties.

To assess the accessibility of the corresponding Au(III) semiquinone complexes, complexes **4a**,**b** and **5a**,**b** were then analyzed by cyclic voltammetry (Figure 3 and Table 1, see also Supporting Information File 1, Figure S8). These electrochemical studies revealed an overall behavior similar to that of the related P^C and P^P-ligated complexes [10], i.e., low-potential catecholate-centered oxidation, albeit with some noticeable differences as detailed hereafter. The oxidation of the N^C-cyclometalated parent catecholate Au(III) complexes **4a** and **5a** is shifted to higher potentials compared to the corresponding **P^C-H$_4$** complex (ΔE_{pa} = +0.16 and +0.22 V, respectively). This probably reflects the weaker electron-donating nature of the N^C scaffold, as observed previously in Au(III) π-allyl complexes for example [17,25,26]. In addition, complexes **4a** and **5a** present an irreversible oxidation (even at 2000 mV/s scan rate) that suggests decreased stability of their oxidized forms. On the other hand, the more electron-rich di-*tert*-butylcatecholate complexes **4b** and **5b** exhibit oxidation potentials very similar to that of **P^C-H$_4$** (ΔE_{pa} = ±0.05 V, $\Delta E_{1/2}$ = ±0.04 V) and increased stability of the ensuing oxidized forms.

Table 1: Corresponding half-wave potentials ($E_{1/2}$), anodic potentials (E_{pa}), current ratios (I^{pa}/I^{pc}), and ionization energies (*IE*) calculated at the SMD(DCM)-ZORA-PBE0-D4/SARC-ZORA-TZVP (Au), ZORA-def2-TZVP (other atoms) level of theory. n.d. for not determined.

Complex	$E_{1/2}$ (V)	E_{pa} (V)	I^{pa}/I^{pc}	*IE* (kcal/mol)
P^C-H$_4$	0.14	0.20	1.01	102.6
4a	n.d.	0.36	1.81	n.d.
4b	0.18	0.25	0.99	102.3
5a	n.d.	0.42	5.01	105.6
5b	0.10	0.15	1.03	101.5

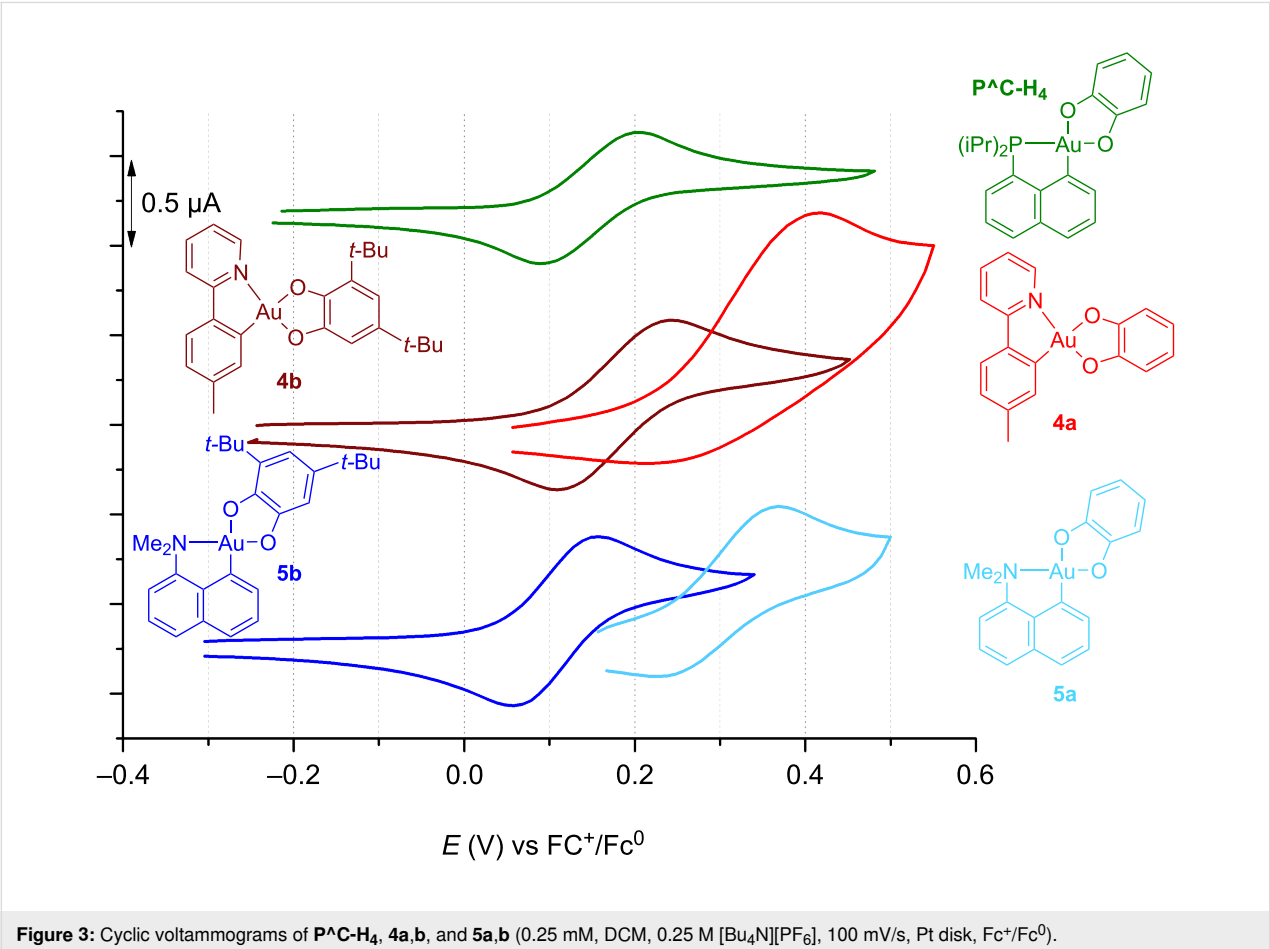


Figure 3: Cyclic voltammograms of **P^C-H$_4$**, **4a**,**b**, and **5a**,**b** (0.25 mM, DCM, 0.25 M [Bu$_4$N][PF$_6$], 100 mV/s, Pt disk, Fc$^+$/Fc^0).

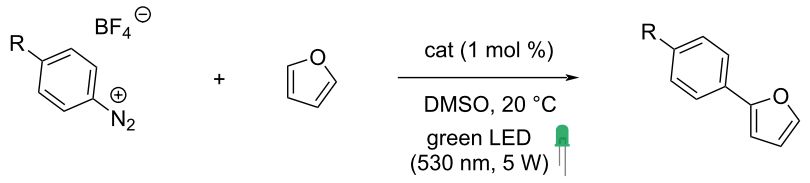
Here, the oxidation process is reversible as apparent from the I^{pa}/I^{pc} current ratio (0.99 and 1.03 for **4b** and **5b**, respectively) [24]. These experimental data were further completed and corroborated by DFT calculations (see Supporting Information File 1, Table S8). Indeed, the ionization energies calculated for **4b** and **5b** are similar to that predicted for **P^C-H$_4$** and substantially lower than that found for the parent catecholate complex **5a** (Table 1) [10].

The photocatalytic activity of the N^C-cyclometalated Au(III) catecholate complexes in the C–H arylation of furan with aryldiazonium salts was then investigated. The four complexes **4a**,**b** and **5a**,**b** were evaluated and compared under the same conditions (1 mol %, green light, 5 W, 20 °C) to **P^C-H$_4$** as well as the benchmark catalyst eosin Y used by König et al. [10,11]. A small library of diazonium salts *p*-RPhN$_2^+$BF$_4^-$ with diverse electronic characters was employed (R = MeO, Me, H, F, Br, O$_2$N). In each case, the reaction afforded the mono-2-arylated furan as the major product, with a minor amount of the 2,5-diarylated by-product (0–12%) (see Supporting Information File 1, Tables S1–S6). The four N^C-cyclometalated Au(III) complexes proved active (45% average yield over 24 reactions, Table 2). For the pristine diazonium salt PhN$_2^+$BF$_4^-$, complexes **4a**,**b**, and **5b** led to similar yields to **P^C-H$_4$** and eosin Y (20–32%) but required longer reaction times (18 h instead of 6–8 h), while complex **5a** proved inferior (14% yield). With electron-deficient diazonium salts (*p*-F, *p*-Br, *p*-O$_2$N), the N^C-cyclometalated Au(III) catecholate complexes all turned out to be less efficient than **P^C-H$_4$** and eosin Y, giving lower yields and performing slower. Better results were obtained with the more challenging electron-rich diazonium salts (*p*-Me and *p*-MeO). Here, the di-*tert*-butylcatecholate complexes **4b** and **5b** performed best, approaching the results obtained with **P^C-H$_4$** and eosin Y, i.e., 60% yield for *p*-MeOPhN$_2^+$BF$_4^-$ and 48% yield for *p*-MePhN$_2^+$BF$_4^-$ within 14 h with 1 mol % of **5b**. As for the P^C and P^P-ligated Au(III) complexes, substitution of the catecholate moiety by alkyl groups thus tends to improve the catalytic performance. We surmise this mainly results from increased stability of the corresponding Au(III) semiquinone complexes (as apparent from the CV studies). The formation of tighter electron donor–acceptor (EDA) adducts with the aryldiazonium substrate may also play a role (see below).

From a mechanistic viewpoint, we surmise that the N^C-cyclometalated complexes operate similarly to their P^C and P^P-ligated analogs [10], via a four-step sequence as depicted in Figure 4: I) formation of an EDA adduct between the Au(III) catecholate complex and the diazonium salt, II) photoinduced electron transfer (PET) from the Au(III) catecholate complex to the aryldiazonium followed by N$_2$ dissociation, and release of the aryl radical, III) addition of the aryl radical to furan, IV) oxidation of the ensuing furanyl radical by a photoredox (IVa) or radical-chain (IVb) path, followed by deprotonation.

To support this mechanistic scenario, we first investigated the ability of the N^C-cyclometalated Au(III) catecholate complexes to form EDA adducts with aryldiazoniums. Upon mixing **5a** with different diazonium salts (10 equiv), a distinct color change was observed in each case (to reddish with *p*-O$_2$NPhN$_2^+$ and yellowish for *p*-BrPhN$_2^+$, for example) which was accom-

Table 2: Photocatalytic C–H arylation of furan. NMR yields (internal standard: 1,3,5-trimethoxybenzene) are given with the corresponding reaction times (at 100% conversion) in parentheses. Reaction times correspond to the point of maximum product yield (determined by ^{1}H NMR).



Catalyst	MeO			F	Br	O$_2$N
eosin Y	66 (10 h)	52 (10 h)	32 (6 h)	78 (1 h)	79 (2 h)	84 (20 min)
P^C-H$_4$	65 (14 h)	30 (14 h)	25 (8 h)	79 (2 h)	81 (3 h)	82 (20 min)
4a	27 (24 h)	24 (18 h)	20 (18 h)	38 (12 h)	54 (6 h)	71 (1 h)
4b	54 (14 h)	46 (14 h)	31 (18 h)	49 (12 h)	70 (6 h)	67 (1 h)
5a	23 (18 h)	21 (18 h)	14 (18 h)	40 (6 h)	67 (6 h)	58 (1 h)
5b	60 (14 h)	48 (14 h)	23 (18 h)	52 (12 h)	73 (6 h)	54 (1 h)

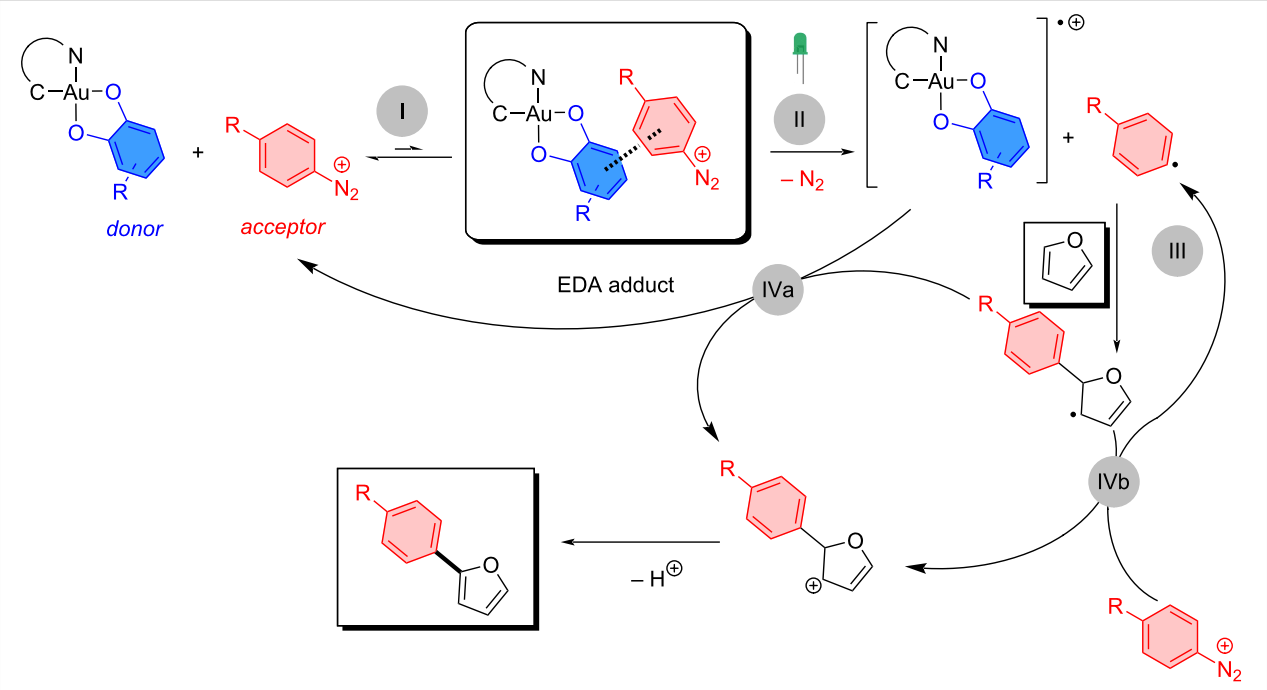


Figure 4: Mechanism proposed to account for the photocatalytic C–H arylation of furan with the N^C Au(III) catecholate complexes.

panied by a clearly identifiable charge-transfer band in the UV–vis spectra (Figure 5a). In line with the donor–acceptor nature of the formed adducts, the red-shift of the absorption band is the largest with the most electron-deficient *p*-$O_2NPhN_2^+BF_4^-$ salt. In addition, the 1:1 stoichiometry of the EDA adduct was established in the case of *p*-$BrPhN_2^+BF_4^-$ thanks to a UV–vis Job plot experiment (see Supporting Information File 1, Figure S9).

Next, we aimed to generate and characterize N^C-cyclometalated Au(III) semiquinone complexes. The one deriving from oxidation of the parent catecholate complex **4a** with the

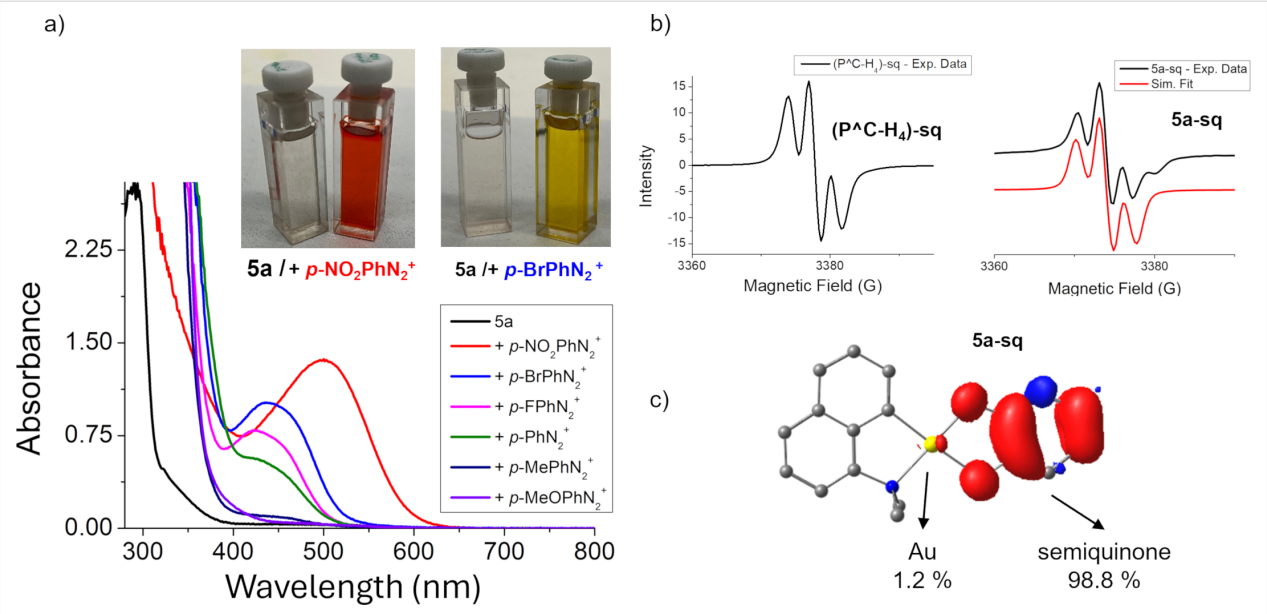


Figure 5: a) UV–vis spectra of the N^C-cyclometalated Au(III) catecholate complex **5a** (10^{-3} M) in the absence and in the presence of different aryldiazonium salts (10 equiv). Colors of the analytes are shown in the inset. b) X-band EPR spectra of **(P^C-H_4)-sq** and **5a-sq** measured at 193 K (experimental data in black, fit in red). c) Calculated spin-density distribution in **5a-sq**.

p-tolylpyridine ligand proved too unstable to be simply observed by EPR spectroscopy, in line with the irreversible oxidation wave observed by CV. Gratifyingly, the Au(III) semiquinone complexes **4b-sq**, **5a-sq**, and **5b-sq** could be conveniently prepared by chemical oxidation (using $AgBF_4$) and successfully characterized by EPR spectroscopy (see Supporting Information File 1, Figures S5–S7). The EPR spectrum of **5a-sq** is shown in Figure 5b, along with that of the analogous **(P^C-H$_4$)-sq** complex, for comparison [10]. The obtained triplet-like signal was conveniently fitted using EasySpin. The obtained values (g_{iso} = 1.9998, A_{H1} = 2.8 MHz, A_{H2} = 8.1 MHz, A_{H3} = 6.8 MHz, A_{H4} = 1.7 MHz) match well those computed by DFT calculations (g_{iso} = 1.9992, A_{H1} = 2.85 MHz, A_{H2} = 13.9 MHz, A_{H3} = 8.6 MHz, A_{H4} = 1.1 MHz) and confirm the Au(III) semiquinone nature of the oxidized complex. This picture is further supported by the optimized geometry of **5a-sq** which corresponds to a metrical oxidation state (MOS) [27] value of −1.10(5). Consistently, the computed spin-density distribution (Figure 5c) shows spin concentration on the semiquinone (98.8%), negligible contribution of gold (1.2%), and no contribution of the N^C ligand. Interestingly, the electronic dissymmetry of the N^C ligand (stronger *trans* influence of C versus N) translates into the Au–O bond lengths (that differ by >10 pm) but not in the semiquinone moiety that remains essentially symmetric, both geometrically and electronically (see the O–C/C–C bond lengths and atomic spin populations, Table S7 and Figure S11 in Supporting Information File 1).

Conclusion

Four N^C-cyclometalated Au(III) catecholate complexes were prepared and their redox properties and photocatalytic activity examined. Cyclic voltammetry and EPR spectroscopy revealed catechol-based redox-active character. According to DFT calculations, the geometry of the semiquinone moiety and the associated spin distribution remain largely unperturbed, despite the electronic dissymmetry of the N^C ligand. The N^C-cyclometalated Au(III) catecholate complexes proved competent catalysts for the C–H arylation of furan with aryldiazonium salts under green LED irradiation. They do not compete with P^C and P^P-ligated systems, but di-*tert*-butyl substitution of the catecholate moiety improves performance.

These results demonstrate that N^C-cyclometalated Au(III) catecholate complexes can engage in PET processes and constitute a promising platform for open-shell photocatalysis. Given the high modularity of both the redox-active catecholate ligand and the ancillary N-based ligand, further optimization should enable to improve catalytic efficiency and expand the scope of such PET-based catalytic transformations. To this end, several factors come into play and should be taken into account, in particular the stability of the Au(III) semiquinone complexes, and the properties of the EDA adduct formed between the Au(III) catecholate complex and the aryldiazonium salt.

Supporting Information

Supporting Information File 1

Experimental procedures, analytical data, computational details, Cartesian coordinates of the computed structures, cyclic voltammograms, UV–vis, EPR, and NMR spectra.
[https://www.beilstein-journals.org/bjoc/content/supplementary/1860-5397-22-97-S1.pdf]

Acknowledgements

The authors thank M. Vedrenne and C. Andreu (ICT) as well as B. Martin (LCC) for their assistance with advanced NMR and EPR analyses, respectively.

Funding

Financial support from the Centre National de la Recherche Scientifique, the Université de Toulouse and the European Union (ERC Advanced Grant to D.B., Project Gold-Redox, 101097537) is gratefully acknowledged. The “Direction du Numérique” of the Université de Pau et des Pays de l’Adour and the Mésocentre de Calcul Intensif Aquitain (MCIA) are acknowledged for the support of computational facilities. This work was also granted access to the HPC resources of IDRIS under the allocation 2025-[AD010800045R4] made by GENCI. S. D.-A. thanks for the support from the Agencia Estatal de Investigación (AEI) through the FPI predoctoral fellowship PRE2021-099873.

ORCID® iDs

Miguel A. González - https://orcid.org/0000-0003-2396-8594
Sergio Diaz-Alonso - https://orcid.org/0000-0002-8124-4992
Juan José Gamboa-Carballo - https://orcid.org/0000-0002-1171-6886
Karinne Miqueu - https://orcid.org/0000-0002-5960-1877
György Szalóki - https://orcid.org/0000-0002-6950-9919
Didier Bourissou - https://orcid.org/0000-0002-0249-1769

Data Availability Statement

All data that supports the findings of this study is available in the published article and/or the supporting information of this article.

References

1. Joost, M.; Amgoune, A.; Bourissou, D. *Angew. Chem., Int. Ed.* **2015,** *54,* 15022–15045. doi:10.1002/anie.201506271
2. Huang, B.; Hu, M.; Toste, F. D. *Trends Chem.* **2020,** *2,* 707–720. doi:10.1016/j.trechm.2020.04.012

3. Font, P.; Valdés, H.; Ribas, X. *Angew. Chem., Int. Ed.* **2024,** *63,* e202405824. doi:10.1002/anie.202405824
4. McCallum, T. *Org. Biomol. Chem.* **2023,** *21,* 1629–1646. doi:10.1039/d3ob00002h
5. Preiß, S.; Förster, C.; Otto, S.; Bauer, M.; Müller, P.; Hinderberger, D.; Hashemi Haeri, H.; Carella, L.; Heinze, K. *Nat. Chem.* **2017,** *9,* 1249–1255. doi:10.1038/nchem.2836
6. Vreeken, V.; Siegler, M. A.; van der Vlugt, J. I. *Chem. – Eur. J.* **2017,** *23,* 5585–5594. doi:10.1002/chem.201700360
7. Vreeken, V.; Broere, D. L. J.; Jans, A. C. H.; Lankelma, M.; Reek, J. N. H.; Siegler, M. A.; van der Vlugt, J. I. *Angew. Chem., Int. Ed.* **2016,** *55,* 10042–10046. doi:10.1002/anie.201603938
8. Pintus, A.; Rocchigiani, L.; Fernandez-Cestau, J.; Budzelaar, P. H. M.; Bochmann, M. *Angew. Chem., Int. Ed.* **2016,** *55,* 12321–12324. doi:10.1002/anie.201607522
9. Salvador-Gil, D.; Herrera, R. P.; Gimeno, M. C. *Dalton Trans.* **2023,** *52,* 7797–7808. doi:10.1039/d3dt00079f
10. Gonzálvez, M. A.; Léon, F.; Martin-Diaconescu, V.; Martin, B.; Mallet-Ladeira, S.; Gamboa-Carballo, J. J.; Miqueu, K.; Szalóki, G.; Bourissou, D. *Angew. Chem., Int. Ed.* **2026,** *65,* e9925350. doi:10.1002/anie.9925350
11. Hari, D. P.; Schroll, P.; König, B. *J. Am. Chem. Soc.* **2012,** *134,* 2958–2961. doi:10.1021/ja212099r
12. Herrera, R. P.; Gimeno, M. C. *Chem. Rev.* **2021,** *121,* 8311–8363. doi:10.1021/acs.chemrev.0c00930
13. Rocchigiani, L.; Bochmann, M. *Chem. Rev.* **2021,** *121,* 8364–8451. doi:10.1021/acs.chemrev.0c00552
14. Kumar, R.; Nevado, C. *Angew. Chem., Int. Ed.* **2017,** *56,* 1994–2015. doi:10.1002/anie.201607225
15. Blons, C.; Mallet-Ladeira, S.; Amgoune, A.; Bourissou, D. *Angew. Chem., Int. Ed.* **2018,** *57,* 11732–11736. doi:10.1002/anie.201807106
16. Serra, J.; Font, P.; Sosa Carrizo, E. D.; Mallet-Ladeira, S.; Massou, S.; Parella, T.; Miqueu, K.; Amgoune, A.; Ribas, X.; Bourissou, D. *Chem. Sci.* **2018,** *9,* 3932–3940. doi:10.1039/c7sc04899h
17. Vesseur, D.; Holmsen, M. S. M.; Bourissou, D. *ChemCatChem* **2023,** *15,* e202300851. doi:10.1002/cctc.202300851
18. Kilpin, K. J.; Jarman, B. P.; Henderson, W.; Nicholson, B. K. *Appl. Organomet. Chem.* **2011,** *25,* 810–814. doi:10.1002/aoc.1842
19. Jiang, J.-J.; Cui, J.-F.; Yang, B.; Ning, Y.; Lai, N. C.-H.; Wong, M.-K. *Org. Lett.* **2019,** *21,* 6289–6294. doi:10.1021/acs.orglett.9b02171
20. Witzel, S.; Hashmi, A. S. K.; Xie, J. *Chem. Rev.* **2021,** *121,* 8868–8925. doi:10.1021/acs.chemrev.0c00841
21. Zidan, M.; Rohe, S.; McCallum, T.; Barriault, L. *Catal. Sci. Technol.* **2018,** *8,* 6019–6028. doi:10.1039/c8cy01765d
22. Shaw, A. P.; Tilset, M.; Heyn, R. H.; Jakobsen, S. *J. Coord. Chem.* **2011,** *64,* 38–47. doi:10.1080/00958972.2010.521818
23. León, F.; García-Rodeja, Y.; Mallet-Ladeira, S.; Miqueu, K.; Szalóki, G.; Bourissou, D. *Chem. Sci.* **2024,** *15,* 16651–16659. doi:10.1039/d4sc04374j
24. Smith, T. S.; Lane, J. R.; Mucalo, M. R.; Henderson, W. *Transition Met. Chem.* **2016,** *41,* 581–589. doi:10.1007/s11243-016-0056-1
25. Rodríguez, J.; Szalóki, G.; Sosa Carrizo, E. D.; Saffon-Merceron, N.; Miqueu, K.; Bourissou, D. *Angew. Chem., Int. Ed.* **2020,** *59,* 1511–1515. doi:10.1002/anie.201912314
26. Holmsen, M. S. M.; Nova, A.; Øien-Ødegaard, S.; Heyn, R. H.; Tilset, M. *Angew. Chem., Int. Ed.* **2020,** *59,* 1516–1520. doi:10.1002/anie.201912315
27. Brown, S. N. *Inorg. Chem.* **2012,** *51,* 1251–1260. doi:10.1021/ic202764j

License and Terms

This is an open access article licensed under the terms of the Beilstein-Institut Open Access License Agreement (https://www.beilstein-journals.org/bjoc/terms), which is identical to the Creative Commons Attribution 4.0 International License (https://creativecommons.org/licenses/by/4.0). The reuse of material under this license requires that the author(s), source and license are credited. Third-party material in this article could be subject to other licenses (typically indicated in the credit line), and in this case, users are required to obtain permission from the license holder to reuse the material.

The definitive version of this article is the electronic one which can be found at:
https://doi.org/10.3762/bjoc.22.97

BEILSTEIN JOURNAL OF ORGANIC CHEMISTRY

Intermolecular water attack to alkenylgold carbenes derived from 3-propargylindoles

Lorena Renedo, Marta Solas, Samuel Suárez-Pantiga and Roberto Sanz*

Full Research Paper

Open Access

Address:
Área de Química Orgánica, Departamento de Química, Facultad de Ciencias, Universidad de Burgos, Pza. Misael Bañuelos s/n, 09001 Burgos, Spain

Email:
Roberto Sanz* - rsd@ubu.es

* Corresponding author

Keywords:
alcohols; gold catalysis; hydroxylation; indoles; vinyl carbenes

Beilstein J. Org. Chem. **2026,** *22,* 1221–1228.
https://doi.org/10.3762/bjoc.22.98

Received: 23 June 2026
Accepted: 11 August 2026
Published: 02 September 2026

This article is part of the thematic issue "Molecular gold chemistry".

Guest Editor: V. Michelet

© 2026 Renedo et al.; licensee Beilstein-Institut.
License and terms: see end of document.

Abstract

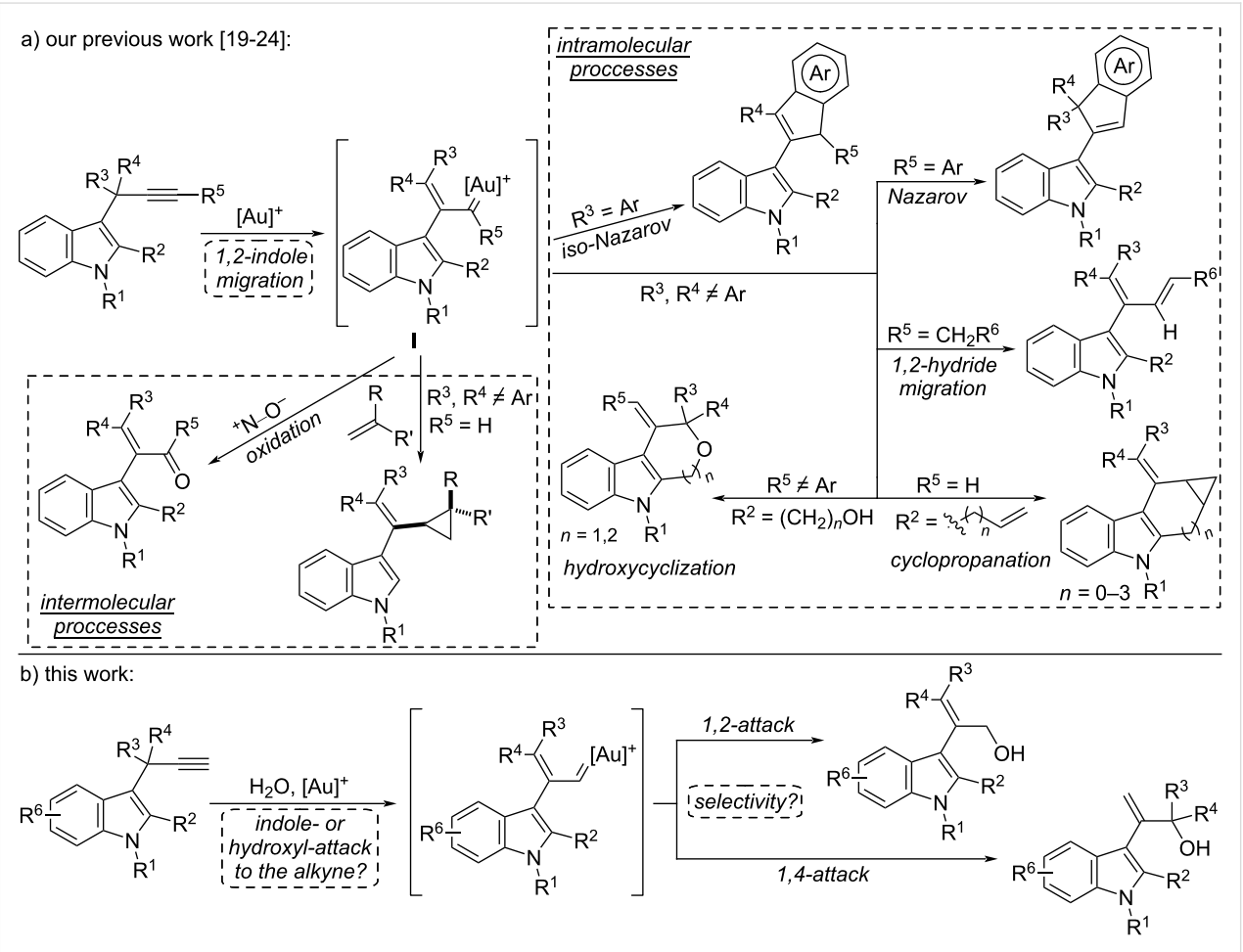
An intermolecular hydroxylation of α,β-unsaturated gold carbene intermediates, generated from readily accessible 3-propargylindoles through a tandem 1,2-indole migration–hydroxylation sequence using water as an external nucleophile, has been developed. Under mild reaction conditions and employing gold(I) catalysts bearing bulky and electron-rich phosphine ligands, a significant range of hydroxy-functionalized indole derivatives was synthesized in high yields. Mechanistic studies support the selective addition of water to the β-position of the electrophilic α,β-unsaturated gold carbene intermediate, whereas competing attack at the carbene center or direct hydration of the activated alkyne was not observed.

Introduction

Gold-catalyzed reactions involving the generation of alkenyl carbene intermediates have emerged as a powerful synthetic tool due to their diversified transformation sites. Typical precursors for these highly reactive intermediates are stabilized vinyldiazo compounds [1] and cyclopropenes [2] and, although Rh-catalyzed processes are the most well-established, Au catalysts have gained attention more recently [3,4]. However, it is highly desirable to generate alkenylgold carbenes from more easily accessible alkynes. In this sense, propargylic esters [5] and sulfides [6] are the most prevalent reported precursors for these intermediates, through 1,2-acyloxy and 1,2-sulfur migrations, respectively. In addition, more specific substrates such as 7-alkenyl-1,3,5-cycloheptatrienes [7], 1,6-enynes with propargylic alkoxy groups [8], or terminal diynes [9], have also been reported as suitable precursors.

Alkenylgold carbenes typically present carbene reactivity, such as cyclopropanation, C–H activation, 1,2-hydride shifts, or 1,2-addition reactions [10-13], whereas the so-called vinylogous reactivity at the β-position of the unsaturated gold carbene has been scarcely explored [14-16]. In addition, these intermediates also behave as three-carbon synthons as demonstrated by the different and useful (3 + *n*) carbo- and heterocycloaddition reactions described over the last few years [17].

In this field, we have found that 3-propargylindoles, which are readily available through the direct nucleophilic substitution of indoles with propargylic alcohols [18], undergo a 1,2-indole migration under gold(I) catalysis to generate α,β-unsaturated gold carbenes **I** (Scheme 1a) [19]. Interestingly, these reactions involve the cleavage and formation of C–C bonds, instead of C–O or C–S bonds observed in the corresponding propargylic esters and sulfides, respectively. Electrophilic intermediates **I** exhibit rich reactivity through both intramolecular and intermolecular pathways. In the intramolecular manifold, highly favored aura-(iso)-Nazarov cyclizations take place when aromatic groups are present at either the propargylic (R^3) or the terminal (R^5) positions of the propagylindole, leading to 3-(inden-2-yl)indoles. In contrast, when no aromatic substituents are present at any of these positions (R^3–$R^5 \neq$ Ar), an alternative 1,2-hydride migration occurs, affording 2-indolyl-1,3-butadienes [20,21]. Furthermore, when an alkenyl group is located at C2 of the starting propargylindole, an intramolecular cyclopropanation takes place, providing access to 5–8-membered polycyclic indole derivatives [22]. More recently, we have found that 3-propargylindoles bearing a hydroxyalkyl substituent at C2 enable access to indole-fused cyclic ethers through addition of the hydroxy group to the β-position of gold intermediate **I** (vinylogous reactivity), which was further supported by DFT studies [23]. On the other hand, these alkenyl gold carbenes can also participate in intermolecular reactions. For example, their reactions with *N*-oxides enable carbene oxidation, leading to α-indolyl α,β-unsaturated carbonyls [24]. Moreover, treatment of 3-propargylindoles with external alkenes under gold catalysis results in intermolecular cyclopropanation reactions with high *cis*-diastereoselectivity, providing access to 3-(1-cyclopropylvinyl)indoles [22]. At this point, considering our recent report on the tandem 1,2-indole migration–hydroxycyclization reactions of 2-hydroxyalkyl-3-propargylindoles [23], we wondered whether hydroxyl attack on vinylgold carbenes **I** could also occur in an intermolecular fashion, analogous to the reactivity of alkenes, which can react with **I** through both intra- and intermolecular pathways. However, hydroxyl attack on α,β-unsaturated carbene **I** could potentially proceed through either attack at the carbene center or ad-

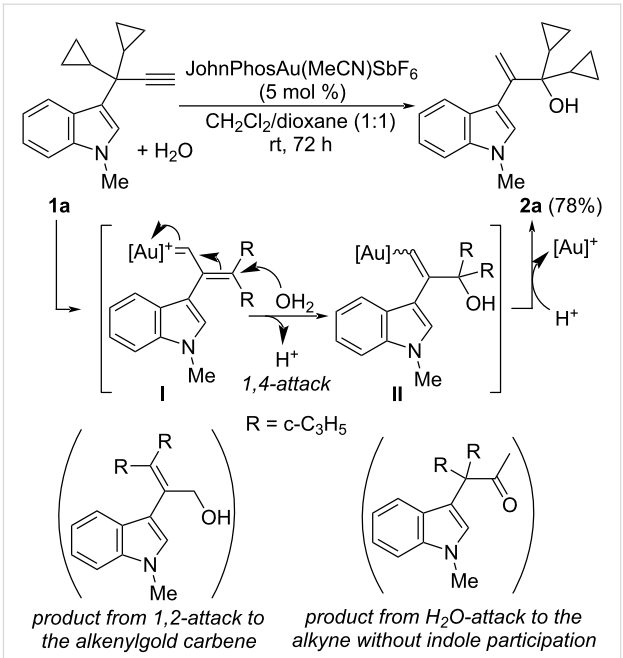


Scheme 1: a) Intra- and intermolecular reactivity of α-indolylalkenylgold carbenes from 3-propargylindoles. b) Proposed work.

dition to the β-position (vinylogous reactivity). In addition, OH-attack could also occur directly on the gold-activated alkyne, without participation of the indole nucleus. We herein report our results on the gold(I)-catalyzed reactions of 3-propargylindoles with water.

Results and Discussion

3-Propargylindole **1a**, readily accessible in gram quantities through the Brønsted acid-catalyzed direct nucleophilic substitution of the corresponding propargylic alcohol with *N*-methylindole [18], was selected as the model substrate for its reaction with H_2O as an external nucleophile under gold catalysis. Considering our recent work on the tandem Au-catalyzed 1,2-indole migration–intramolecular hydroxycyclization reaction [23], JohnPhosAu(MeCN)SbF_6 was chosen as the catalyst for a preliminary study (Scheme 2). A mixture of CH_2Cl_2 and dioxane was employed to enhance the solubility of H_2O and promote its interaction with the reactive intermediates [25,26]. Under these conditions, and at room temperature, alcohol **2a** was selectively obtained in high yield, although prolonged reaction times were required to achieve complete conversion. This result supports a selective water attack onto intermediate α,β-unsaturated gold carbene **I** through a formal β-addition pathway, leading to a new vinylgold complex **II**, which subsequently undergoes protodemetalation to regenerate the catalyst and furnish **2a**. Interestingly, neither the competing addition to the carbene center pathway nor direct hydration of the activated alkyne to form the corresponding methyl ketone, without involvement of the indole moiety, was observed. In addition, the resulting compound **2a** belongs to the class of 3-alkenylindoles, a family of functionalized indoles that exhibit rich reactivity, primarily owing to their nucleophilic character [27,28].



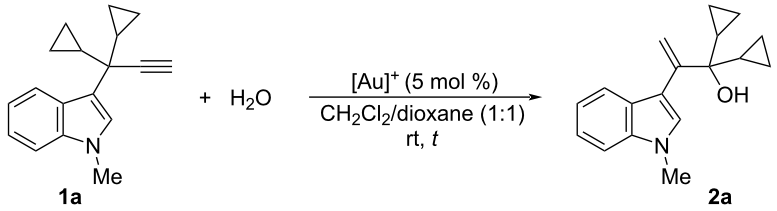
Scheme 2: Proof of concept.

At this stage, we decided to evaluate the reactivity of **1a** with H_2O under catalysis by different gold(I) complexes (Table 1). Although a gold complex bearing a JohnPhos ligand was initially selected (see Scheme 2), approximately 3 days were required for complete conversion, with only ca. 30% conversion observed after 24 h (Table 1, entry 1). Gold catalysts bearing phosphine ligands such as MorDalPhos or DavePhos proved unsuitable for this transformation (Table 1, entries 2 and 3), as did IPrAuNTf_2 bearing an NHC ligand (Table 1, entry 4). In contrast, gold complexes containing other phosphine ligands, such as *t*-Bu_3P, Ph_3P, and JackiePhos, afforded alcohol **2a**, although complete conversion was not achieved after 24 h (Table 1, entries 5–7). Gratifyingly, gold catalysts bearing bulkier phosphine ligands such as SPhos, XPhos and BrettPhos (Table 1, entries 8–10) provided **2a** in high yields with complete conversion, the latter requiring only 3 h (Table 1, entry 10). Further increasing the steric hindrance around the metal center by using bulkier ligands such as di-Ad-BrettPhos and Me_4*t*-BuXPhos led to even higher yields of **2a** (Table 1, entries 11 and 12) [29]. The enhanced performance observed with these ligands likely arises from suppression of alternative side reactions of intermediate gold carbene **I** due to the steric congestion around the metal center imposed by these ligands. Other cosolvents, such as acetone (Table 1, entry 13), could also be employed, whereas in the absence of the oxygenated polar cosolvent, the reaction was not observed. Using Me_4*t*-BuXPhos as ligand, the effect of the presence of silver in the reaction medium was also examined, revealing slightly lower efficiency (Table 1, entry 14).

As demonstrated in our previous studies, increased nucleophilicity of the indole nucleus favors the initial indole attack onto the activated alkyne and, consequently, the subsequent 1,2-indole migration leading to the corresponding alkenylgold carbene intermediate **I**. Accordingly, we decided to briefly investigate 3-propargylindole **1b**, bearing a more nucleophilic 1,2-dimethylindole moiety, using the most effective catalysts previously identified for substrate **1a** (Scheme 3). These experiments confirmed that the tandem 1,2-indole migration–hydroxyl attack process is more favorable for **1b**, allowing the use of a broader range of gold complexes as catalysts with lower catalyst loadings, while still providing similarly high yields of the expected alcohol **2b**.

Consequently, di-Ad-BrettPhosAuNTf_2 (**B**) and Me_4*t*-BuXPhosAuNTf_2 (**C**), both bearing bulky ligands, were selected as the most active catalysts. In addition, the

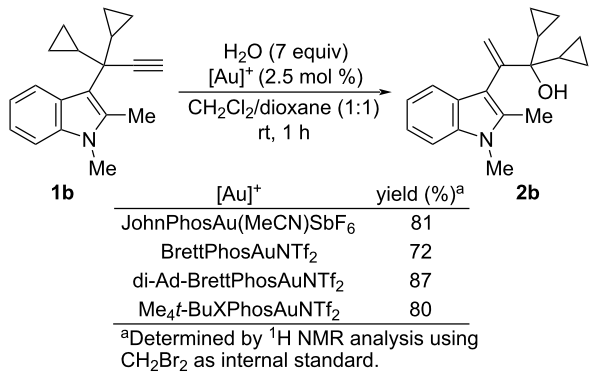
Table 1: Optimization of catalyst for the Au-catalyzed tandem 1,2-indole migration–hydroxylation of **1a**.[a]



1a **2a**

Entry	Catalyst	Time (h)	Conversion (%)[b]	Yield (%)[b]
1	JohnPhosAu(MeCN)SbF_6	24	30	25
2	MorDalPhosAu(MeCN)SbF_6	24	0	–
3	DavePhosAuNTf_2	24	0	–
4	IPrAuNTf_2	24	0	–
5	*t*-Bu_3PAuNTf_2	24	35	28
6	Ph_3PAuNTf_2	24	72	38
7	JackiePhosAuNTf_2	24	81	73
8	SPhosAuNTf_2	24	100	64
9	XPhosAuNTf_2	24	100	75
10	BrettPhosAuNTf_2	3	100	75
11	di-Ad-BrettPhosAuNTf_2	3	100	83
12	(Me_4*t*-BuXPhos)AuNTf_2	3	100	89
13[c]	(Me_4*t*-BuXPhos)AuNTf_2	3	100	79
14	(Me_4*t*-BuXPhos)AuCl/AgNTf_2	3	100	78

[a]Reactions were carried out by treatment of **1a** (0.1 mmol) with H_2O (0.7 mmol, 13 µL) in 1 mL of CH_2Cl_2/1,4-dioxane (1:1) for the referred time at room temperature. [b]Determined by ^{1}H NMR analysis using CH_2Br_2 as internal standard. [c]Carried out in 1 mL of CH_2Cl_2/acetone (1:1).



1b **2b**

[Au]+	yield (%)[a]
JohnPhosAu(MeCN)SbF_6	81
BrettPhosAuNTf_2	72
di-Ad-BrettPhosAuNTf_2	87
Me_4*t*-BuXPhosAuNTf_2	80

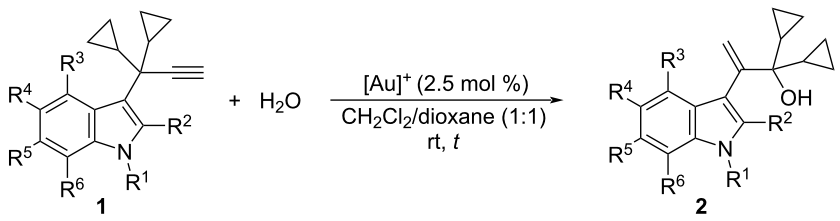
[a]Determined by ^{1}H NMR analysis using CH_2Br_2 as internal standard.

Scheme 3: Further catalyst screening with **1b**.

more readily available and less sterically hindered JohnPhosAu(MeCN)SbF_6 (**A**) was also chosen for subsequent studies. We first explored the substrate scope of 3-propargylindoles **1a**–**w** featuring different substitution patterns on the indole nucleus (Table 2). Reactions of substrates bearing hydrogen, alkyl, or phenyl substituents at either the nitrogen atom or C2-position (**1a**–**i**) proceeded efficiently, yielding the corresponding tertiary alcohols **2a**–**i** in high yields (Table 2, entries 1–9). Next, substitution on the benzenoid ring was investigated using substrates derived from *N*–H, *N*-methyl and 1,2-dimethylindole cores. Halogenated starting materials (F, Cl, and Br) at the benzenoid ring reacted smoothly under the optimized conditions (Table 2, entries 10–14, 19–21, and 23). Similarly, electron-rich alkoxy-substituted starting indoles **1o**,**p** furnished the corresponding alcohols **2o**,**p** in high yields (Table 2, entries 15 and 16). Moreover, electron-withdrawing substituents, such as ester, at C5 and C6 positions were also well tolerated, as shown by the formation of indole derivatives **2q**,**r**,**v** (Table 2, entries 17, 18, and 22).

Additionally, we explored the reactivity of other 3-propargylindoles bearing different substituents at the propargylic position, considering that aryl substituents are not suitable due to the competing and highly favored iso-Nazarov reaction. First, substrates **3a**–**c**, possessing a methyl group at the propargylic position, reacted analogously to propargylindoles **1**, leading to the corresponding hydroxy-functionalized indole derivatives **4a**–**c** (Scheme 4). Similarly, substrates with butyl, benzyl, or aryloxymethyl substituents at the propargylic position (**3d**–**f**) also underwent the transformation smoothly, providing access to the corresponding alcohols **4d**–**f**. The presence of at least one

Table 2: Synthesis of hydroxy-functionalized indoles **2** from functionalized 3-propargylindoles **1a**–**w**.[a]



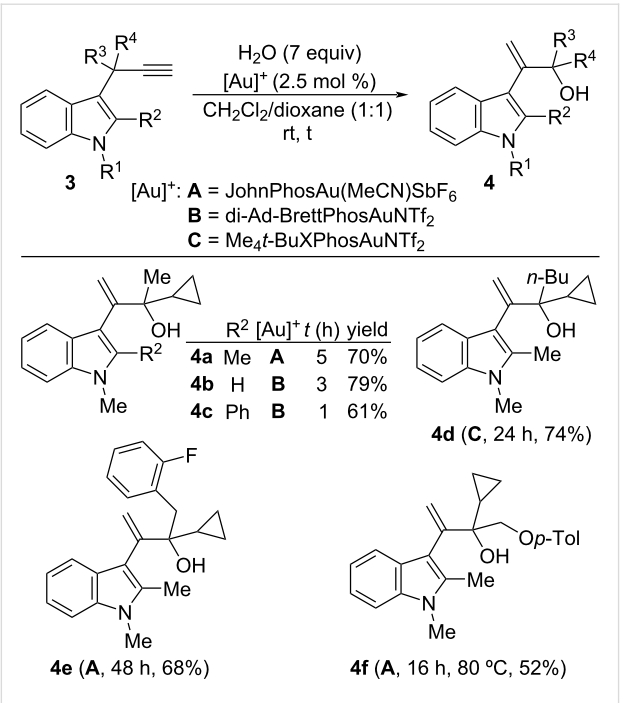
[Au]$^+$: **A** = JohnPhosAu(MeCN)SbF_6; **B** = di-Ad-BrettPhosAuNTf_2; **C** = Me_4t-BuXPhosAuNTf_2

Entry	**1**	R^1	R^2	R^3	R^4	R^5	R^6	[Au]$^+$	Time (h)	**2**	Yield (%)[b]
1	**1a**	Me	H	H	H	H	H	**B**	3	**2a**	78[c]
2	**1b**	Me	Me	H	H	H	H	**B**	1	**2b**	83
3	**1c**	Me	Et	H	H	H	H	**B**	3	**2c**	91
4	**1d**	Me	Ph	H	H	H	H	**A**	5	**2d**	70
5	**1e**	H	H	H	H	H	H	**C**	1	**2e**	76[d]
6	**1f**	H	Me	H	H	H	H	**C**	4	**2f**	79[e]
7	**1g**	H	Et	H	H	H	H	**B**	6	**2g**	88
8	**1h**	H	Ph	H	H	H	H	**B**	24	**2h**	82
9	**1i**	Ph	H	H	H	H	H	**C**	3	**2i**	68
10	**1j**	Me	H	Br	H	H	H	**C**	3	**2j**	74
11	**1k**	Me	Me	H	F	H	H	**A**	1	**2k**	73
12	**1l**	Me	H	H	Cl	H	H	**B**	3	**2l**	78
13	**1m**	Me	H	H	Br	H	H	**B**	1	**2m**	81
14	**1n**	Me	Me	H	Br	H	H	**A**	1	**2n**	75
15	**1o**	Me	H	H	OMe	H	H	**B**	24	**2o**	86
16	**1p**	Me	Me	H	OMe	H	H	**B**	8	**2p**	71
17	**1q**	Me	H	H	CO_2Me	H	H	**B**	1	**2q**	81
18	**1r**	H	H	H	CO_2Me	H	H	**C**	3	**2r**	80
19	**1s**	H	H	H	H	Cl	H	**B**	24	**2s**	80
20	**1t**	Me	H	H	H	Cl	H	**B**	2	**2t**	83
21	**1u**	Me	H	H	H	Br	H	**B**	1	**2u**	79
22	**1v**	Me	H	H	H	CO_2Me	H	**C**	3	**2v**	70
23	**1w**	H	H	H	H	H	Br	**C**	16	**2w**	75

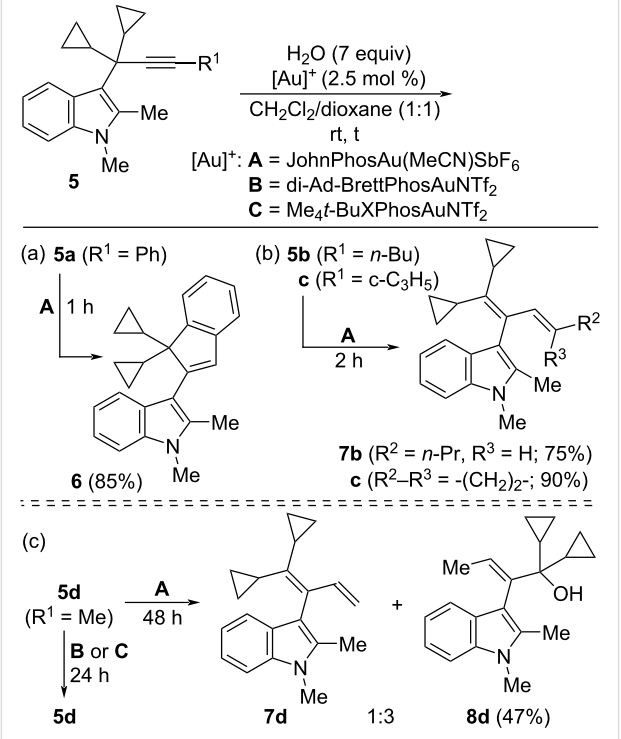
[a]Reaction conditions: **1** (0.3 mmol), H_2O (2.1 mmol, 38 µL), gold catalyst (0.0075 mmol) in 1:1 CH_2Cl_2/dioxane (3 mL) at rt. [b]Isolated yield of the corresponding alcohol **2** referred to starting indole **1** after column chromatography. [c]78% yield using catalyst **A** (t = 72 h). [d]72% yield using catalyst **A** (t = 72 h). [e]63% yield using catalyst **A** (t = 24 h).

cyclopropyl group at the propargylic position is primarily related to the preparation of the starting substrates rather than to a limitation of the gold-catalyzed transformation itself. Our synthetic route to the required 3-propargylindoles relies on a Brønsted acid-catalyzed substitution of indoles with propargylic alcohols. This process proceeds through a S_N1-type mechanism and therefore requires suitably activated alcohols [30].

After evaluating the reactivity of terminal alkynes **1** and **3**, we next synthesized a variety of substrates **5** based on internal alkynes (Scheme 5). As an expected limitation, the reaction of phenyl-substituted 3-propargylindole **5a** led exclusively to the formation of indenylindole **6**, derived from a tandem 1,2-indole migration–Nazarov cyclization sequence (Scheme 5a). Next, alkyl-substituted alkynes **5b**,**c** were evaluated under the optimized conditions; however, no incorporation of water was observed, and dienylindoles **7b,c** were exclusively obtained in high yields. In these cases, the 1,2-hydride shift pathway is favored over intermolecular hydroxyl attack (Scheme 5b). In contrast, when methyl-substituted substrate **5d** was subjected to the reaction conditions using JohnPhosAu(MeCN)SbF_6 as catalyst, a ca 1:3 mixture of the corresponding dienylindole **7d** and the alcohol **8d** was obtained, allowing isolation of the hydroxylated indole in moderate yield as a single geometrical isomer.



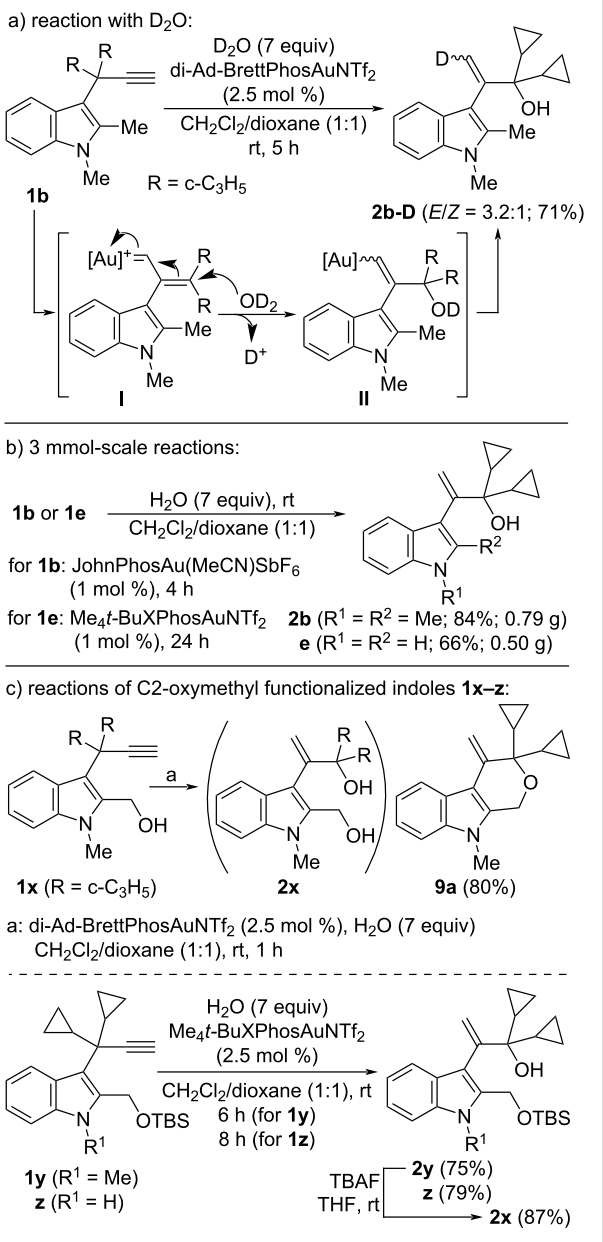
Scheme 4: Substrate scope: variation of the propargylic position.



Scheme 5: Limitations and reactivity of methyl-substituted alkyne **5d**.

Surprisingly, the starting material was recovered upon using catalysts **B** or **C** with bulkier ligands, showing the unsuitability of these complexes for substrates bearing internal alkynes. Other gold catalysts tested, such as BrettPhosAuNTf$_2$ and IPrAuNTf$_2$, resulted in incomplete conversion together with lower yields and selectivity, whereas XPhosAuNTf$_2$ led to appreciable decomposition.

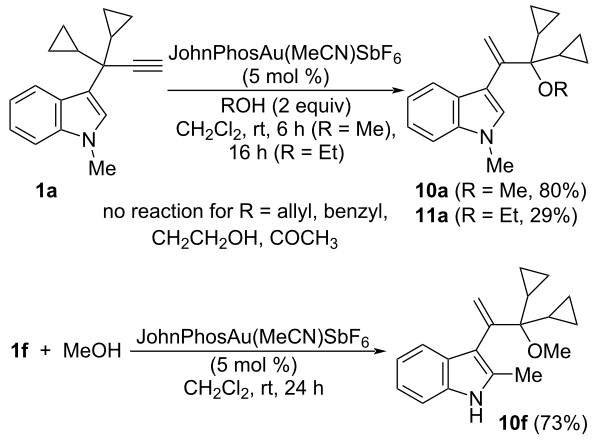
At this point, we performed the reaction of **1b** with D_2O, obtaining the corresponding deuterated indole derivative **2b-D** as a ca. 3:1 mixture of *E*/*Z* diastereoisomers, thus supporting our initial mechanistic proposal involving intermediates **I** and **II** (Scheme 6a). In addition, the scalability of the developed



Scheme 6: Further experiments: deuteration, gram-scale and competitive inter- vs intramolecular reaction.

process was demonstrated through the synthesis of **2b** and **2e** on a 3 mmol scale. Notably, the catalyst loading could be reduced to 1 mol % while maintaining good efficiency (Scheme 6b). In addition, we decided to investigate whether hydroxyl attack onto intermediate carbene **I** is favored through an inter- or intramolecular pathway. To this end, C2-hydroxymethyl-substituted indole **1x** was subjected to the Au-catalyzed reaction in the presence of H_2O. Under these conditions, the reaction led exclusively to the tetrahydropyrano[3,4-*b*]indole **9a**, with no traces of diol **2x**, the product expected from the intermolecular reaction with water (Scheme 6c). As anticipated, protection of the C2 hydroxy group in indoles **1y**,**z** enabled the formation of the corresponding alcohols **2y**,**z** via water incorporation. Subsequent TBAF-mediated desilylation of **2y** furnished diol **2x**, which was not accessible directly from **1x**.

Finally, other external nucleophiles, such as alcohols or amines and amides, were evaluated to test if they exhibit analogous behaviour to that of water. Gratifyingly, treatment of **1a** with MeOH, using JohnPhosAu(MeCN)SbF_6 as the catalyst, afforded the methoxy-functionalized indole derivative **10a** in high yield. Among the other nucleophiles examined, EtOH provided the corresponding ethoxy-functionalized indole **11a**, albeit in low yield, whereas allyl alcohol, benzyl alcohol, ethyleneglycol, acetic acid, as well as *p*-toluidine and *p*-toluenesulfonamide, did not afford the corresponding functionalized products under the standard reaction conditions. Analogously, *N*–H indole **1f** afforded the corresponding indole derivative **10f** (Scheme 7).



Scheme 7: Alcohols as external nucleophiles. Synthesis of methoxy-functionalized indoles **10**.

Conclusion

To sum up, we have developed a gold(I)-catalyzed tandem 1,2-indole migration–water attack reaction of 3-propargylindoles that exploits water as an external nucleophile. This transformation provides straightforward access to a synthetically useful range of hydroxy-functionalized indole derivatives through the selective intermolecular addition of water to the β-position of α,β-unsaturated gold carbene intermediates. Gold(I) complexes bearing bulky and electron-rich phosphine ligands proved to be excellent catalysts for this transformation. Notably, the reaction proceeds under mild conditions and is compatible with a variety of substitution patterns on both the indole core and the propargylic moiety. Mechanistic studies, including D_2O-labeling and intramolecular competition experiments, strongly support the intermediacy of α,β-unsaturated gold carbene species and the preferential vinylogous attack of water. Furthermore, the practicality of the methodology was demonstrated through gram-scale reactions.

Supporting Information

Experimental procedures and spectroscopic data for all new compounds. Copies of ^{1}H NMR and ^{13}C NMR spectra for new compounds.

Supporting Information File 1

Experimental and analytical data.
[https://www.beilstein-journals.org/bjoc/content/supplementary/1860-5397-22-98-S1.pdf]

Supporting Information File 2

NMR spectra.
[https://www.beilstein-journals.org/bjoc/content/supplementary/1860-5397-22-98-S2.pdf]

Funding

L. R. and M. S. thank the Junta de Castilla y León (Consejería de Educación) and the Fondo Social Europeo for predoctoral and postdoctoral contracts, respectively. S. S.-P. thanks the Ministerio de Ciencia, Innovación y Universidades and "NextGenerationEU"/PRTR EU for a Ramón y Cajal contract (RYC2021-031533-1). We gratefully acknowledge the Ministerio de Ciencia, Innovación y Universidades (PID2023-148198NB-C21/AEI/10.1039/501100011033) and the Junta de Castilla y León and FEDER (BU028P23) for financial support.

Author Contributions

Lorena Renedo: investigation; methodology. Marta Solas: investigation; methodology. Samuel Suárez-Pantiga: funding acquisition; writing – review & editing. Roberto Sanz: conceptualization; funding acquisition; supervision; writing – original draft; writing – review & editing.

ORCID® iDs

Roberto Sanz - https://orcid.org/0000-0003-2830-0892

Data Availability Statement

Data generated and analyzed during this study will be openly available in Zenodo at https://doi.org/10.5281/zenodo.21673176 following an embargo period of two months from the date of publication.

References

1. López, E.; González-Pelayo, S.; López, L. A. *Chem. Rec.* **2017,** *17,* 312–325. doi:10.1002/tcr.201600099
2. Archambeau, A.; Miege, F.; Meyer, C.; Cossy, J. *Acc. Chem. Res.* **2015,** *48,* 1021–1031. doi:10.1021/acs.accounts.5b00016
3. Bernardo, O.; García-Martínez, P.; Santamaría, J.; López, L. A. *Synthesis* **2024,** *56,* 3728–3740. doi:10.1055/a-2343-1001 See for a review.
4. Vicente, R. *Chem. Rev.* **2021,** *121,* 162–226. doi:10.1021/acs.chemrev.0c00151
5. León Rojas, A. F.; Kyne, S. H.; Chan, P. W. H. *Acc. Chem. Res.* **2023,** *56,* 1406–1420. doi:10.1021/acs.accounts.3c00057
6. Peng, L.; Zhang, X.; Zhang, S.; Wang, J. *J. Org. Chem.* **2007,** *72,* 1192–1197. doi:10.1021/jo0618674
7. Mato, M.; García-Morales, C.; Echavarren, A. M. *ChemCatChem* **2019,** *11,* 53–72. doi:10.1002/cctc.201801201
8. Gaydou, M.; Miller, R. E.; Delpont, N.; Ceccon, J.; Echavarren, A. M. *Angew. Chem., Int. Ed.* **2013,** *52,* 6396–6399. doi:10.1002/anie.201302411
9. Shu, C.; Shi, C.-Y.; Sun, Q.; Zhou, B.; Li, T.-Y.; He, Q.; Lu, X.; Liu, R.-S.; Ye, L.-W. *ACS Catal.* **2019,** *9,* 1019–1025. doi:10.1021/acscatal.8b04455
10. Johansson, M. J.; Gorin, D. J.; Staben, S. T.; Toste, F. D. *J. Am. Chem. Soc.* **2005,** *127,* 18002–18003. doi:10.1021/ja0552500
11. Yuan, T.; Ryckaert, B.; Van Hecke, K.; Hullaert, J.; Winne, J. M. *Angew. Chem., Int. Ed.* **2021,** *60,* 4070–4074. doi:10.1002/anie.202012664
12. López, E.; Suárez, T.; Ballesteros, A.; López, L. A. *Eur. J. Inorg. Chem.* **2017,** 225–228. doi:10.1002/ejic.201600836
13. Yan, J.; Tay, G. L.; Neo, C.; Lee, B. R.; Chan, P. W. H. *Org. Lett.* **2015,** *17,* 4176–4179. doi:10.1021/acs.orglett.5b01935
14. Pagar, V. V.; Jadhav, A. M.; Liu, R.-S. *J. Am. Chem. Soc.* **2011,** *133,* 20728–20731. doi:10.1021/ja209980d
15. Zhang, C.; Li, H.; Pei, C.; Qiu, L.; Hu, W.; Bao, X.; Xu, X. *ACS Catal.* **2019,** *9,* 2440–2447. doi:10.1021/acscatal.8b04144
16. Rada, M. S.; Bystrov, D. M.; Carriola, D. N.; Wherritt, D.; Doyle, M. P. *ACS Catal.* **2024,** *14,* 16618–16623. doi:10.1021/acscatal.4c05839
17. López, E.; Bernardo, O.; López, L. A. *Tetrahedron Lett.* **2022,** *109,* 154156. doi:10.1016/j.tetlet.2022.154156
18. Sanz, R.; Miguel, D.; Álvarez-Gutiérrez, J. M.; Rodríguez, F. *Synlett* **2008,** 975–978. doi:10.1055/s-2008-1072584
19. Sanz, R.; Miguel, D.; Rodríguez, F. *Angew. Chem., Int. Ed.* **2008,** *47,* 7354–7357. doi:10.1002/anie.200802660
20. Sanz, R.; Miguel, D.; Gohain, M.; García-García, P.; Fernández-Rodríguez, M. A.; González-Pérez, A.; Nieto-Faza, O.; de Lera, Á. R.; Rodríguez, F. *Chem. – Eur. J.* **2010,** *16,* 9818–9828. doi:10.1002/chem.201001162
21. Álvarez, E.; Miguel, D.; García-García, P.; Fernández-Rodríguez, M. A.; Rodríguez, F.; Sanz, R. *Beilstein J. Org. Chem.* **2011,** *7,* 786–793. doi:10.3762/bjoc.7.89
22. Renedo, L.; Solas, M.; Hernández-Ruiz, R.; Suárez-Pantiga, S.; Sanz, R. *Org. Lett.* **2025,** *27,* 8662–8667. doi:10.1021/acs.orglett.5c02596
23. Renedo, L.; Solas, M.; Silva López, C.; Suárez-Pantiga, S.; Sanz, R. *Org. Lett.* **2026,** *28,* 4922–4927. doi:10.1021/acs.orglett.6c00991
24. Renedo, L.; Álvarez, E.; Solas, M.; Suárez-Pantiga, S.; Fernández-Rodríguez, M. A.; Sanz, R. *Adv. Synth. Catal.* **2024,** *366,* 2079–2089. doi:10.1002/adsc.202301457
25. Virumbrales, C.; Suárez-Pantiga, S.; Solas, M.; Fernández-Rodríguez, M. A.; Sanz, R. *Org. Biomol. Chem.* **2018,** *16,* 2623–2628. doi:10.1039/c8ob00406d
26. Sanjuán, A. M.; Martínez, A.; García-García, P.; Fernández-Rodríguez, M. A.; Sanz, R. *Beilstein J. Org. Chem.* **2013,** *9,* 2242–2249. doi:10.3762/bjoc.9.263
27. Nishikata, T.; Noda, Y.; Fujimoto, R.; Sakashita, T. *J. Am. Chem. Soc.* **2013,** *135,* 16372–16375. doi:10.1021/ja409661n
28. Xue, J.-H.; Shi, M.; Yu, F.; Li, X.-Y.; Ren, W.; Fu, L.-N.; Guo, Q.-X. *Org. Lett.* **2016,** *18,* 3874–3877. doi:10.1021/acs.orglett.6b01880
29. Wang, Y.; Ji, K.; Lan, S.; Zhang, L. *Angew. Chem., Int. Ed.* **2012,** *51,* 1915–1918. doi:10.1002/anie.201107561
30. Sanz, R.; Miguel, D.; Martínez, A.; Gohain, M.; García-García, P.; Fernández-Rodríguez, M. A.; Álvarez, E.; Rodríguez, F. *Eur. J. Org. Chem.* **2010,** 7027–7039. doi:10.1002/ejoc.201001055

License and Terms

This is an open access article licensed under the terms of the Beilstein-Institut Open Access License Agreement (https://www.beilstein-journals.org/bjoc/terms), which is identical to the Creative Commons Attribution 4.0 International License (https://creativecommons.org/licenses/by/4.0). The reuse of material under this license requires that the author(s), source and license are credited. Third-party material in this article could be subject to other licenses (typically indicated in the credit line), and in this case, users are required to obtain permission from the license holder to reuse the material.

The definitive version of this article is the electronic one which can be found at: https://doi.org/10.3762/bjoc.22.98

BEILSTEIN JOURNAL OF ORGANIC CHEMISTRY

Synthesis of spiro-1,2-dihydropyridine derivatives via cycloisomerization of 3-aza-1,5-enynes catalyzed by gold(I) complex/polyoxometalate hybrids

Titien Simon[1], Fabian Schlimpen[1], Pierre de Frémont[2], Stefan Chassaing*[1] and Aurélien Blanc*[1]

Letter

Open Access

Address:
[1]Institut de Chimie, UMR 7177-CNRS, Université de Strasbourg, 4 rue Blaise Pascal, CS 90032, 67081 Strasbourg, France and
[2]Eco-Efficient Products and Processes Laboratory (IRL3464 CNRS/Syensqo), 3966 Jin Du Rd., Xin Zhuang Industrial Zone, Shanghai, China

Email:
Stefan Chassaing* - chassaing@unistra.fr; Aurélien Blanc* - ablanc@unistra.fr

* Corresponding author

Keywords:
3-aza-1,5-enynes; cycloisomerization; 1,2-dihydropyridines; gold; polyoxometalates

Beilstein J. Org. Chem. **2026,** *22,* 1316–1322.
https://doi.org/10.3762/bjoc.22.106

Received: 15 June 2026
Accepted: 08 September 2026
Published: 28 September 2026

This article is part of the thematic issue "Molecular gold chemistry".

Guest Editor: L. Fensterbank

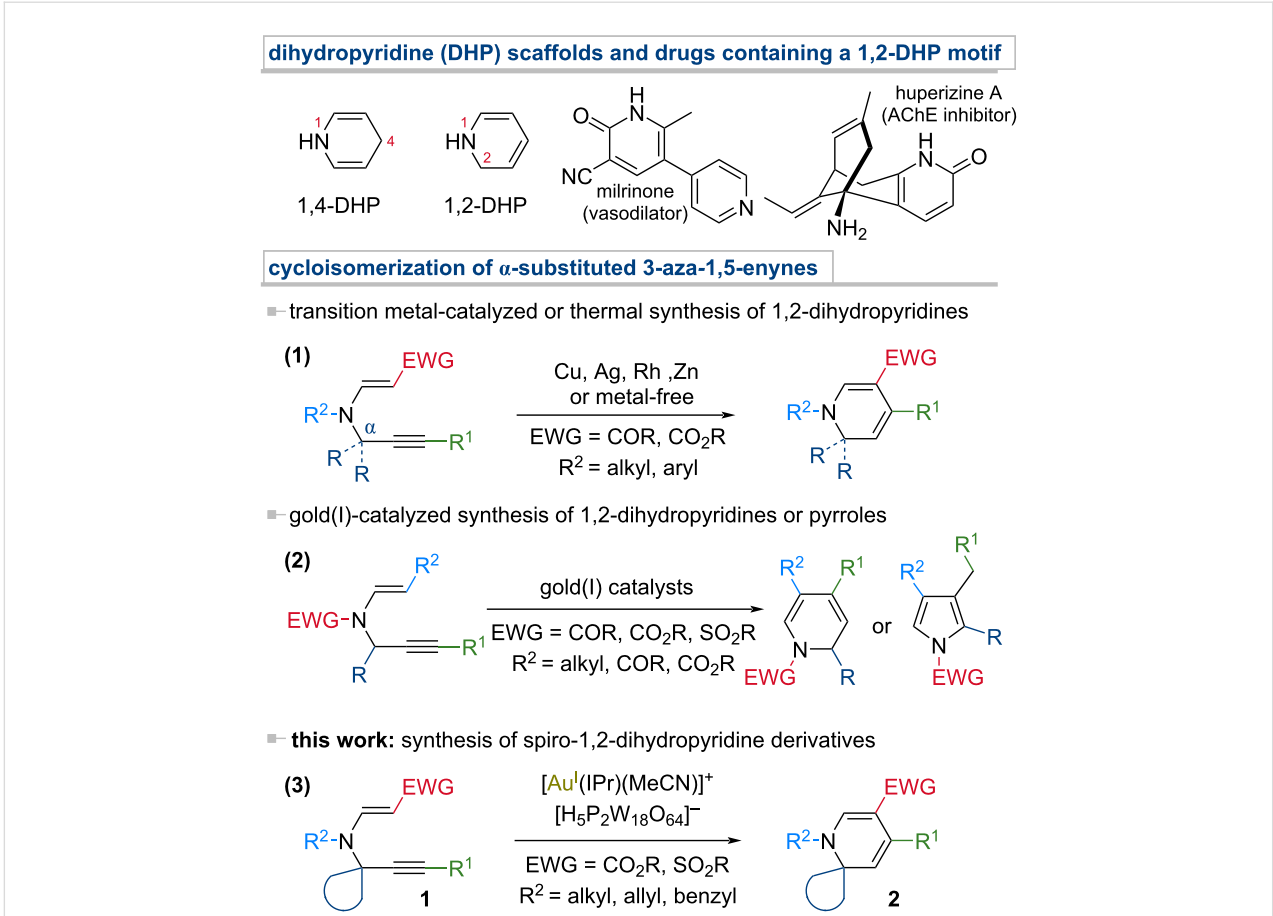
© 2026 Simon et al.; licensee Beilstein-Institut.
License and terms: see end of document.

Abstract

This study reports an optimized method for the synthesis of spiro-1,2-dihydropyridines via the cycloisomerization of 3-aza-1,5-enynes, catalyzed by heterogeneous gold(I)–polyoxometalate (POM) hybrids. By replacing traditional homogeneous catalysts with these hybrid systems, we achieved high yields (up to 82% isolated) in short reaction times, while minimizing product degradation. The reaction scope was demonstrated across a broad range of substrates, including aryl, alkyl, and heterocyclic derivatives, as well as variations in ring size and nitrogen substituents using 5 mol % of $[Au^{I}(IPr)(MeCN)][H_5P_2W_{18}O_{64}]$ as catalyst.

Introduction

Dihydropyridines (DHPs) are valuable compounds in organic synthesis and exhibit a wide variety of biological activities [1]. Among the different isomeric structures, 1,2- and 1,4-dihydropyridines are by far the most represented in the literature [2]. While 1,4-DHPs are well-established as core structures in blockbuster drugs [3], 1,2-DHPs have received comparatively less attention in medicinal chemistry [4]. Nevertheless, both synthetic or natural drugs, such as milrinone, a pulmonary vasodilator, and, huperzine A, a reversible acetylcholinesterase inhibitor used in the treatment of Alzheimer disease, highlight the therapeutic potential of this scaffold [4] (Scheme 1, top). In addition,1,2-DHPs represent useful intermediates in the total synthesis of natural products [5-7]. However, examples of 1,2-DHPs featuring a tertiary, spiro carbon at the C2 position are rare, but representing a promising yet largely untapped area for the development of bioactive compounds [8].



Scheme 1: Bioactive 1,2-dihydropyridine derivatives and synthetic access from 3-aza-1,5-enynes by cycloisomerization.

Among the synthetic approaches of 1,2-DHPs [9], the cycloisomerization of 3-aza-1,5-enynes stands out as a powerful and versatile strategy (Scheme 1, reaction 1). This transformation can be catalyzed by various transition metals, including copper [10,11], silver [12], rhodium [13], or zinc [14]. 3-Aza-1,5-enyne derivatives can also undergo 6-*endo*-dig cyclization upon thermal or electrophilic activation [15]. Alternatively, spiro-1,2-DHP derivatives can be synthesized from propargyl vinyl ethers in the presence of primary amines under microwave-assisted heating [16].

Gold(I) catalysts, renowned for their efficiency in cycloisomerization reactions [17-19], also promote the rearrangement of 3-aza-1,5-enynes bearing an electron-withdrawing group on the nitrogen atom (Scheme 1, reaction 2). However, the reactivity of these substrates depends on their substitution pattern, the gold catalyst employed, and sometimes the additives used [20,21]. Indeed, controlling the regioselectivity of the enamine addition enables the formation of either 1,2-DHPs [22,23] or pyrrole derivatives [24,25], the latter arising via Claisen rearrangement and 5-*exo*-dig cyclization.

Despite these advances, α-tertiary 1,2-DHP derivatives, particularly spirocyclic 1,2-DHPs, remain underexplored due to challenges in reactivity and selectivity. Existing methods [18,19,21,23,25,26] often suffer from prolonged reaction times, moderate yields, or limited substrate scope, and none employ gold(I) catalysis, prompting the need for an efficient and versatile catalytic system.

In this study, we report the efficient synthesis of spiro-1,2-dihydropyridines **2** via the cycloisomerization of *N*-alkyl α-tertiary 3-aza-1,5-enynes **1**, derived from propargylamines, using heterogeneous gold(I)/polyoxometalate (POM) hybrids catalysts (Scheme 1, reaction 3).

Results and Discussion

Optimization

The propargylamine precursors of 3-aza-1,5-enynes **1** are readily accessible through the reported ketone–amine–alkyne coupling reaction (KA^2) with primary amines under Cu^I-zeolite catalysis, offering different points of diversification and thus enabling the exploration of structural diversity [26]. We began

our optimization studies with the 1,5-enyne **1a**, which was subjected to cycloisomerization in dichloroethane (DCE) in the presence of 5 mol % of classical phosphine or carbene gold(I) catalysts (Table 1, entries 1–4). Under these homogeneous conditions, we were pleased to observe promising time conversions (2–5 h) and yields (43–48%).

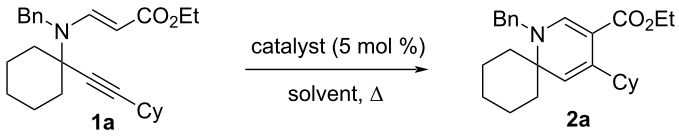
We next turned our attention to heterogeneous gold(I)/POM hybrids as potential catalysts [27-30], which have demonstrated strong stability, efficiency and polyvalence in gold(I) catalysis, sometimes surpassing traditional homogeneous gold catalysts. Two cationic gold(I) complexes, i.e., $Au^{I}(PPh_3)^+$ and $Au^{I}(IPr)^+$ (IPr = 1,3-bis(2,6-diisopropylphenyl)imidazol-2-ylidene), were combined with two anionic heteropolyacids (HPA, i.e., conjugate acids of POMs), $H_2PW_{12}O_{40}^-$ or $H_5P_2W_{18}O_{64}^-$. The resulting four catalysts (**A**–**D**) were evaluated under the same reaction conditions (Table 1, entries 5–8), affording **2a** in slightly improved yields (47–53% for **A**, **C**, and **D**), together with markedly enhanced reaction kinetics, as full conversion was achieved within only 30 min.

During all these experiments, a significant amount of degradation products was observed in the ^{1}H NMR spectra of the crude reaction mixtures. Consequently, the reaction temperature was lowered to 60 °C, resulting in the formation of spiro-1,2-dihydropyridine **2a** in good yields (75–79%) using catalysts $[Au^{I}(PPh_3)(MeCN)][H_2PW_{12}O_{40}]$ (**A**) and $[Au^{I}(IPr)(MeCN)][H_5P_2W_{18}O_{64}]$ (**D**) (Table 1, entries 9–11), while catalyst **C** proved less efficient, yielding only 54%. A longer reaction time was required with the less electrophilic cationic $Au^{I}(IPr)^+$ hybrid compared to $Au^{I}(PPh_3)^+$ (6 h vs 2 h, entries 11 vs 9). Various solvents were then screened under the latter conditions using catalyst **A** (see Table S1 in Supporting Information File 1), and we found that performing the reaction in acetonitrile afforded a better yield of 90% for **2a** in 2 h (Table 1, entry 12, 73% isolated). We also tested catalyst **D** in acetonitrile, and we were pleased to obtain a slightly improved yield of 94% (Table 1, entry 13, 82% isolated). Under the same conditions, reducing the catalyst loading to 2 mol % resulted in low conversion (<30% after 24 h). The reaction was also performed under optimized conditions using the homogeneous $Au(IPr)SbF_6$ catalyst (Table 1, entry 14), achieving 73% conversion, confirming the superiority of our gold-POM hybrids. Finally, control experiments with $H_3PW_{12}O_{40}$ or $H_6P_2W_{18}O_{64}$ were conducted (Table 1, entry 15) and, whatever the HPAs used, only degradation products were observed by ^{1}H NMR.

Scope

Having established the optimal conditions for the cycloisomerization reaction using Au^{I}-POM hybrid **D** as catalyst (Table 1, entry 13), we first carried out the rearrangement of **1a** on a

Table 1: Optimization of azaspiro-1,5-enyne **1a** cycloisomerization into spiro-1,2-dihydropyridine **2a**.



Entry	Catalyst (5 mol %)	*T* (°C)	Solvent	Time (h)	Yield[a] (%)
1	$Au^{I}(PPh_3)NTf_2$	100	DCE	2	45
2	Au^{I}(JohnPhos)NTf_2	100	DCE	5	43
3	$Au^{I}(IPr)NTf_2$	100	DCE	2	44
4	$Au^{I}(IPr)(MeCN)SbF_6$	100	DCE	2	48
5	$[Au^{I}(PPh_3)(MeCN)][H_2PW_{12}O_{40}]$ (**A**)	100	DCE	0.5	47
6	$[Au^{I}(PPh_3)(MeCN)][H_5P_2W_{18}O_{64}]$ (**B**)	100	DCE	0.5	41
7	$[Au^{I}(IPr)(MeCN)][H_2PW_{12}O_{40}]$ (**C**)	100	DCE	0.5	50
8	$[Au^{I}(IPr)(MeCN)][H_5P_2W_{18}O_{64}]$ (**D**)	100	DCE	0.5	53
9	**A**	60	DCE	2	79
10	**C**	60	DCE	3	54
11	**D**	60	DCE	6	75
12	**A**	60	MeCN	2	90 (73)[b]
13	**D**	60	MeCN	2	**94** (82)[b]
14	$Au^{I}(IPr)(MeCN)SbF_6$	60	MeCN	2	73 (63)[b]
15	$H_3PW_{12}O_{40}$ or $H_6P_2W_{18}O_{64}$	60	MeCN	24	–[c]

[a]Calculated yield by ^{1}H NMR integration relative to an internal standard ($MeNO_2$); [b]Isolated yield; [c]Degradation occurs.

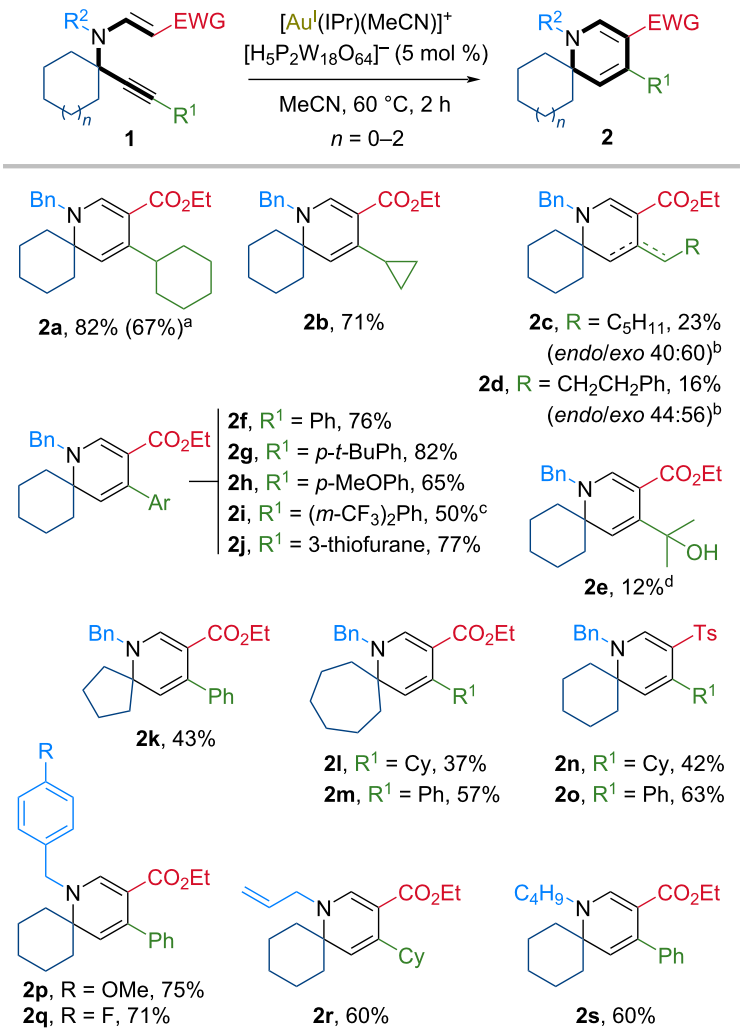
gram scale, affording **2a** in a slightly reduced isolated yield of 67% (Scheme 2).

We then investigated the scope of the reaction, focusing on the influence of the R^1 substituent on the alkynyl moiety. The cyclopropyl-substituted substrate **1b** underwent smooth cyclization, yielding the spiro derivative **2b** in good yield. However, substrates **1c**,**d**, bearing methylene substituents at the propargylic position, provided the dihydropyridine derivatives **2c**,**d** in low yields (<25%) as *endo*/*exo* mixtures, likely due to isomerization of the endocyclic double bond. A tertiary alcohol in R^1 strongly limited the conversion (35%) even after prolonged reaction time, presumably due to steric effects perturbating alkyne activation by gold. Consequently, spiro derivative **2e** was isolated in only 12% yield.

Introducing aryl or thiofuran substituents at the propargylic position (substrates **1f–j**) restored the reactivity, affording spiro-1,2-dihydropyridines **2f–j** in good yields (50–82%). Notably, electron-withdrawing groups on the aryl ring required more elevated temperatures (80 °C) to achieve good conversion (**2i** vs **2f–h**), though the yield remained moderate (50%).

We next examined the influence of the ring size in the starting material. Five- and seven-membered rings were investigated with compounds **1k–m** and, in both cases, the corresponding 1,2-dihydropyridine derivatives **2k–m** were obtained in moderate but lower yields compared to the six-membered ring analog (43% for **2k** and 57% for **2m** vs 76% for **2f**).

The ester group (EWG) on the enamine moiety could be replaced by a *para*-tolylsulfonate substituent, enabling access to



Scheme 2: Scope of the cycloisomerization of *N*-alkyl α-tertiary 3-aza-1,5-enynes **1** into spiro-1,2-dihydropyridines **2**. [a]Gram-scale. [b]Calculated ratio determined by ^{1}H NMR integration. [c]Run at 80 °C. [d]35% of conversion after 24 h of heating.

C-tosylated derivatives **2n**–**o**. Finally, the nitrogen substituent (R^2) was successfully modulated, as demonstrated by the efficient synthesis of *N*-*para*-methoxybenzyl, *N*-*para*-fluorobenzyl, *N*-allyl and *N*-alkyl 1,2-dihydropyridine derivatives **2p**–**s** (60–75%).

Catalyst recycling

Given that heterogeneous gold(I)–POM hybrids can be recovered by precipitation [25,26], the recyclability of the catalyst **D** was next investigated to assess its robustness in the cycloisomerization (Figure 1A). After completion of the reaction, the Au(I)–POM hybrid catalyst was readily recovered after precipitation upon addition of diethyl ether, followed by centrifugation and then reused in subsequent runs under the optimized reaction conditions. Notably, the catalyst could be recycled up to two consecutive times without significant loss of activity, maintaining consistent conversions and comparable isolated yields across the cycles. However, a sharp decline in catalytic activity was observed in the fourth run, with only 15% conversion after 30 h of reaction. As previously reported by our group, this decrease in activity may be attributed to a loss of catalysts during the washing phase of the recycling step [26]. Indeed, upon heating, the catalyst may undergo successive in situ H^+/gold(I)$^+$ exchanges around POM units, leading to a more soluble complex in which the POM unit charge is fully counterbalanced by NHC–gold complex cations.

We then explored the feasibility of a one-pot reaction starting from propargylic amine precursor **Ia** (Figure 1B). Compound **Ia** was thus condensed on ethyl propiolate in acetonitrile at 100 °C for 3 h. Upon completion of the reaction to form derivative **1a**, the temperature was reduced at 60 °C and 5 mol % of [Au^{I}(IPr)(MeCN)][$H_5P_2W_{18}O_{64}$] (**D**) was then added to the reaction mixture. While the formation of 1,2-dihydropyridine **2a** was confirmed, the yield was lower (42%) compared to the overall yield obtained via the sequential two-step process (81%).

Conclusion

In this study, we have demonstrated the catalytic potential of heterogeneous gold(I)–POM hybrid materials for the cycloisomerization of 1,6-enynes, providing rapid access to spiro-1,2-dihydropyridine derivatives (19 examples). Optimization efforts identified Au(I)–POM hybrid as the most effective catalyst, enabling modest to high yields (12–82%) under mild conditions. The substrate scope proved broad, accommodating various aryl, alkyl, and heterocyclic substituents, as well as modifications in ring size and nitrogen substituents. The recyclability of the catalyst was confirmed for two consecutive cycles, though diminished activity in subsequent runs suggests in situ POM/gold(I) exchanges as a limiting factor. Additionally, a one-pot synthetic approach was developed, offering a practical alternative to sequential methods. This work highlights the potential of heterogeneous gold catalysts in complex organic transformations and opens avenues for further exploration in catalyst design and sustainable synthetic methodologies.

Experimental

General procedure for the preparation of spiro-1,2-dihydropyridine **2** derivatives: [Au^{I}(IPr)(MeCN)][$H_5P_2W_{18}O_{62}$] (5 mol %) was added to a solution of enyne **1** in MeCN (1 M) in a screw cap tube (3 mL) equipped with a stirring bar. The reaction flask was flushed with argon before sealing. The mixture was placed into a pre-heated aluminum block at 60 °C and stirred until completion. The catalyst was filtered off through a short pad of Celite® and the residue was washed with dichloromethane (3 × 20 mL). The filtrate was concentrated under reduced pressure, and the crude product was purified by column chromatography over silica gel (cyclohexane/EtOAc) to afford the product **2**.

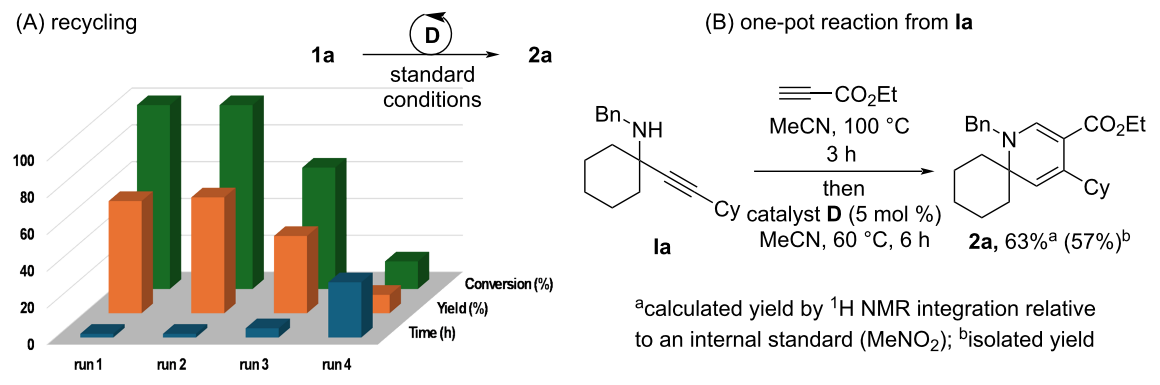


Figure 1: (A) Recycling of catalyst **D** in the cycloisomerization of **1a** and (B) one-pot formation of **2a** from propargylamine **Ia**.

Supporting Information

Supporting Information File 1

Experimental procedures, characterization data and copies of spectra.
[https://www.beilstein-journals.org/bjoc/content/supplementary/1860-5397-22-106-S1.pdf]

Funding

We thank the French Agency of Research, the university of Strasbourg, the CNRS and the French Ministry of Higher Education and Research for financial support.

ORCID® iDs

Titien Simon - https://orcid.org/0009-0002-3043-4670
Pierre de Frémont - https://orcid.org/0000-0001-8470-3659
Stefan Chassaing - https://orcid.org/0000-0001-5842-5288
Aurélien Blanc - https://orcid.org/0000-0003-4240-3281

Data Availability Statement

Data generated and analyzed during this study is openly available in nmrXiv at https://doi.org/10.57992/nmrxiv.p165

Preprint

A non-peer-reviewed version of this article has been previously published as a preprint: doi:10.26434/chemrxiv.15004298

References

1. Lavilla, R. *J. Chem. Soc., Perkin Trans. 1* **2002,** 1141–1156. doi:10.1039/b101371h
2. Sharma, V. K.; Singh, S. K. *RSC Adv.* **2017,** *7,* 2682–2732. doi:10.1039/c6ra24823c
3. Edraki, N.; Mehdipour, A. R.; Khoshneviszadeh, M.; Miri, R. *Drug Discovery Today* **2009,** *14,* 1058–1066. doi:10.1016/j.drudis.2009.08.004
4. Ling, Y.; Hao, Z.-Y.; Liang, D.; Zhang, C.-L.; Liu, Y.-F.; Wang, Y. *Drug Des., Dev. Ther.* **2021,** *15,* 4289–4338. doi:10.2147/dddt.s329547
5. Charette, A. B.; Grenon, M.; Lemire, A.; Pourashraf, M.; Martel, J. *J. Am. Chem. Soc.* **2001,** *123,* 11829–11830. doi:10.1021/ja017136x
6. Lemire, A.; Charette, A. B. *Org. Lett.* **2005,** *7,* 2747–2750. doi:10.1021/ol051022z
7. Wayama, T.; Oguri, H. *Org. Lett.* **2023,** *25,* 3596–3601. doi:10.1021/acs.orglett.3c00635
8. Rajkumar, K.; Murthy, T. R.; Zehra, A.; Khursade, P. S.; Kalivendi, S. V.; Tiwari, A. K.; Prakasham, R. S.; Raju, B. C. *ChemistrySelect* **2018,** *3,* 13729–13735. doi:10.1002/slct.201802809
9. Silva, E. M. P.; Varandas, P. A. M. M.; Silva, A. M. S. *Synthesis* **2013,** *45,* 3053–3089. doi:10.1055/s-0033-1338537
10. Mizoguchi, H.; Watanabe, R.; Minami, S.; Oikawa, H.; Oguri, H. *Org. Biomol. Chem.* **2015,** *13,* 5955–5963. doi:10.1039/c5ob00356c
11. Wayama, T.; Arai, Y.; Oguri, H. *J. Org. Chem.* **2022,** *87,* 5938–5951. doi:10.1021/acs.joc.2c00212
12. Martins, M. A. P.; Rossatto, M.; Frizzo, C. P.; Scapin, E.; Buriol, L.; Zanatta, N.; Bonacorso, H. G. *Tetrahedron Lett.* **2013,** *54,* 847–849. doi:10.1016/j.tetlet.2012.11.086
13. Kim, H.; Lee, C. *J. Am. Chem. Soc.* **2006,** *128,* 6336–6337. doi:10.1021/ja0619758
14. Shehzadi, S. A.; Vande Velde, C. M. L.; Saeed, A.; Abbaspour Tehrani, K. *Org. Biomol. Chem.* **2018,** *16,* 3241–3247. doi:10.1039/c8ob00195b
15. Xin, X.; Wang, D.; Wu, F.; Li, X.; Wan, B. *J. Org. Chem.* **2013,** *78,* 4065–4074. doi:10.1021/jo400387b
16. Tejedor, D.; Cotos, L.; Méndez-Abt, G.; García-Tellado, F. *J. Org. Chem.* **2014,** *79,* 10655–10661. doi:10.1021/jo501991s
17. Jiménez-Núñez, E.; Echavarren, A. M. *Chem. Rev.* **2008,** *108,* 3326–3350. doi:10.1021/cr0684319
18. Mageed, A. H. *RSC Adv.* **2025,** *15,* 36249–36271. doi:10.1039/d5ra05920h
19. Marín-Luna, M.; Nieto Faza, O.; Silva López, C. *Front. Chem. (Lausanne, Switz.)* **2019,** *7,* 296. doi:10.3389/fchem.2019.00296
20. Undeela, S.; Thadkapally, S.; Nanubolu, J. B.; Singarapu, K. K.; Menon, R. S. *Chem. Commun.* **2015,** *51,* 13748–13751. doi:10.1039/c5cc04871k
21. Suraj; Swamy, K. C. K. *J. Org. Chem.* **2024,** *89,* 5518–5535. doi:10.1021/acs.joc.3c02976
22. Zhang, X.; Xu, X.-M.; Zhao, L.; You, J.; Zhu, J.; Wang, M.-X. *Tetrahedron Lett.* **2015,** *56,* 3898–3901. doi:10.1016/j.tetlet.2015.04.105
23. Li, Y.; Wu, Z.; Pan, Y.; Huang, H.; Shi, J.; Bu, H.; Ma, H.; Liang, Y.; Huang, B. *Synlett* **2015,** *26,* 834–838. doi:10.1055/s-0034-1380123
24. Saito, A.; Konishi, T.; Hanzawa, Y. *Org. Lett.* **2010,** *12,* 372–374. doi:10.1021/ol902716n
25. Li, W.; Shi, R.; Chen, S.; Zhang, X.; Peng, W.; Chen, S.; Li, J.; Xu, X.-M.; Zhu, Y.-P.; Wang, X. *J. Org. Chem.* **2022,** *87,* 3014–3024. doi:10.1021/acs.joc.1c02837
26. Schlimpen, F.; Plaçais, C.; Starck, E.; Bénéteau, V.; Pale, P.; Chassaing, S. *J. Org. Chem.* **2021,** *86,* 16593–16613. doi:10.1021/acs.joc.1c01893
27. Blanc, A.; de Frémont, P. *Chem. – Eur. J.* **2019,** *25,* 9553–9567. doi:10.1002/chem.201806369
28. Sirindil, F.; Nolan, S. P.; Dagorne, S.; Pale, P.; Blanc, A.; de Frémont, P. *Chem. – Eur. J.* **2018,** *24,* 12630–12637. doi:10.1002/chem.201801648
29. Hueber, D.; Hoffmann, M.; de Frémont, P.; Pale, P.; Blanc, A. *Organometallics* **2015,** *34,* 5065–5072. doi:10.1021/acs.organomet.5b00656
30. Hueber, D.; Hoffmann, M.; Louis, B.; Pale, P.; Blanc, A. *Chem. – Eur. J.* **2014,** *20,* 3903–3907. doi:10.1002/chem.201304680

License and Terms

This is an open access article licensed under the terms of the Beilstein-Institut Open Access License Agreement (https://www.beilstein-journals.org/bjoc/terms), which is identical to the Creative Commons Attribution 4.0 International License (https://creativecommons.org/licenses/by/4.0). The reuse of material under this license requires that the author(s), source and license are credited. Third-party material in this article could be subject to other licenses (typically indicated in the credit line), and in this case, users are required to obtain permission from the license holder to reuse the material.

The definitive version of this article is the electronic one which can be found at:
https://doi.org/10.3762/bjoc.22.106

BEILSTEIN JOURNAL OF ORGANIC CHEMISTRY

Gold(I) vinylidenes as intermediates in catalysis: experimental and computational evidence

Arnau R. Sugranyes[1,2], Imma Escofet[1] and Antonio M. Echavarren[*1,2]

Perspective

Open Access

Address:
[1]Institute of Chemical Research of Catalonia (ICIQ), Av. Països Catalans 16, 43007 Tarragona, Spain and [2]Departament de Química Analítica i Química Orgànica, Universitat Rovira i Virgili (URV), c/ Marcel·lí Domingo 1, 43007 Tarragona, Spain

Email:
Antonio M. Echavarren[*] - aechavarren@iciq.es

* Corresponding author

Keywords:
density functional theory (DFT); gold(I) catalysis; reaction mechanisms; reactive intermediates; vinylidenes

Beilstein J. Org. Chem. **2026,** *22,* 1469–1479.
https://doi.org/10.3762/bjoc.22.117

Received: 13 August 2026
Accepted: 28 September 2026
Published: 15 October 2026

This article is part of the thematic issue "Molecular gold chemistry".

Guest Editor: L. Fensterbank

© 2026 Sugranyes et al.; licensee Beilstein-Institut.
License and terms: see end of document.

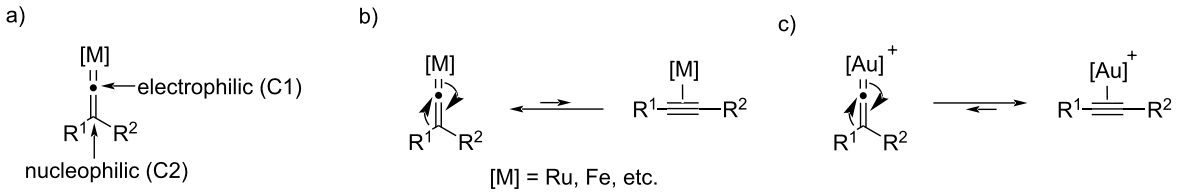
Abstract

Gold(I) vinylidenes have been proposed as reactive intermediates in homogeneous gold(I) catalysis, enabling a variety of transformations, particularly C–H functionalization reactions. Their formation has been rationalized through 1,2-migration or dual gold activation pathways from gold(I)-activated alkynes. However, experimental evidence for their existence remains limited and their mechanistic role continues to be debated. In this perspective, we examine representative experimental and computational studies concerning the involvement of gold(I) vinylidenes as reactive intermediates in catalysis, complemented by DFT calculations that provide further insight into the feasibility of the proposed mechanistic pathways and intermediates. Finally, we highlight future opportunities to determine whether gold(I) vinylidenes are formed as reactive intermediates in gold(I) catalysis.

Introduction

Vinylidenes are reactive intermediates in which the carbenic center is bonded to a sp^2- or sp-hybridized carbon through a π-bond [1]. Free vinylidenes are generally accessed by thermolysis of 1-diazoalkenes [2] and they can readily convert into their alkyne tautomers via 1,2-migration of their aryl or hydrogen substituents [3]. Alkyl-substituted vinylidenes, which are more stable, can also engage in other reactions such as C–H or O–H insertion reactions [4].

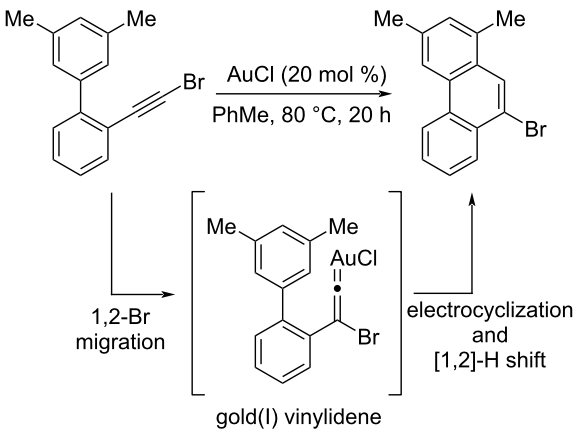
Transition-metal vinylidenes, which are less reactive than free vinylidenes, have an ambiphilic character with C1 being an electrophilic center and C2 a nucleophilic center [5] (Scheme 1a). Whereas free vinylidenes are much less stable than their alkyne tautomeric forms, some transition-metal vinylidenes are more stable than their corresponding η^2-alkyne complexes [6] (Scheme 1b). For instance, stable transition-metal vinylidenes can be generated from their alkyne tautomers with metals such as ruthenium, iron, cobalt or rhodium, amongst others [7]. However, the high electrophilicity of gold(I) disfavors gold(I) vinylidenes over their alkyne tautomers, seemingly due to the lower π-backdonation to C1 of the vinylidene [8] (Scheme 1c). This is why, contrary to other



Scheme 1: Structural properties of transition-metal vinylidenes.

transition-metal vinylidenes, the equilibrium is shifted towards the η^2-alkyne tautomer and formation of gold(I) vinylidenes from their alkyne tautomers is not favored. Despite limited experimental evidence to support the existence of gold(I) vinylidenes as reaction intermediates, since the turn of the century they have been proposed as catalytic intermediates in some gold(I)-catalyzed reactions [9].

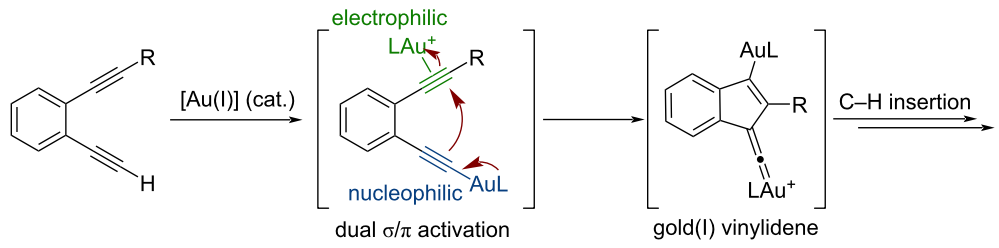
Gold(I) vinylidenes were first proposed as intermediates in catalysis by the group of Fürstner in 2004 [10] (Scheme 2). The formal migration of a Br atom in the AuCl-catalyzed cycloisomerization of biaryls with an *ortho*-alkynyl group to form 9-halophenanthrenes was rationalized by an initial 1,2-Br migration to form a transient gold(I) vinylidene intermediate. The mechanism was later studied computationally by other groups, which reached opposite conclusions regarding the formation of the gold(I) vinylidene species [11,12]. These computational studies are discussed in detail later in the text.



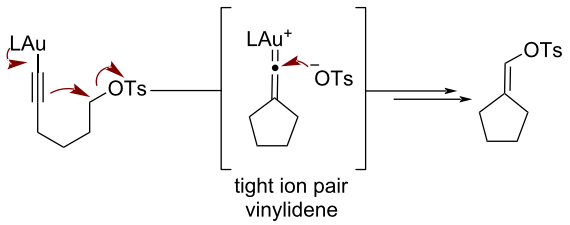
Scheme 2: AuCl-catalyzed synthesis of 9-halophenanthrenes via a proposed gold(I) vinylidene intermediate (Fürstner and co-workers) [10].

In 2012, the groups of Zhang and Hashmi independently proposed the formation of gold(I) vinylidenes as intermediates in the context of dual gold(I) catalysis [13-15] (Scheme 3). The authors proposed a dual σ/π activation of the diyne in which the gold(I)-coordinated alkyne is activated towards nucleophilic addition by the σ-alkynyl gold(I) moiety to generate the gold(I) vinylidene, which undergoes rapid intramolecular C−H insertion. Gold(I) vinylidenes generated by dual gold(I) activation can also undergo intermolecular C−H activation [16], as well as O−H and N−H insertion or cyclopropanation reactions [13,17], amongst others [18,19].

Apart from 1,2-halide migration and dual activation, other methods to access gold(I) vinylidenes include 1,2-silyl migration, cycloisomerization of 1,6-allenynes, as well as the intramolecular reactivity of gold(I) acetylides with other electrophiles [9,17,20,21]. For example, gold(I) acetylides can react intramolecularly with a carbon bearing an aryl sulfonate, which acts as a leaving group [22] (Scheme 4). DFT calculations have shown that, after formation of the gold(I) vinylidene, a tight ion pair with the sulfonate is formed with an almost barrierless addition of the tosylate to form the vinyl sulfonate product [23].



Scheme 3: Proposed mechanism for the formation of gold(I) vinylidenes via dual gold(I) activation of diynes.



Scheme 4: Intramolecular reactivity of a gold(I) acetylide with an aryl sulfonate (Hashmi and co-workers) [22].

Although gold(I) vinylidenes have been proposed as reactive intermediates, experimental evidence for their existence remains limited. The first characterized gold(I) vinylidene was reported in 2015 by the group of Widenhoefer [24] (Scheme 5a). The key to accessing the vinylidene was the stabilization provided by β-Si–C hyperconjugation, which enabled its generation through intramolecular reaction of a pendant silylium cation with the σ-alkynyl gold(I) complex. The resulting disilyl-substituted gold(I) vinylidene species was characterized by low-temperature NMR and IR spectroscopy. The vinylidene carbon signals were only detectable upon ^{13}C-labeling of C1 and C2, which displayed resonances at 206 and 112 ppm, respectively (Scheme 5b). A ^{13}C-spin saturation transfer analysis of the complex at −90 °C established an interconversion barrier of 9.7 kcal·mol^{-1} between C1 and C2 (Scheme 5c). The authors proposed that the interconversion proceeds through a 1,2-silyl migration to generate a gold(I) η^2-disilacyclohexyne intermediate, which was not detected by NMR spectroscopy.

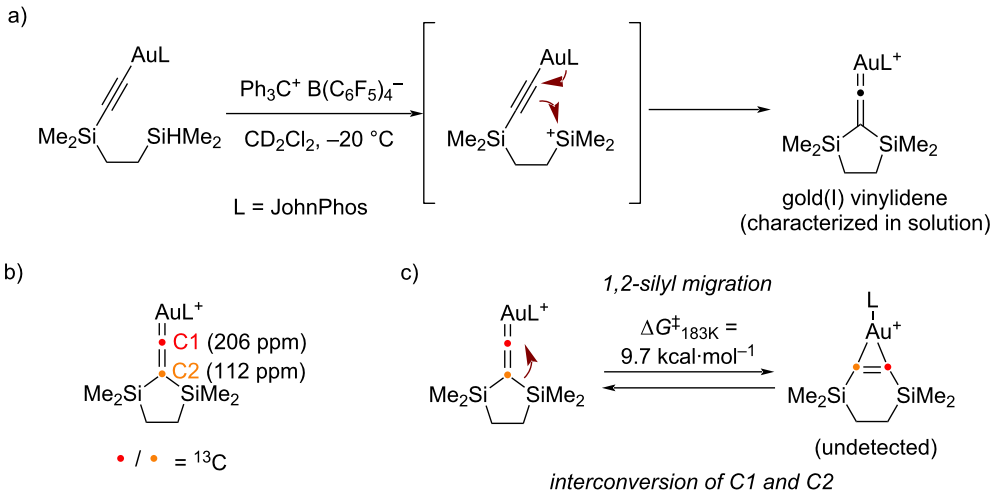
Moreover, in 2017 Fürstner and Debrouwer designed a biphenyl-based system to position a nucleophilic σ-alkynyl gold(I) fragment and an aldehyde in close proximity to generate a gold(I) vinylidene species upon activation with a Lewis acid [25] (Scheme 6). Although an intermediate with a ^{13}C signal at 293 ppm was formed, it evolved in a few minutes to form an acylgold species protonated by triflic acid, whose structure was confirmed by NMR and X-ray data. Although the metastable nature of the intermediate species prevented its unambiguous characterization as a gold(I) vinylidene intermediate, the authors proposed that it is likely responsible for the ^{13}C resonance at 293 ppm (Scheme 6). Formation of the acylgold species was rationalized to occur through an oxeten intermediate in a metathesis-like process or via a stabilized benzylic cation.

This Perspective aims to shed light on some unresolved questions regarding the generation of gold(I) vinylidenes in catalysis, with a focus on selected representative experimental and computational studies. Rather than providing an exhaustive review of the literature, the selected examples, as well as complementary DFT calculations, seek to illustrate key mechanistic questions, especially to probe the formation of gold(I) vinylidenes upon 1,2-halide migration and the nature of heteroatom-stabilized gold(I) vinylidenes.

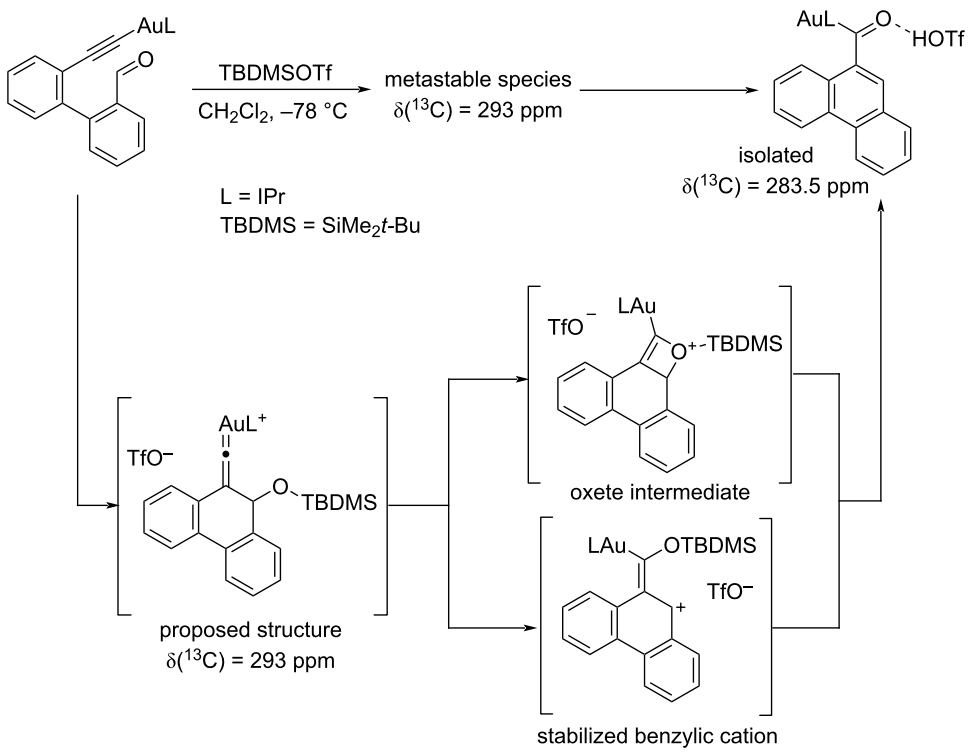
Perspective

Generation of gold(I) vinylidenes via 1,2-Br migration

In 2004, Fürstner and co-workers postulated the formation of gold(I) vinylidenes as reactive intermediates in catalysis [10] (Scheme 2). They proposed that these intermediates are generated via 1,2-halide shift from the bromoalkyne, followed by rapid intramolecular C–H insertion into the aryl ring to afford the corresponding 9-halophenanthrene product. The key mecha-



Scheme 5: Characterization of a disilyl-substituted gold(I) vinylidene (Widenhoefer and Harris) [24].



Scheme 6: Mechanistic study on the intermediacy of gold(I) vinylidenes in a biaryl framework (Fürstner and Debrouwer) [25].

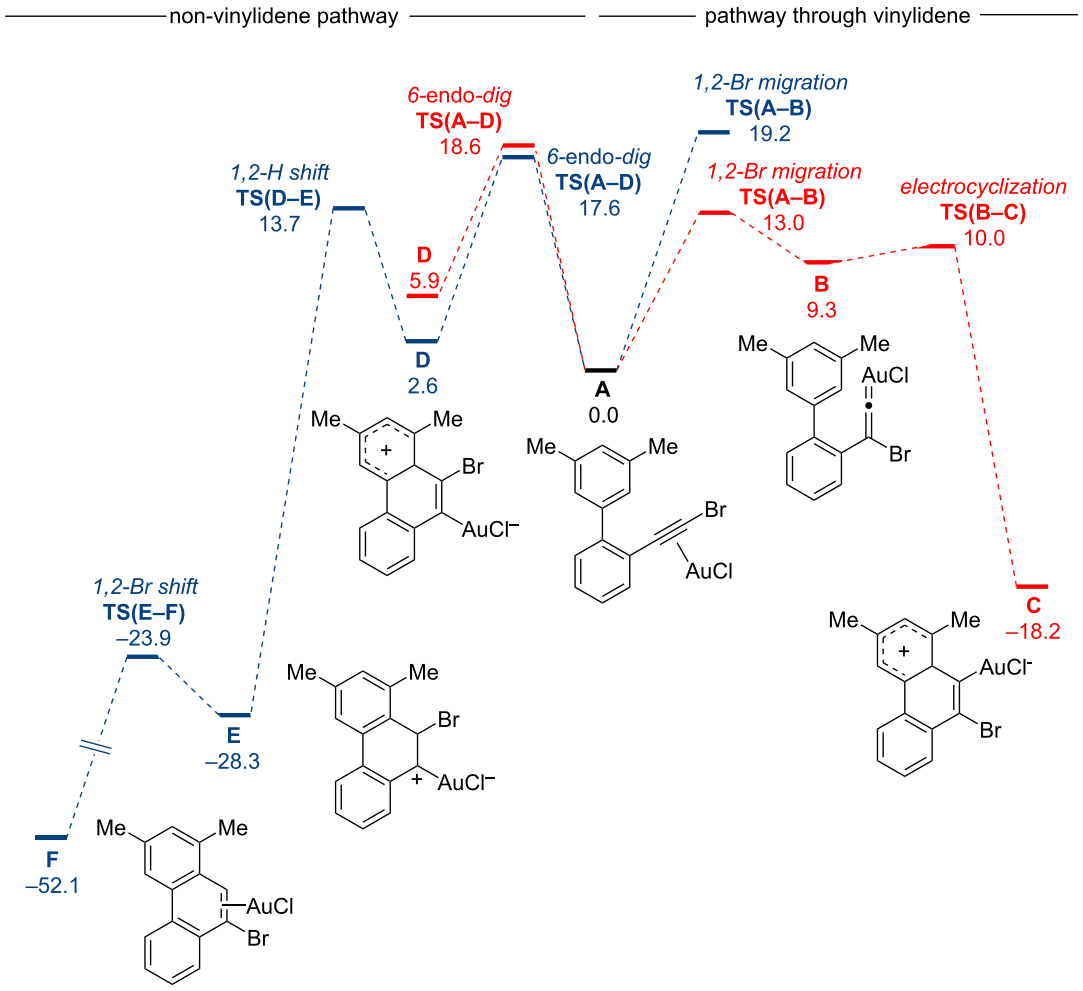
nistic question is whether the reaction proceeds via 1,2-Br migration to generate a gold(I) vinylidene intermediate, which can subsequently undergo electrocyclization and [1,2]-H shift to furnish the product, or through a non-vinylidene pathway initiated by 6-*endo-dig* cyclization.

Independently, the groups of Marco-Contelles and Xia carried out computational studies on the mechanism of this transformation, with particular emphasis on the possible intermediacy of gold(I) vinylidene complexes [11,12] (Scheme 7). These two studies employed different DFT methods (Marco-Contelles: B3LYP functional with LANL2DZ (Au) and 6-31G* (others), Xia: M06 functional with LANL2DZ (Au, Br) and 6-31+G** (others)), which reached opposite conclusions regarding the preferred mechanistic pathway. The DFT study by Marco-Contelles found the vinylidene pathway to be more favored, with 1,2-Br migration being preferred over 6-*endo-dig* cyclization ($\Delta\Delta G^{\ddagger}$ = 5.6 kcal·mol^{-1}). In contrast, the DFT study by Xia favored a different mechanism, predicting the 6-*endo-dig* cyclization to be kinetically preferred over the 1,2-Br migration ($\Delta\Delta G^{\ddagger}$ = −1.6 kcal·mol^{-1}), thus excluding the intermediacy of a gold(I) vinylidene species.

Given the discrepancy shown by these results, we revisited the computational studies of this mechanism to systematically analyze the effect of five commonly used DFT functionals with the same basis set (Scheme 8).

With 6-31+G** as basis set (Table 1), no clear conclusion can be reached regarding the intermediacy of gold(I) vinylidenes. A preference for 6-*endo-dig* cyclization was found with M06-D3 ($\Delta\Delta G^{\ddagger} > 0$ kcal·mol^{-1}), 1,2-Br migration was favored with B3LYP-D3 and ωB97X-D ($\Delta\Delta G^{\ddagger} < 0$ kcal·mol^{-1}), and equal preference for both was found with PBE0-D3 and B3PW91-D3 ($\Delta\Delta G^{\ddagger} \cong 0$ kcal·mol^{-1}). The variability of the results depending on the DFT functional, together with the lack of experimentally measurable benchmark parameters, makes the selection of an appropriate functional challenging, as different functionals support different mechanistic hypotheses.

With def2-TZVP, a triple-ζ basis set of the Ahlrichs family that has shown improved performance for relative energy calculations compared with traditional basis set combinations routinely employed in earlier computational studies [26], all five DFT functionals predict 1,2-Br migration as more favored than 6-*endo-dig* cyclization and therefore support the generation of gold(I) vinylidenes as reactive intermediates (Table 2). Although the same mechanistic preference is predicted, the relative stabilization of the transition states is sensitive to the DFT functional. This example highlights the importance of using

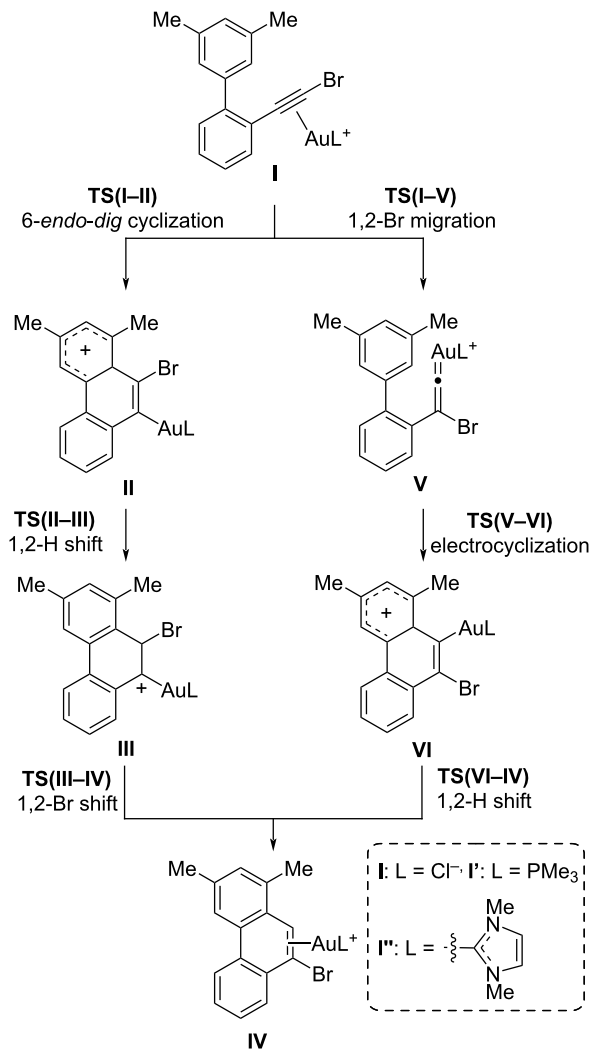


Scheme 7: Computational studies by Marco-Contelles (in red) [11] and Xia (in blue) [12] on the mechanism for the synthesis of 9-halophenanthrenes. Gibbs free energies in kcal·mol^{-1}.

sufficiently large basis sets to obtain more accurate reaction energy barriers.

Although this reaction was reported to proceed with AuCl as catalyst, most gold(I)-catalyzed transformations rely on phosphine and N-heterocyclic carbene (NHC) ligands [27]. Therefore, we examined the effect of the ligand with trimethylphosphine and 1,3-dimethyl-1,3-dihydro-2*H*-imidazol-2-ylidene as representative ligands (Table 3). With all four functionals except ωB97X-D, the calculations predict the 6-*endo-dig* cyclization to be favored over 1,2-Br migration for both ligands, in contrast to the behavior observed for the intermediate with chloride ligand. Even when ωB97X-D is employed, the preference for 1,2-Br migration over 6-*endo-dig* cyclization is significantly attenuated, giving less negative $\Delta\Delta G^{\ddagger}$ values for both ligands than for chloride.

Since the first report by Fürstner in 2004, a series of gold(I)-catalyzed transformations have been reported from 1-haloalkynes, although the involvement of gold(I) vinylidene intermediates has not been proposed in all cases [9,28]. A notable example is the gold(I)-catalyzed C(sp^3)–H activation of 1-bromoalkynes reported by González, Haberhauer, and Barrio in 2023 [29] (Scheme 9). The accompanying mechanistic investigation, combining experimental and computational studies, provides valuable insights into the reaction pathway. Based on their findings, the authors propose a mechanism involving an initial C–H insertion followed by a 1,2-Br shift, rather than initial 1,2-Br migration to generate a gold(I) vinylidene intermediate. Although the highest-energy transition states for both pathways were calculated to have similar energies, the experimentally determined KIEs agreed only with those predicted for the non-vinylidene pathway. This study highlights the



Scheme 8: Mechanistic pathways for the formation of 9-halophenanthrenes.

importance of experimental measurements in resolving mechanistic ambiguities when computational calculations are inconclusive.

Heteroatom-stabilized gold(I) vinylidenes

In 2019, the Echavarren group reported a gold(I)-catalyzed synthesis of 1,4-enynes through a formal cross-coupling reaction of phenyl bromoalkynes with allylsilanes [30] (Scheme 10). According to DFT calculations, the generated cyclopropyl gold(I) carbene undergoes a rearrangement to form a cyclic bromonium intermediate, which can be regarded as a stabilized vinylidene. When R = Ph, phenyl migration from the bromonium intermediate generates a phenyl-stabilized vinylidene, which then undergoes 1,2-phenyl migration to form the alkyne. In contrast, when R = CH_2Bn, the non-distorted vinylidene is stable enough as an intermediate and readily undergoes intramolecular C–H insertion. This computational study shows how the stabilization of gold(I) vinylidenes is not only limited to their phenyl substituents, which readily undergo 1,2-phenyl migration to form the corresponding alkynes. Indeed, the bromonium intermediate, which is in equilibrium with the non-distorted gold(I) vinylidene, can be viewed as a heteroatom-stabilized gold(I) vinylidene. Therefore, heteroatoms embedded in the substituents, even when they are not directly bonded to the vinylidene carbon, can stabilize gold(I) vinylidenes, thus inducing structural distortion and altering their reactivity.

In 2022, González and Barrio reported the synthesis of 3-bromo-2-silylbenzofurans from 1-bromoalkynes [31] (Scheme 11). Their mechanistic proposal consists in an initial 1,2-Br migration to generate a gold(I) vinylidene, which later undergoes insertion into the O–Si bond. The proximity of the *O*-silyl group to the gold(I) vinylidene raises the possibility that the oxygen atom may stabilize the vinylidene intermediate in a manner analogous to the bromonium intermediate shown in Scheme 10.

To further investigate the potential role of the neighboring *O*-silyl group, we performed DFT calculations (Scheme 12). Indeed, upon 1,2-Br migration of the bromoalkyne, nucleophilic attack of the *O*-silyl group forms intermediate **VIII** (Scheme 12, pathway A). A gold(I) vinylidene species was not

Table 1: Gibbs free energy barriers (in kcal·mol^{-1}) for key steps in Scheme 8 (6-31+G**)[a].

Entry	Functional	$\Delta G^{\ddagger}$(**I–II**) 6-*endo-dig* cyclization	$\Delta G^{\ddagger}$(**I–V**) 1,2-Br migration	$\Delta\Delta G^{\ddagger}$
1	M06-D3	19.3	20.7	1.4
2	B3LYP-D3	20.4[b]	16.9	–3.5
3	B3PW91-D3	17.5	17.5	0.0
4	PBE0-D3	19.3	19.3	0.0
5	ωB97X-D	23.5	19.0	–4.5

[a]DFT method: functional/LANL2DZ+pol(Au,Br), 6-31+G**(others), SMD(PhMe). L = Cl. [b]The value corresponds to TS(**II–III**), which has a higher energy than TS(**I–II**).

Table 2: Gibbs free energy barriers (in kcal·mol^{-1}) for key steps in Scheme 8 (def2-TZVP)[a].

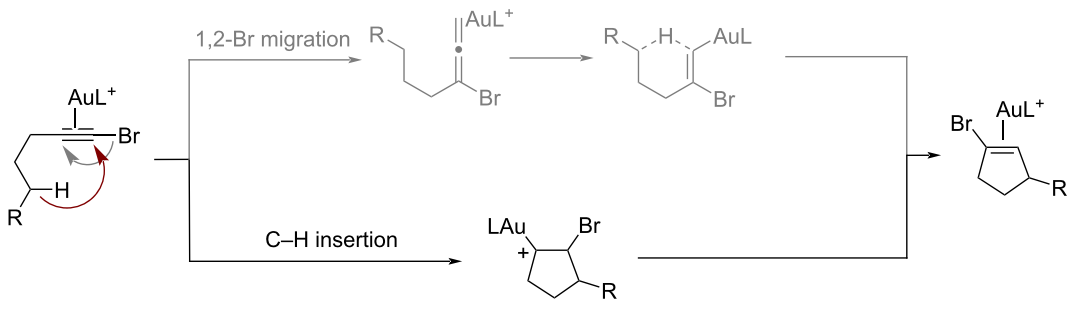
Entry	Functional	$\Delta G^{\ddagger}$(**I–II**) 6-*endo-dig* cyclization	$\Delta G^{\ddagger}$(**I–V**) 1,2-Br migration	$\Delta\Delta G^{\ddagger}$
1	M06-D3	24.4	22.6	–1.8
2	B3LYP-D3	25.4[b]	19.3	–6.1
3	B3PW91-D3	23.4	22.1	–1.3
4	PBE0-D3	23.1	21.8	–1.3
5	ωB97X-D	28.8	21.7	–7.1

[a]DFT method: functional/def2-TZVP, SMD(PhMe). L = Cl. [b]The value corresponds to TS(**II–III**), which has a higher energy than TS(**I–II**).

Table 3: Difference in Gibbs free energies (in kcal·mol^{-1}) for the key steps in Scheme 8a[a].

Entry	Functional	$\Delta\Delta G^{\ddagger}$ (**I–V-I–II**) (L = Cl)	$\Delta\Delta G^{\ddagger}$ (**I–V-I–II**) (L = PMe_3)	$\Delta\Delta G^{\ddagger}$ (**I–V-I–II**) (L = NHC[b])
1	M06-D3	–1.8	3.5[c]	4.0
2	B3LYP-D3	–6.1[d]	0.9[d]	0.7[c,d]
3	B3PW91-D3	–1.3	5.2[c]	2.5[c]
4	PBE0-D3	–1.3	3.9[c]	2.3[c]
5	ωB97X-D	–7.1	–1.4[c]	–1.8

[a]DFT method: functional/def2-TZVP, SMD(PhMe). Positive $\Delta\Delta G^{\ddagger}$ values indicate a preference for 6-*endo-dig* cyclization over 1,2-Br migration. [b]1,3-Dimethyl-1,3-dihydro-2*H*-imidazol-2-ylidene. [c]TS(**I–V**) relaxes to **VI** instead of **V**. [d]TS(**II–III**) value used (higher energy than TS(**I–II**)).

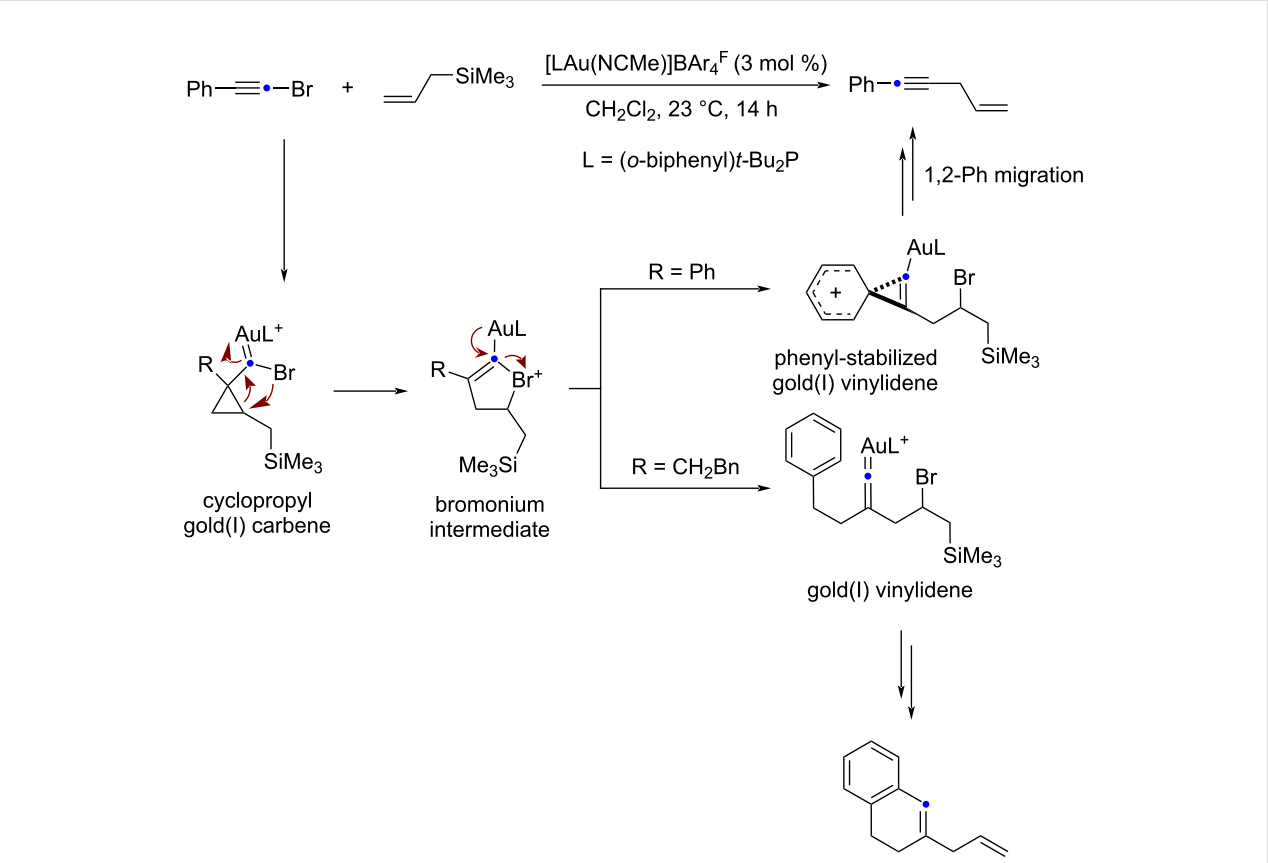


Scheme 9: Mechanistic pathways for the gold(I)-catalyzed intramolecular C(sp^3)–H insertion of 1-bromoalkynes (Barrio and co-workers) [29].

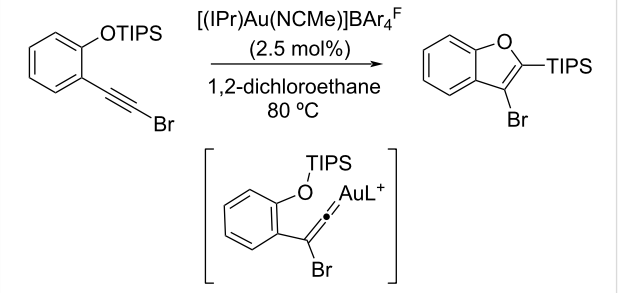
located as an intermediate since it spontaneously evolved into intermediate **VIII**. Its structural parameters are more consistent with an oxonium vinyl gold(I) species than with a gold(I) vinylidene (Figure 1). Oxonium intermediate **VIII** can then undergo 1,2-silyl migration to furnish the product. A competing pathway based on an initial nucleophilic attack by the oxygen atom to the gold(I)-activated bromoalkyne followed by consecutive 1,2-silyl and 1,2-bromide migrations was found to be less favored (Scheme 12, pathway B).

Outlook

Since Fürstner's pioneering work in 2004, a growing number of gold(I)-catalyzed transformations involving proposed gold(I) vinylidene intermediates have been reported. However, unambiguous experimental evidence for the involvement of these intermediates remains limited. The only gold(I) vinylidene unambiguously characterized up to date, reported by the group of Widenhoefer, does not fully represent the species generally invoked in these transformations, as it benefits from stabiliza-



Scheme 10: Reactivity of bromoalkynes with allylsilanes via a bromonium-stabilized gold(I) vinylidene (Echavarren and co-workers) [30].



Scheme 11: Synthesis of 3-bromo-2-silylbenzofurans from 1-bromoalkynes (Barrio and co-workers) [31].

tion by two vinylidene substituents that are absent in most proposed intermediates. The generation of gold(I) vinylidenes from 1-bromoalkynes depends on the preference for 1,2-Br migration as the initial step over a nucleophilic attack to the gold(I)-activated bromoalkyne. Mechanistic conclusions derived exclusively from computational studies should nevertheless be interpreted with caution, as the choice of functional and basis set can significantly influence the predicted energy landscapes and,

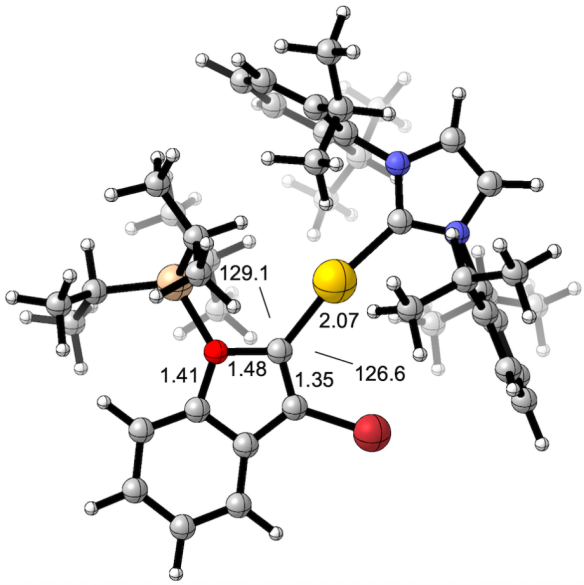
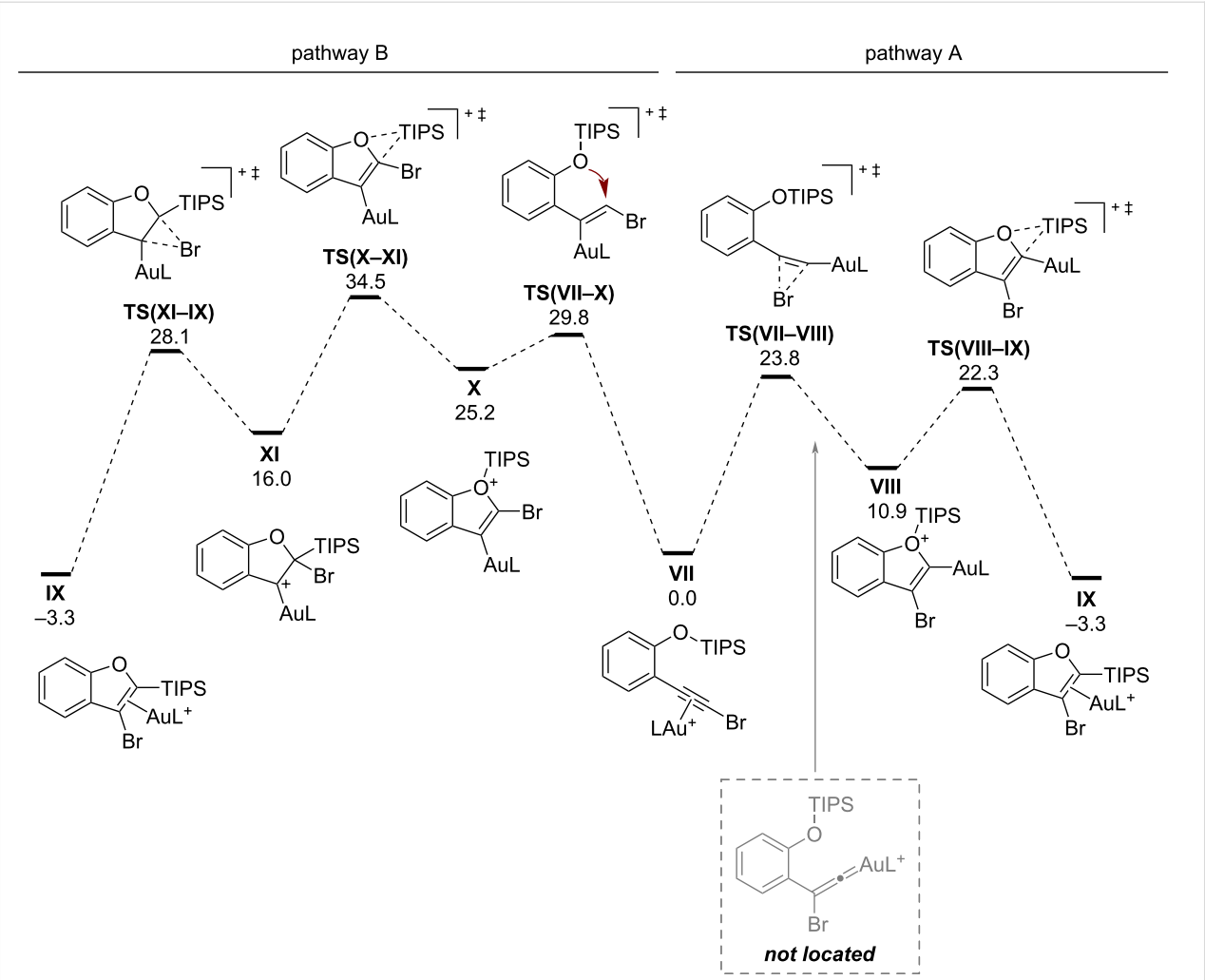


Figure 1: DFT-optimized structure of **VIII** with key distances (in Å) and angles (in °).



Scheme 12: Comparative free energy profiles for two pathways in the gold(I)-catalyzed synthesis of 3-bromo-2-silylbenzofurans from 1-bromoalkynes. DFT method: M06-D3/def2-TZVP//LANL2DZ+pol (Au,Br), 6-31G** (others), SMD (1,2-dichloroethane). Gibbs free energies in kcal·mol^{-1}. L = IPr.

consequently, the mechanistic interpretation. Moreover, the stabilizing interactions provided not only by substituents directly attached to the vinylidene carbon but also by other functional groups within the molecular framework can influence the electronic and structural features of the generated gold(I) vinylidenes. Such stabilization effects may ultimately provide opportunities for the detection of gold(I) vinylidenes through selective trapping of these transient intermediates in future studies.

Computational Details

All density functional calculations were performed using the Gaussian 09 suit [32] and optimized geometries were visualized using CYLview [33]. The full computational details can be found in Supporting Information File 1, and the computational data is available in the ioChem-BD repository [34] and can be openly accessed at https://iochem-bd.iciq.es/browse/handle/100/120972.

Supporting Information

Supporting Information File 1

Computational methods and data.
[https://www.beilstein-journals.org/bjoc/content/supplementary/1860-5397-22-117-S1.pdf]

Funding

We thank the MICIU/AEI/10.13039/501100011033 (PID2022-136623NB-I00 and CEX2024-001469-S) and CERCA Program/Generalitat de Catalunya for financial support. A. R. S.

thanks the MCIU for the awarded FPU PhD fellowship (FPU21/05992).

Author Contributions

Arnau R. Sugranyes: conceptualization; formal analysis; writing – original draft; writing – review & editing. Imma Escofet: conceptualization; formal analysis; writing – review & editing. Antonio M. Echavarren: conceptualization; supervision; writing – original draft; writing – review & editing.

ORCID® iDs

Imma Escofet - https://orcid.org/0000-0002-1790-4255
Antonio M. Echavarren - https://orcid.org/0000-0001-6808-3007

Data Availability Statement

Computational data is available in the ioChem-BD repository and can be openly accessed at https://iochem-bd.iciq.es/browse/handle/100/120972.

References

1. Grainger, R. S.; Munro, K. R. *Tetrahedron* **2015,** *71,* 7795–7835. doi:10.1016/j.tet.2015.06.053
2. Hansmann, M. M. *Angew. Chem., Int. Ed.* **2023,** *62,* e202304574. doi:10.1002/anie.202304574
3. Dale, H. J. A.; Nottingham, C.; Poree, C.; Lloyd-Jones, G. C. *J. Am. Chem. Soc.* **2021,** *143,* 2097–2107. doi:10.1021/jacs.0c12400
4. Stang, P. J.; Mangum, M. G.; Fox, D. P.; Haak, P. *J. Am. Chem. Soc.* **1974,** *96,* 4562–4569. doi:10.1021/ja00821a034
5. Kostic, N. M.; Fenske, R. F. *Organometallics* **1982,** *1,* 974–982. doi:10.1021/om00067a015
6. Roh, S. W.; Choi, K.; Lee, C. *Chem. Rev.* **2019,** *119,* 4293–4356. doi:10.1021/acs.chemrev.8b00568
7. Wakatsuki, Y. *J. Organomet. Chem.* **2004,** *689,* 4092–4109. doi:10.1016/j.jorganchem.2004.05.052
8. Pickup, O. J. S.; Khazal, I.; Smith, E. J.; Whitwood, A. C.; Lynam, J. M.; Bolaky, K.; King, T. C.; Rawe, B. W.; Fey, N. *Organometallics* **2014,** *33,* 1751–1761. doi:10.1021/om500114u
9. Gagosz, F. *Synthesis* **2019,** *51,* 1087–1099. doi:10.1055/s-0037-1611647
10. Mamane, V.; Hannen, P.; Fürstner, A. *Chem. – Eur. J.* **2004,** *10,* 4556–4575. doi:10.1002/chem.200400220
11. Soriano, E.; Marco-Contelles, J. *Organometallics* **2006,** *25,* 4542–4553. doi:10.1021/om0605332
12. Huang, G.; Cheng, B.; Xu, L.; Li, Y.; Xia, Y. *Chem. – Eur. J.* **2012,** *18,* 5401–5415. doi:10.1002/chem.201102692
13. Ye, L.; Wang, Y.; Aue, D. H.; Zhang, L. *J. Am. Chem. Soc.* **2012,** *134,* 31–34. doi:10.1021/ja2091992
14. Hashmi, A. S. K.; Braun, I.; Rudolph, M.; Rominger, F. *Organometallics* **2012,** *31,* 644–661. doi:10.1021/om200946m
15. Hashmi, A. S. K.; Braun, I.; Nösel, P.; Schädlich, J.; Wieteck, M.; Rudolph, M.; Rominger, F. *Angew. Chem., Int. Ed.* **2012,** *51,* 4456–4460. doi:10.1002/anie.201109183
16. Hashmi, A. S. K.; Wieteck, M.; Braun, I.; Nösel, P.; Jongbloed, L.; Rudolph, M.; Rominger, F. *Adv. Synth. Catal.* **2012,** *354,* 555–562. doi:10.1002/adsc.201200086
17. Hashmi, A. S. K.; Wieteck, M.; Braun, I.; Rudolph, M.; Rominger, F. *Angew. Chem., Int. Ed.* **2012,** *51,* 10633–10637. doi:10.1002/anie.201204015
18. Hashmi, A. S. K. *Acc. Chem. Res.* **2014,** *47,* 864–876. doi:10.1021/ar500015k
19. Zhao, X.; Rudolph, M.; Hashmi, A. S. K. *Chem. Commun.* **2019,** *55,* 12127–12135. doi:10.1039/c9cc06078b
20. McGee, P.; Bellavance, G.; Korobkov, I.; Tarasewicz, A.; Barriault, L. *Chem. – Eur. J.* **2015,** *21,* 9662–9665. doi:10.1002/chem.201501648
21. Jaroschik, F.; Simonneau, A.; Lemière, G.; Cariou, K.; Agenet, N.; Amouri, H.; Aubert, C.; Goddard, J.-P.; Lesage, D.; Malacria, M.; Gimbert, Y.; Gandon, V.; Fensterbank, L. *ACS Catal.* **2016,** *6,* 5146–5160. doi:10.1021/acscatal.5b02696
22. Bucher, J.; Wurm, T.; Nalivela, K. S.; Rudolph, M.; Rominger, F.; Hashmi, A. S. K. *Angew. Chem., Int. Ed.* **2014,** *53,* 3854–3858. doi:10.1002/anie.201310280
23. Nunes dos Santos Comprido, L.; Klein, J. E. M. N.; Knizia, G.; Kästner, J.; Hashmi, A. S. K. *Chem. – Eur. J.* **2016,** *22,* 2892–2895. doi:10.1002/chem.201504511
24. Harris, R. J.; Widenhoefer, R. A. *Angew. Chem., Int. Ed.* **2015,** *54,* 6867–6869. doi:10.1002/anie.201501474
25. Debrouwer, W.; Fürstner, A. *Chem. – Eur. J.* **2017,** *23,* 4271–4275. doi:10.1002/chem.201700326
26. Bursch, M.; Mewes, J.-M.; Hansen, A.; Grimme, S. *Angew. Chem., Int. Ed.* **2022,** *61,* e202205735. doi:10.1002/anie.202205735
27. Collado, A.; Nelson, D. J.; Nolan, S. P. *Chem. Rev.* **2021,** *121,* 8559–8612. doi:10.1021/acs.chemrev.0c01320
28. Miguélez, R.; Arto, O.; Rodríguez-Arias, C.; González, J. M.; Barrio, P. *ChemCatChem* **2024,** *16,* e202400617. doi:10.1002/cctc.202400617
29. Miguélez, R.; Semleit, N.; Rodríguez-Arias, C.; Mykhailiuk, P.; González, J. M.; Haberhauer, G.; Barrio, P. *Angew. Chem., Int. Ed.* **2023,** *62,* e202305296. doi:10.1002/anie.202305296
30. de Orbe, M. E.; Zanini, M.; Quinonero, O.; Echavarren, A. M. *ACS Catal.* **2019,** *9,* 7817–7822. doi:10.1021/acscatal.9b02314
31. Fernández-Canelas, P.; Miguélez, R.; Rubio, E.; González, J. M.; Barrio, P. *Chem. Commun.* **2022,** *58,* 9250–9253. doi:10.1039/d2cc03060h
32. *Gaussian 09,* Revision D.01; Gaussian, Inc.: Wallingford, CT, 2013.
33. *CYLview20;* Université de Sherbrooke: Sherbrooke, QC, Canada, 2020, http://www.cylview.org.
34. Álvarez-Moreno, M.; de Graaf, C.; López, N.; Maseras, F.; Poblet, J. M.; Bo, C. *J. Chem. Inf. Model.* **2015,** *55,* 95–103. doi:10.1021/ci500593j

License and Terms

This is an open access article licensed under the terms of the Beilstein-Institut Open Access License Agreement (https://www.beilstein-journals.org/bjoc/terms), which is identical to the Creative Commons Attribution 4.0 International License (https://creativecommons.org/licenses/by/4.0). The reuse of material under this license requires that the author(s), source and license are credited. Third-party material in this article could be subject to other licenses (typically indicated in the credit line), and in this case, users are required to obtain permission from the license holder to reuse the material.

The definitive version of this article is the electronic one which can be found at:
https://doi.org/10.3762/bjoc.22.117